PhD degree in Molecular Medicine (curriculum in Molecular Oncology)

European School of Molecular Medicine (SEMM),

University of Milan and University of Naples "Federico II"

Settore disciplinare: Bio/10

Molecular contribution of the Aurora-A kinase and the junctional protein Afadin to oriented cell divisions

Sara Gallini

European Institute of Oncology (IEO), Milan

Matricola n. R09863

Supervisor: **Dr. Marina Mapelli**

European Institute of Oncology (IEO), Milan

Internal Advisor: **Prof. Giorgio Scita**

IFOM, The FIRC Institute of Molecular Oncology, Milan

External Advisor: **Prof. Cayetano González**

Institute for Research in Biomedicine (IRB Barcelona)

Anno accademico 2014-2015

TABLE OF CONTENTS

ABBREVIATIONS

Abl-1	Ableson Leukemia Kinase-1
ACD	Asymmetric Cell Division
AF-6	Afadin
AJ	Adherens Junction
BD	Binding Domain
BSA	Bovine Serum Albumin
Caco-2	Human Colorectal Adenocarcinoma Cells
CDK1	Cyclin-Dependent Kinase 1
Co-IP	Co-Immunoprecipitation
Cos-7	Monkey *Cercopithecus Aethiops* Fibroblast-Like Kidney Cells
DIC	Differential Interference Contrast Microscopy
Dlg	Disc Large
DMSO	Dimethyl Sulfoxide
ECM	Extracellular Matrix
Eg5	Kinesin-5
F-actin	Filamentous Actin
FG	Force Generator
FRAP	Fluorescence Recovery After Photobleaching
GEF	Guanine Nucleotide Exchange Factors
GL2	Luciferase
GSH	Glutathione Sepharose
GTP/GDP	Guanosine Triphosphate/Diphosphate
Gαi	The Alpha Subunit Of Adenyl-Cyclase-Inibitory Heterotrimeric G Protein
HEK293t	Human Embryonic Kidney 293 Cells
HeLa	Human Cervical Cancer Cells
hTERT-RPE-1	Human Telomerase-Immortalized Retinal Pigment Epithelial Cell Line
K-fiber	Kinetochore-Fiber
KD	Kinase-Dead
Lgl	Lethal Giant Larvae
LGN	Leu-Gly-Asn Repeat-Enriched Protein
MAR	Matrix Attachment Region
MDCK	Madin-Darby Canine Kidney Cells
MEF	Mouse Embryo Fibroblast
MT	Microtubule
MTOC	Microtubule-Organizing Centers
NB	Neuroblast
NLS	Nuclear Localization Signal
NuMA	Nuclear Mitotic Apparatus
Par	Partitioning-Defective
PCM	Pericentriolar Material
PFA	Paraformaldehyde
Plk1	Polo-Kinase-1
qPCR	Quantitative-PCR
Ran	Ras Related Nuclear Protein
RCC1	Regulator Of Chromosome Condensation
Ric8A	Resistance To Inhibitors Of Cholinesterase 8
RNAi	RNA Interference
SAF	Spindle Assembly Factor
Scrib	Scribble
SEC	Size Exclusion Chromatography
shRNA	Short-Hairpin RNA
SOP	Sensory Organ Precursor
STLC	S-Trityl-L-Cysteine
TPR	Tetratrico-Peptide Repeats
TPX2	Xenopus Kinesin-Like Protein 2

FIGURES INDEX

ABSTRACT

Correct spindle positioning is essential for tissue morphogenesis and homeostasis. The orientation of the mitotic spindle is determined by cortical force generators formed on NuMA:LGN:Gαi complexes, which anchor astral microtubules emanating from the spindle poles at specialized domains of the plasma membrane via direct interaction with the motor proteins Dynein/Dynactin. Cortical polarity cues and actin-associated proteins synergize with extrinsic signals (such as cell-to-cell and cell-to-extracellular matrix contacts) in recruiting NuMA:LGN:Gαi complexes at the cell cortex. In addition, spindle placement is coordinated with mitotic progression by mitotic kinases regulating the timely cortical recruitment of NuMA:LGN:Gαi above the spindle poles.

My PhD project focused on the study of the molecular mechanisms accounting for the spindle orientation functions of the Aurora-A kinase, the polarity protein Lgl2, and the junctional protein Afadin.

The Aurora-A kinase is known for being implicated in spindle alignment, however the molecular events underlying this function remain to date unclear. To study the spindle orientation functions of Aurora-A, I developed protocols for the partial inhibition of its activity in transformed and non-transformed cells in culture. Under these conditions, in metaphase NuMA and Dynactin accumulate abnormally at the spindle poles without reaching the cortex, while the cortical distribution of LGN remains unperturbed. Fluorescence Recovery After Photobleaching (FRAP) experiments conducted on GFP-NuMA revealed that Aurora-A governs the dynamic exchange between the cytoplasmic and the spindle-pole-localized pools of NuMA. Molecularly, Aurora-A phosphorylates directly the C-terminus of NuMA on three serine residues, among which Ser-1969 is the major determinant for the dynamic behaviour of NuMA at the spindle poles. Most interestingly, we identify a new microtubule-binding domain of NuMA, which does not overlap with the LGN-binding motif, thus suggesting that NuMA can associate

concomitantly with LGN and microtubules. This finding indicates that the microtubule-binding activity of NuMA might contribute to anchor microtubule +TIPs at cortical sites with LGN. Collectively, my studies demonstrate that in metaphase the direct phosphorylation of NuMA by Aurora-A controls its cortical enrichment, and that this is the major event underlying the spindle orientation functions of Aurora-A in cultured cells. Phosphorylation of NuMA by Aurora-A does not affect its affinity for microtubules nor for LGN, but rather determines the mobility of the protein at the spindle-poles.

Biochemical studies suggested that Lgl2 can associate with LGN, hinting at a possible role of this protein in spindle orientation in mammalian system. On these premises, I found that depletion of Lgl2 misorients the spindle in HeLa cells plated on fibronectin. However, I could not reproduce the Lgl2:LGN interaction *in vitro* nor *ex vivo*. Interestingly, by immunoprecipitation experiments I detected an interaction between NuMA and Lgl2, which could explain the phenotype of spindle misorientation resulting from the silencing of Lgl2 in HeLa cells. Further studies will be required to gain a molecular understanding of the relevance Lgl2:NuMA interaction in oriented divisions.

Part of my PhD studies addressed the role of Afadin in spindle orientation; I demonstrated that Afadin is required for spindle positioning, and correct epithelial morphogenesis of Caco-2 three-dimensional cysts. At a molecular level, Afadin binds directly and concomitantly to F-actin and to LGN. Indeed, in mitotic HeLa cells, Afadin is required for cortical accumulation of LGN, NuMA and Dynein above the spindle poles, in a F-actin dependent manner. Collectively, these results uncovered a pivotal role of Afadin in governing the enrichment of LGN and NuMA at the lateral cortex of polarized epithelia. They also depict that Afadin as the first mechanical anchor between Dynein and cortical F-actin.

1. INTRODUCTION

1.1 Mitosis and the Mitotic Spindle

1.1.1 Mitosis

The ordered sequence of events that leads to cell duplication is called cell cycle. The cell cycle is constituted by two principal phases: the synthesis (S) phase, in which DNA, centrosome, and organelles are replicated, and the mitotic (M) phase, when the duplicated chromosomes are equally distributed to the daughter cells, physically divided during the cytokinesis (Figure 1).

Mitotic events can be further divided into five distinct phases: prophase, prometaphase, metaphase, anaphase, and telophase. During prophase, the chromatin released after nuclear envelope breakdown begins to condense to form chromosomes. Meanwhile the two centrosomes close to the nuclear envelope segregate to the opposites sides of the cell to form a bipolar spindle. The newly formed mitotic spindle captures chromosomes (prometaphase), aligns the chromosomes along the cell equator (metaphase), and then separates them (anaphase), so that the genetic material can be segregated to each daughter cell (telophase). After mitosis, the cell divides by cytokinesis (Figure 1) (Morgan, 2006).

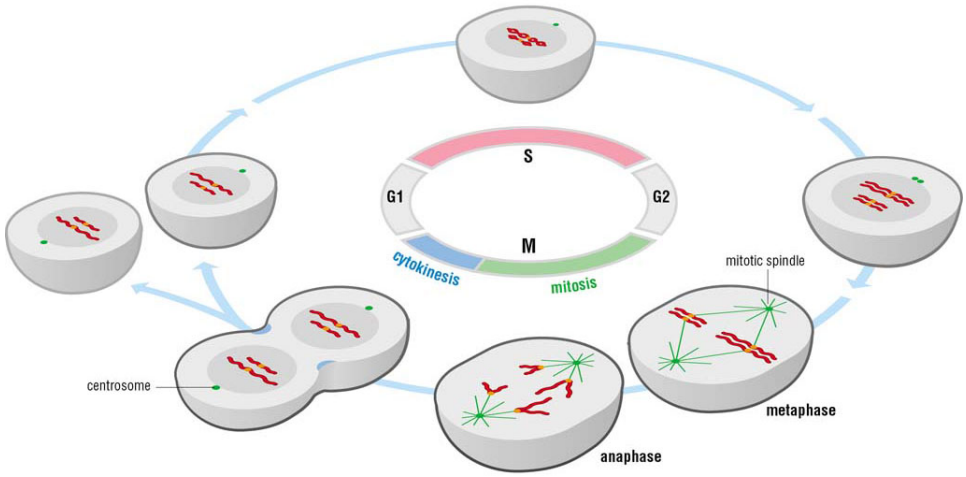

Adapted from David O.Morgan, The Cell Cycle: Principles of Control, 2006

Figure 1 - The cell cycle is a sequence of different phases, which takes place in eukaryotic cells to generate two daughter cells. In S-phase the DNA, centrosome and organelles are duplicated. In mitosis (M) the duplicated chromosomes are attached to the mitotic spindle and aligned at the metaphase plate. Then each sister chromatids is pulled to opposite side of the cell. Mitosis is

followed by cytokinesis, which distributes the cellular content in the resulting daughter cells. G1 phase is the gap phase between M and S phases; G2 phase is the gap between S and M phases (Morgan, 2006).

1.1.2 Mitotic spindle assembly

The mitotic spindle is a bipolar array of microtubules (MTs) focused and anchored at the spindle poles. Three classes of MTs form the mitotic spindle: kinetochore MTs, interpolar MTs and astral MTs. Kinetochore MTs assemble in bundles known as K-fibers, which are attached to chromosomes at the kinetochores, and in anaphase physically pull sister chromatids apart to separate the two genomes. Interpolar MTs form an antiparallel array between the spindle poles and are implicated in positioning of the cleavage furrow (Glotzer, 2009; Izumi et al., 2006; Schober et al., 1999; Siller et al., 2006; Zhu et al., 2011b). Astral MTs radiate out form the spindle poles and dynamically anchor the mitotic spindle to the cell cortex to participate in spindle alignment and elongation (Izumi et al., 2006; Kotak and Gonczy, 2013). Each MT is composed of α and β tubulin subunits. Tubulin dimers associate head-to-tail in a polar structure with a plus-end where β-tubulin is exposed, and a minus-end where α-tubulin emerges (Desai and Mitchison, 1997). In somatic cells, MTs nucleate from the centrosomes, which are regarded as the major microtubule-organizing centers (MTOCs). In mitosis, centrosomes are located at the spindle poles, where spindle MTs converge. Centrosome consists of two barrel-shaped centrioles embedded within a protein-dense matrix, the pericentriolar material (PCM) (Meraldi and Nigg, 2002).

In G2/M transition, the PCM increases in size and develops the capacity to nucleate and anchor MTs in a process called centrosome maturation (Meraldi and Nigg, 2002). This process requires the activity of several mitotic kinases such as the cyclin-dependent kinase 1 (CDK1), the Polo-like kinases (Plk1) and Aurora-A (Wang et al., 2014). The centrosomes and the nucleated MTs are then arranged in a bipolar spindle by different factors. The activity of the plus-end motor protein Eg5 (kinesin-5) and the minus-end

motor protein Dynein are essential for establishment of spindle bipolarity (Gadde and Heald, 2004) (Figure 2). Eg5 has been shown to be required for the separation of the centrosomes by crosslinking and sliding antiparallel MTs emanating form each centrosome, this way pushing centrosomes apart. Mechanistically, Eg5 forms homotetramers containing four motor domains. Tetrameric Eg5 can crosslink two adjacent antiparallel MTs and slide them on one another (Figure 2) (Sawin et al., 1992). Selective removal of Eg5 or chemical inhibition of its motor activity prevents centrosome separation, resulting in the formation of monopolar spindles (Mayer et al., 1999). Centrosome separation requires the activity of the additional microtubule motor Dynein (Figure 2). Dynein is a multisubunit ATPase composed by the Dynein heavy chain motor protein, and Dynein intermediate and light chains. The ancillary subunit Dynactin is also required for its motor activity (Kardon and Vale, 2009). In mitosis Dynein localizes to several cellular compartments including the plus-ends of growing MTs, the cell cortex, and the nuclear envelope (Kardon and Vale, 2009)(Figure 2).

In mitosis Dynein localizes at the spindle poles together with Dynactin and NuMA (Nuclear Mitotic Apparatus) to focus and tether the minus-ends of MTs close to the centrosomes (Merdes et al., 2000; Merdes et al., 1996). Beside contributing to bipolar spindle formation, mitotic cortical Dynein plays a prominent role in spindle positioning by pulling on astral MTs, as described in more details in the next paragraphs (Figure 2) (Kotak et al., 2012).

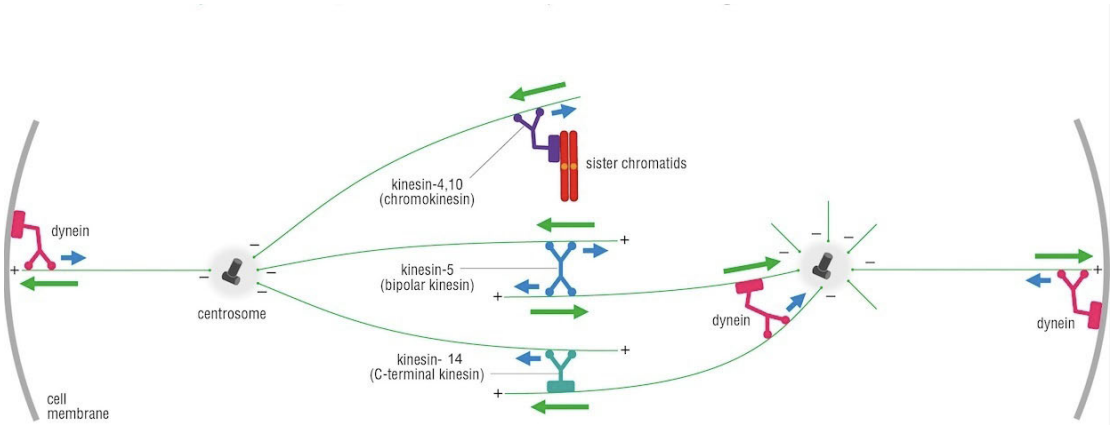

Adapted from David O.Morgan, The Cell Cycle Principles of Control, 2006

Figure 2 - The motor proteins in spindle assembly. During mitosis, centrosome separation is coordinated by the minus-end-directed motor protein Dynein and the plus-end-directed motor protein Eg5 (kinesin-5). The homotetrameric Eg5 crosslinks and slides antiparallel interpolar MTs to push centrosomes apart. On the other side, Dynein anchors the astral MTs at the cortex and pull the centrosomes toward the cell membrane. Moreover, Dynein focuses the MTs at the spindle poles. Also kinesin-4 and kinesin-10 promote centrosome separation. (Morgan, 2006).

Chromosome-derived signals transduced by the small GTP-binding protein Ran (Ras-related nuclear protein) are also necessary for mitotic spindle assembly (Kalab and Heald, 2008). Ran was originally characterized as a regulator of the nucleo-cytoplasmic transport in association with importins and exportins. Later it was found that the GTP-loaded form of Ran promotes MT assembly by favouring the release of spindle assembly factors (SAFs) from importins, which inhibit their function (Gorlich and Kutay, 1999; Kalab and Heald, 2008; Mattaj and Englmeier, 1998). SAFs stimulate MT nucleation and organization by regulating MT dynamics. The Ran-GTP cycle is regulated in turn by the guanine nucleotide exchange factor (GEF) RCC1 (regulator of chromosome condensation), which promotes the dissociation of GDP and enhances the GTP bound state of Ran (Figure 3). Since RCC1 is associated with chromatin, in mitosis it generates a gradient of Ran-GTP centred on chromosomes. In this situation, proteins containing a nuclear localization signal (NLS), which are bound to β-importin, are released form this interaction by Ran-GTP in proximity of the chromosomes (Figure 3)(Clarke and Zhang, 2008).

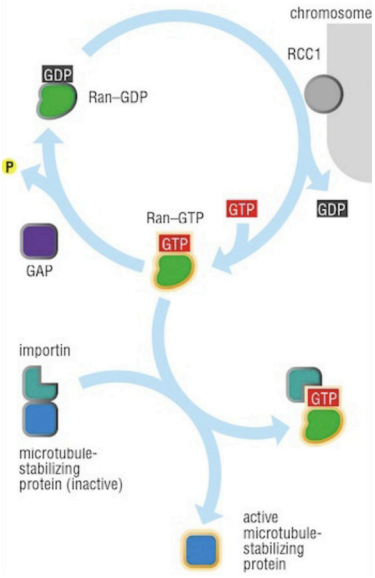

Figure 3 – Ran-GTP: a chromosome-derived signal to drive spindle assembly. The GEF factor RCC1 localized on chromosomes determines the production of a Ran-GTP gradient. The Ran-GTP gradient is required to dissociate the MT-stabilizing proteins from importins, and to activate them. MT-stabilizing proteins such as NuMA and TPX2 are then required to assemble the mitotic spindle (Morgan, 2006).

Adapted from David O.Morgan, The Cell Cycle: Principles of Control, 2006.

1.2 Spindle orientation

In metaphase, the mitotic spindle is placed centrally to the cytoplasm, and its position is stabilized to allow elongation and sisters' separation in anaphase. The position and the orientation of the mitotic spindle are determined by cortical force generators (FGs), which anchor astral MTs emanating from the spindle poles to specialized domains of the plasma membrane (Kiyomitsu, 2015). Besides sustaining elongation, the spindle orientation also regulates the position of the cleavage furrow and hence the placement of daughter cells within a growing tissue. For this reasons, during development, correct spindle orientation is required for morphogenesis and maintenance of tissue architecture (Kulukian and Fuchs, 2013; Peyre and Morin, 2012). In addition, during asymmetric stem cell divisions, spindle orientation plays a fundamental role in determining the size, the content, and ultimately the fate of the resulting daughter cells (Knoblich, 2010; Siller and Doe, 2009). An emerging concept in the stem cell field is that contacts to specialized microenvironments called niches are essential to maintain stemness (Fuchs and Chen, 2013). In this view, the partitioning of adhesion molecules resulting form a given orientation impacts on the fate choice of sibling cells. Studies conducted in several systems including *C.elegans* zygotes, *Drosophila* neuroblasts (NBs) and more recently vertebrate epithelia led to the

identification of a number of proteins involved in spindle positioning, however the molecular mechanisms governing this process still remain incompletely understood (Bergstralh et al., 2013a; Lu and Johnston, 2013).

1.2.1 Spindle orientation machinery

Studies in *C. elegans*, *Drosophila* and mammalian cells revealed that the core constituents of the spindle orientation machinery are complexes formed by NuMA, the Leu-Gly-Asn repeat-enriched protein LGN and the Gαi subunit of the heterotrimeric G-proteins (Bergstralh et al., 2013a) (Table 1 and Figure 4). They assemble in a conserved trimeric NuMA:LGN:Gαi complex that contributes to orientation by recruiting Dynein to the cell cortex via interaction with NuMA (Figure 4) (Kotak et al., 2012).

Vertebrate	*Drosophila*	*C.elegans*
NuMA	Mud	LIN-5
LGN	Pins	GPR-1/2
Gαi	Gαi/Gαo	GOA-1/GPA-16
mInsc	Insc	-
Par3	Bazooka (Baz)	PAR-3
Par6	DmPar6	PAR-6
aPKC	D-aPKC	PKC-3
Lgl1 / Lgl2	D-Lgl	LGL-1
hDlg	Dlg	DLG-1
Afadin/AF-6	Canoe	AFD-1

Table 1 – Spindle orientation proteins in the different model systems considered in this thesis. Orthologues of proteins involved in spindle orientation and in polarity in vertebrates, *Drosophila* and in *C.elegans*.

Interestingly, only the GDP-loaded form of Gαi is able to interact with LGN, implying that a non-canonical GTP-cycle governs the timely assembly of active NuMA:LGN:Gαi complexes at the membrane. Heterotrimeric G-protein complexes are composed by α, β and γ subunits binding to the plasma membrane through lipid modifications on Gα (myristoylation) and Gγ (prenylation) (Manahan et al., 2000). Canonical receptor-dependent heterotrimeric G-protein signalling pathways are activated by ligand-binding to

G-protein coupled receptors, which promotes the release of Gα-GTP from Gβ-Gγ to activate signal transduction (Neer, 1995). In contrast, the receptor–independent G-protein cycle implicated in spindle positioning relies on the GEF Ric-8A (Resistance to inhibitors of cholinesterase 8A) to generate a pool of Gαi-GDP molecules targeting LGN at the cortex (Figure 4). Gαi-GDP binds the four GoLoco motifs present at the C-terminus of LGN targeting LGN and NuMA at the membrane (Bellaiche and Gotta, 2005) (Figure 4). Studies on HeLa and MDCK cells revealed that inhibition or ablation of Ric-8A, as well as depletion of Gαi or disruption of the Gαi:LGN interaction, reduce cortical enrichment of LGN, NuMA and Dynein/Dynactin, and cause spindle randomization. These data provided an experimental prove of the importance of the Gαi GTP-cycle in spindle alignment processes (Peyre et al., 2011; Woodard et al., 2011; Zheng et al., 2010). Since Gαi-GDP distributes uniformly at the cortex, what restrict the localization of the NuMA:LGN above the spindle poles is still unclear (Du and Macara, 2004; Kiyomitsu and Cheeseman, 2013; Peyre et al., 2011).

LGN acts as a molecular scaffold, which can simultaneously interact with Gαi-GDP and NuMA. Its N-terminal domain consists of eight tetratrico-peptide repeats (TPRs), which bind to NuMA, while its C-terminal domain containing four GoLoco motifs interacting with Gαi-GDP. In the absence of binding partners, the TPR domain and the GoLoco motifs interact intramolecularly to hold the protein in an inactive conformation (Du and Macara, 2004; Pan et al., 2013) (Figure 4). This *closed* conformation is released upon binding of LGN to Gαi-GDP at the membrane, which makes the TPR domain available to interact with NuMA (Du and Macara, 2004; Du et al., 2001; Du et al., 2002; Pan et al., 2013). Cortical NuMA mediates the interaction with Dynein/Dynactin. The minus-end directed movement of Dynein anchored at the membrane with NuMA:LGN:Gαi results in traction forces pulling on astral MTs toward the poles (Kotak et al., 2012) (Figure 4).

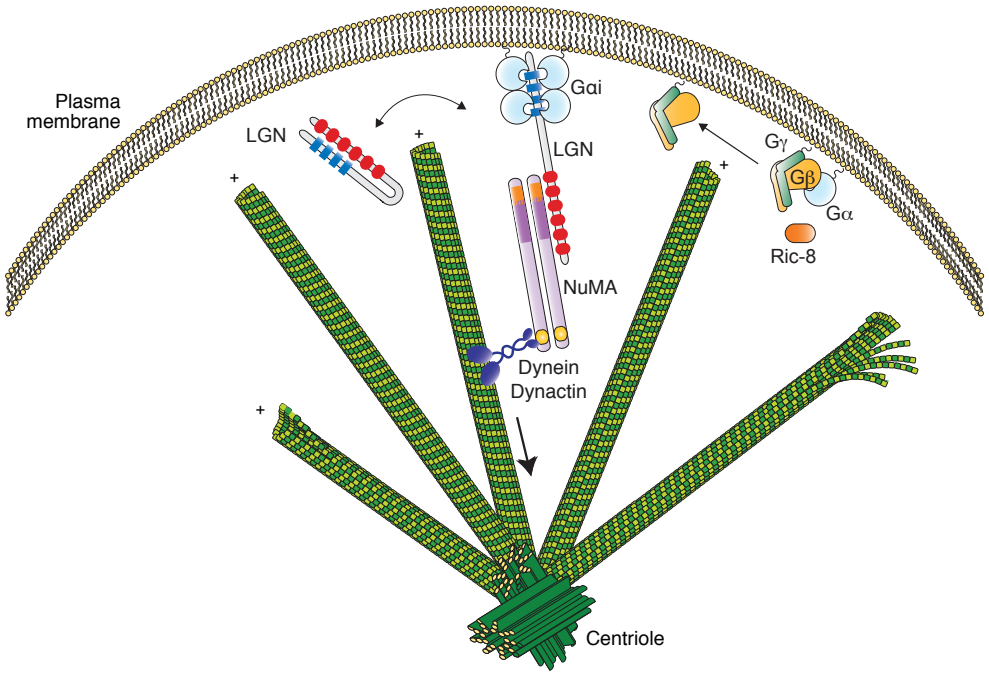

Figure 4 - The evolutionary conserved spindle orientation machinery. Cortical trimeric NuMA:LGN:Gαi complexes are required to orient the spindle by anchoring astral MTs to the cell cortex. The N-terminal domain of NuMA interacts with the minus-end motor proteins Dynein/Dynactin that pull on astral MTs. The scaffolding protein LGN interacts with NuMA through the N-terminal TPR domain (red), and with the C-terminal GoLoco motifs (blue) it binds the Gαi-GDP subunits anchored at the plasma membrane via myristoyl groups (light blue). LGN acts as a conformational switch: in the closed state the N-terminal part of LGN interacts with its own C-terminal domain, but when Gαi-GDP and NuMA bind to LGN, it opens up and localizes at the cell cortex. The Ric-8A GEF-activity is necessary to produce Gαi-GDP, which recruits Dynein/Dynactin:NuMA:LGN at the cortex.

1.2.2 Mitotic spindle centering

Spindle positioning is achieved through the activity of cortical Dynein/Dynactin, which links the cell cortex to the astral MTs, and exerts pulling forces to center or displace the spindle (Kiyomitsu, 2015).

Recently, intrinsic signals derived from chromosomes and spindle poles have been demonstrated to regulate Dynein-dependent pulling forces in unpolarised cells in culture (Kiyomitsu and Cheeseman, 2012). In mitotic HeLa cells, LGN localizes in crescents above the spindle poles. In metaphase, oscillatory movements back and forth along the pole-to-pole axis center the mitotic spindle. Imaging studies revealed that when the spindle

pole approaches the cell cortex, the cortical Dynein/Dynactin crescent disappears and a new crescent appears on the opposite side. This mechanism is regulated by Plk1, which localizes at the spindle poles and whose activity causes the dissociation of Dynein/Dynactin from the NuMA:LGN:Gαi complex (Kiyomitsu and Cheeseman, 2012) (Figure 5A). The Plk1-centering pathway seems to function cooperatively with a chromosome–derived Ran-GTP gradient. In fact NuMA is a Ran-importin-β regulated factor. Near to the chromosomes, NuMA is released from importin-β and this assists spindle assembly ((Nachury et al., 2001) and see **paragraph 1.1.2**). Recently, studies in HeLa cells showed that Ran-GTP prevents cortical enrichment of LGN and NuMA above the metaphase plate, confining their localization to polar regions of the cortex above the spindle poles (Kiyomitsu and Cheeseman, 2012) (Figure 5A). The molecular bases for this phenotype are to date unclear. The position of the spindle set in metaphase is maintained during the elongation occurring in anaphase thanks to the expansion and remodelling of the plasma membrane close to the spindle pole. A possible cause of this mechanism could be the reduction of Anillin, a protein involved in cytoskeletal dynamics, from cortical areas in proximity of the chromosomes by the Ran-GTP gradient (Kiyomitsu and Cheeseman, 2013) (Figure 5B).

In unequal-sized cell divisions, such as in *C.elegans* zygotes and *Drosophila* NBs, the mitotic spindle is not central but it is displaced toward one side of the cell. In *C.elegans*, displacement toward the posterior cell cortex is achieved by asymmetric cortical distribution of force generators assembled on LIN-5:GPR1/2:GOA-1/GPA-16 (the counterpart of NuMA:LGN:Gαi in nematodes; Table 1)(Nguyen-Ngoc et al., 2007). In fly NBs, the spindle is assembled asymmetrically so that the distance between the apical pole and the metaphase plate is longer than the corresponding distance between the basal pole and the metaphase plate (Cai et al., 2003). This configuration determines the difference in

size between the larger apical cell that will remain a NB and the smaller basal cell that will commit to become a ganglion mother cell (Siller and Doe, 2009).

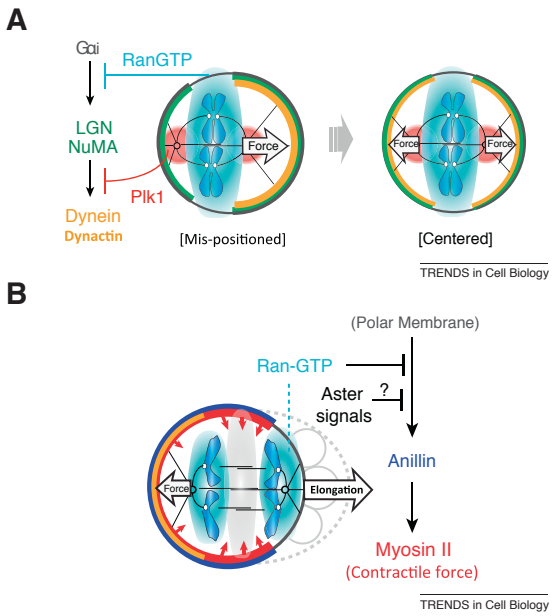

Adapted from Kiyomitsu, T., Trends in cell biology, 2015.

Figure 5 - Spindle-centering mechanisms in metaphase and in anaphase. (**A**) Schematic representation of the Ran-GTP gradient and Plk1 kinase activity required to center the spindle in metaphase supported by studies of the Cheeseman laboratory. The chromosome-derived Ran-GTP gradient (blue) excludes NuMA:LGN complexes from the cell cortex near to the DNA. On the other hand, Plk1 activity localized at the spindle poles (red) impairs the interaction between NuMA:LGN complexes and the motor-proteins Dynein/Dynactin. (**B**) Schematic illustration of asymmetrical plasma membrane-elongation during anaphase. In this context, the Ran-GTP gradient promotes a cortical reduction of Anillin and Myosin in the cell cortex near to the chromosomes, promoting membrane elongation (Kiyomitsu, 2015).

1.3 Functional role of the mitotic spindle

The mitotic spindle is the main actor coordinating cell division with fate choice and positioning. The position of the spindle, and hence the division plane, is particularly relevant in the so called *oriented divisions*, including epithelial symmetric divisions and asymmetric stem cell divisions (Morin and Bellaiche, 2011).

1.3.1 Spindle orientation in Symmetric Cell Division

Epithelial sheets enlarge by symmetric divisions generating two identical daughters. In these systems, the spindle is oriented parallel to the epithelial plane, giving rise to two daughter cells that lie within the epithelial layer, this way maintaining the integrity of the epithelium (Ragkousi and Gibson, 2014). Symmetric polarized cell divisions have been studied in systems, such as epithelial tissues and three-dimensional cultures of MDCK and Caco-2 cells, which provided a simple model of monolayered epithelia. 3D cysts grow by oriented divisions in which the spindle aligns perpendicularly to the apico-basal polarity axis (Hao et al., 2010; Jaffe et al., 2008; Wei et al., 2012; Zheng et al., 2010). Spindle positioning pathways have also be analysed in non-polarized cells in culture, such as HeLa cells, which undergo symmetrical divisions with the spindle axis aligned to the cell-substrate adhesion plane in a β1-integrin-dependent manner (Toyoshima and Nishida, 2007). In all these systems, prominent roles of LGN and NuMA in maintaining the correct orientation have been described.

Silencing of Gαi or LGN in HeLa cells demonstrated that in metaphase LGN is required for cortical targeting of NuMA and Dynein/Dynactin motors (Kotak et al., 2012; Woodard et al., 2011). Reduction of NuMA levels in turn prevents cortical enrichment of Dynein/Dynactin, and randomizes the spindle. Interestingly, overexpression of LGN or Gαi causes excessive spindle movements and results in misoriented divisions, indicating that appropriate levels of the NuMA:LGN:Gαi complex are crucial for proper spindle positioning (Du and Macara, 2004; Kotak et al., 2012). In MDCK cysts, LGN becomes

enriched at the lateral cortex of mitotic cells similarly to what observed in chick neuroepithelial cells. In both systems, a lateral cortical belt of LGN is required to capture astral MTs and to keep the spindle within the epithelial plane (Peyre et al., 2011; Zheng et al., 2010). In MDCK cells, spindle misorientation induced by LGN ablation causes defective cystogenesis, leading to multiple-lumen cysts rather than single-lumen monolayered cellular spheres (Zheng et al., 2010). Notably, aberrant cystogenesis is not only a read-out for orientation errors but can also be ascribed to apico-basal polarity defects (Yamanaka et al., 2006). What recruits and maintains the lateral belt of LGN in growing polarized epithelia is not completely clear. Seminal studies from the Macara's lab revealed that phosphorylation of LGN on the linker region between the TPR domain and the GoLoco motifs excludes LGN from the apical site of MDCK cysts by preventing association with Gαi (Hao et al., 2010). The association of LGN with the baso-lateral protein Dlg1 (disc large 1) has also been implicated in cortical localization of LGN in several systems (Bergstralh et al., 2013b; Saadaoui et al., 2014), as will be further discussed later. Whether these are the unique cortical cues targeting LGN laterally during planar cell divisions is an interesting open issue.

1.3.2 Spindle orientation in Asymmetric Cell Division

Asymmetric cell divisions (ACDs), or self-renewing stem cell divisions, generate daughter cells endowed with distinct fate. During asymmetric divisions cellular components generally referred to as *fate determinants* are unequally partitioned between the resulting cells. In addition, sibling cells are positioned differentially within the tissue, and only one of them retains contact to the "niche", this way maintaining stem cell identity (Fuchs and Chen, 2013). Historically, ACDs has been described to require different steps: 1) the establishment of a cellular polarity axis; 2) the asymmetric localization of fate determinants, and 3) the alignment mitotic spindle along the polarity axis (Figure 6)

(Morin and Bellaiche, 2011). In this configuration, fate determinants and polarity proteins are inherited only by one of the daughter cells.

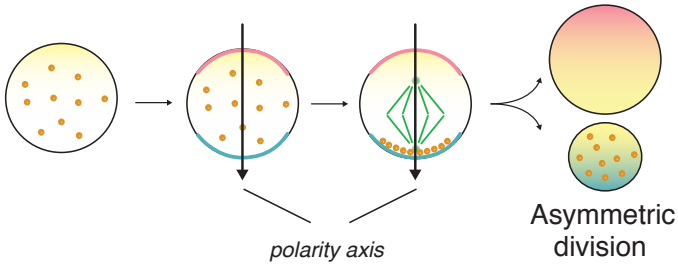

Figure 6 - Model of asymmetric cell division. Schematic representation of the steps required for the asymmetric cell division and of the relationship between the orientation of the mitotic spindle and the asymmetric outcome of a cell division. The orange dots are the *fate determinates* and the pink and blue lines represent proteins, which define the apico-basal polarity.

Most of our knowledge of the molecular events underlying ACDs comes from studies in model systems such as *C.elegans* zygotes, and *Drosophila* NBs (the stem cell of the *Drosophila* central nervous system), later paralleled in vertebrate neuroepithelial cells and basal progenitors of the developing skin (Betschinger and Knoblich, 2004; Gonczy and Rose, 2005; Kulukian and Fuchs, 2013; Peyre and Morin, 2012; Siller and Doe, 2009) (BOX 1 and Figure 7). Collectively, these analyses showed that conserved functions of the polarity proteins Par3:Par6:aPKC coordinate the cellular polarity axis with the spindle axis by asymmetrical recruitment at the cortex of force generators assembled on NuMA:LGN:Gαi complexes (Figure 7). Loss of polarity proteins or force generators' components compromises spindle positioning and the asymmetric outcome of the cell division. More specifically, in *Drosophila mud* mutants, NBs fail to orient the metaphase spindle with the cortical polarity axis (Bowman et al., 2006; Izumi et al., 2006; Siller et al., 2006), and overproliferate aberrantly by symmetric cell divisions (Cabernard and Doe, 2009), indicating that proper spindle orientation is a prerequisite for correct fate specification of NBs. Silencing of GPR-1/2 and LIN-5 in *C. elegans* zygotes impairs spindle placement (**see paragraph 1.2.2**), and generates daughter cells equal in size (Gotta et al., 2003; Park and Rose, 2008; Srinivasan et al., 2003).

Seminal studies from the Fuchs's laboratory revealed that during embryonic development, murine basal skin progenitors divide asymmetrically with the spindle perpendicular to the basement membrane to develop a functional stratified epidermis (Lechler and Fuchs, 2005). These oriented perpendicular divisions generate a basal progenitor and a suprabasal cells that differentiate in a Notch-dependent manner (BOX 1 and Figure 7C)(Williams et al., 2011). Inactivation by *in utero* electroporation of LGN or NuMA in asymmetrically dividing progenitors at day E9.5 disrupts both perpendicular divisions and skin stratification indicating a prominent role of oriented ACDs in skin morphogenesis (Williams et al., 2011). The function of oriented divisions in the development of the brain is less clear, likely due to the complexity of the tissue architecture and morphogenesis. Depletion of LGN in dividing progenitors of the chick and mouse neuroepithelium randomizes the spindle. Notably, this does not seem to affect the fate of the progeny, as both daughters retain the molecular signature of apical progenitors although they loose the attachment to the ventricular surface (Konno et al., 2008; Morin et al., 2007). Together, evidence collected in very diverse systems demonstrates the functional importance of asymmetric oriented divisions in generating daughter cells unequal in fate, in spatial position or in size, and in sustaining correct morphogenetic programs.

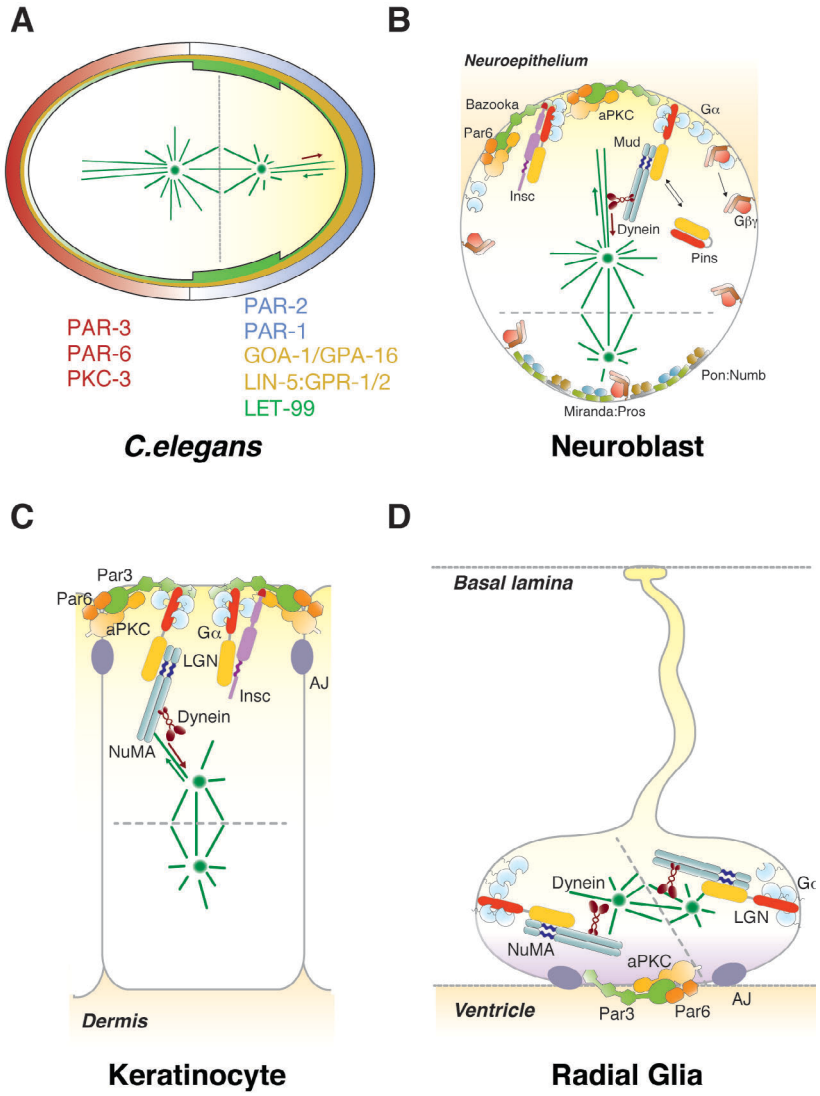

Adapted from Culurgioni S. and·Mapelli M., Cellular and Molecular Life Sciences, 2013.

Figure 7 - Spindle positioning in model systems of asymmetric cell division. Schematic representation of cortical polarity and mitotic spindle orientation in (**A**) *C.elegans* zygots, (**B**) *Drosophila* NBs, (**C**) murine skin basal progenitors and (**D**) vertebrate neuroepithelial cells. For detailed description see BOX 1.

BOX 1

In ***C.elegans* zygote**, the first cell division gives rise to two daughter cells different in size and in fate. Before division, zygotes polarize along an anterior-posterior axis through the segregation of PAR-3:PAR-6:PKC-3 at the anterior cortex and PAR-1 and PAR-2 at the posterior cortex (Grill et al., 2001). Spindle orientation is coupled at anterior-posterior polarity by the cortical localization of LIN-5:GPR-1/2:GOA-1/GPA-16. LIN-5:GPR-1/2:GOA-1/GPA-16 are enriched at the posterior cortex determining an asymmetric cortical pulling force (Couwenbergs et al., 2007; Nguyen-Ngoc et al., 2007; Park and Rose, 2008) (Figure 7A).

After delamination from the neuroepithelium, ***Drosophila* NB** divides asymmetrically generating one self-renewing NB and one ganglion mother cell, which in turn produces two neurons or glial cells. Pins is recruited at the apical surface by interaction with the adaptor protein Inscutable (Insc) that localizes at the apical side with Bazooka (Schober et al., 1999; Wodarz et al., 1999). Bazooka together with Par6 and aPKC marks the apical cortical domain (Petronczki and Knoblich, 2001; Wodarz et al., 2000). Apical Pins interacts with Gαi-GDP and Mud to orient the spindle (Bowman et al., 2006; Izumi et al., 2006; Siller et al., 2006). The binding of Pins with Insc and Mud is mutually exclusive, indicating that the two apical Pins complexes work synergistically to promote asymmetric divisions (Culurgioni et al., 2011; Zhu et al., 2011b). At the basal site of the neuroblast cortex, the adaptor proteins: Miranda and Pon promote the basal localization of the fate determinants Pros and Numb, respectively (Knoblich et al., 1995) (Figure 7B).

In asymmetrically dividing murine **skin basal progenitors**, the mitotic spindle is aligned perpendicular to the basement membrane, leading to differentiation and stratification of the epidermis. Molecularly, the bridging protein mInsc is required to recruit apically NuMA:LGN:Gαi complexes together with the Par proteins. The ternary NuMA:LGN:Gαi complex in turn recruits Dynein/Dynactin at the cortex to orient the spindle parallel to the apico-basal polarity axis (Lechler and Fuchs, 2005; Williams et al., 2011) (Figure 7C).

In **vertebrate neural progenitors**, NuMA:LGN:Gαi complexes enrich to a lateral belt to direct planar division, maintaining the spindle axis parallel to the ventricular surface (Mora-Bermudez et al., 2014; Peyre et al., 2011). In this system, a minimal tilt in the spindle axis results in asymmetric divisions generating daughter cells with unequal partitioning of the apical end-foot and Par proteins. This division gives rise to two daughter cells with different fates and attachment to the ventricular zone (Peyre and Morin, 2012) (Figure 7D).

1.4 NuMA

The Nuclear Mitotic Apparatus protein NuMA is a 238 kDa protein, whose nuclear functions are still largely unclear. During mitosis NuMA localizes at the spindle poles and at the polar regions of the cortex above the spindle poles to organize and position the mitotic spindle (Du and Macara, 2004; Du et al., 2001; Fant et al., 2004).

1.4.1 Essential function of NuMA in mitosis

NuMA is a master regulator of spindle functions, implicated not only in spindle placement but also in spindle organization and maintenance. At mitotic entry, it assists MT focussing toward the spindle poles and physically tethers centrosomes to spindle MTs (Khodjakov et al., 2003; Merdes et al., 1996; Silk et al., 2009). For all mitotic activities NuMA works in association with Dynein/Dynactin, whose motor functions are required to transport NuMA along MTs to the spindle poles (Merdes et al., 2000). The NuMA:Dynein complex provides a tethered matrix by crosslinking parallel MTs, which resists at the opposite tension of the K-fibers (Merdes et al., 2000; Silk et al., 2009). Studies in Xenopus mitotic extracts and in HeLa cells revealed that the activities of NuMA at the spindle poles are centrosome-independent. Depletion of NuMA resulted in pole fragmentation, dissociation of the centrosome from the spindle, and defects in chromosome alignment (Haren et al., 2009; Heald et al., 1996; Merdes et al., 2000; Merdes et al., 1996). Interestingly, recent studies in mouse embryo fibroblasts (MEFs) demonstrated that the pole-organizing functions of NuMA are redundant with centrosomes in the early phases of spindle assembly, but they become essential for spindle maintenance after the establishment of tension on K-fibers. In mouse MEFs removal of exon-22 from the NuMA locus generates a NuMA protein lacking residues 1926-1985 that is unable to focus the spindle poles and to maintain centrosomes attached to K-fibers (Silk et al., 2009). Consistently, work by the Dumont lab revealed that NuMA and Dynein contribute to repair the spindle architecture upon K-fiber laser-ablation by pulling the free minus-end of severed MTs back to into

spindle poles (Elting et al., 2014).

Although in mitosis the bulk of NuMA works at the spindle poles, a portion of NuMA molecules is recruited at the cortex in crescents above the spindle poles by direct interaction with LGN (Du and Macara, 2004; Du et al., 2001). This pool of cortical NuMA is responsible for cortical recruitment of Dynein and for spindle orientation (Kotak et al., 2012). In asymmetric metaphases characterized so far, including *Drosophila* NBs and murine keratinocytes, NuMA localizes only above the apical pole together with the Par proteins and LGN (Izumi et al., 2006; Lechler and Fuchs, 2005; Seldin et al., 2013). This distribution is required to align the mitotic spindle along the apico-basal polarity axis. In symmetrically dividing cells of polarized epithelia, NuMA is found with LGN in two crescents above both the spindle poles, and promotes planar spindle orientation (Peyre et al., 2011; Zheng et al., 2010). A similar distribution is observed in HeLa cells in culture (Kotak et al., 2013; Machicoane et al., 2014; Woodard et al., 2011).

In metaphase, LGN is the major cortical receptor for NuMA (Du and Macara, 2004; Kotak et al., 2012; Seldin et al., 2013). However other factors control its cortical distribution. In HeLa cells and mouse epidermis, Abl1 phosphorylation on Tyr-1774 of NuMA is required to maintain the cortical localization of NuMA in metaphase (Matsumura et al., 2011). In the same system, removal of poly-ubiquitin chains from Dishevelled-3 by the deubiquitinase activity of CYLD has been shown to enhance the interaction between NuMA and Dishevelled, which is required to promote spindle alignment (Yang et al., 2014). These results are consistent with previous findings implicating Wnt-signalling in oriented cell divisions of *Drosophila* sensory organ precursor (SOP) cells through direct interaction between Mud and Dishevelled (Segalen et al., 2010). Collectively, these discoveries seem to suggest that in metaphase NuMA and Dynein are targeted to the membrane not only by LGN but also by Wnt-dependent mechanisms.

During symmetric and asymmetric anaphases, NuMA accumulates at two cortical crescents above the spindle poles (Kiyomitsu and Cheeseman, 2013; Kotak et al., 2013;

Seldin et al., 2013; Zheng et al., 2014). Increased levels of cortical NuMA result in the enrichment of Dynein/Dynactin at the opposite sites of the cortex, which generate robust pulling forces in opposite directions to elongate the spindle and separate sister chromatids. Studies in HeLa and in Cos-7 cells have revealed that in anaphase NuMA is targeted to the cortex by direct association with the lipid bilayer, which is precluded in metaphase by phosphorylation of Thr-2055 by CDK1 (Kotak et al., 2013; Zheng et al., 2014) (Figure 8). Inactivation of CDK1 at anaphase onset allows LGN-independent binding of NuMA to the polar region of the membrane above spindle poles (Kotak et al., 2013; Zheng et al., 2014) (Figure 8). In this way, spindle positioning is coordinated with cell cycle progression.

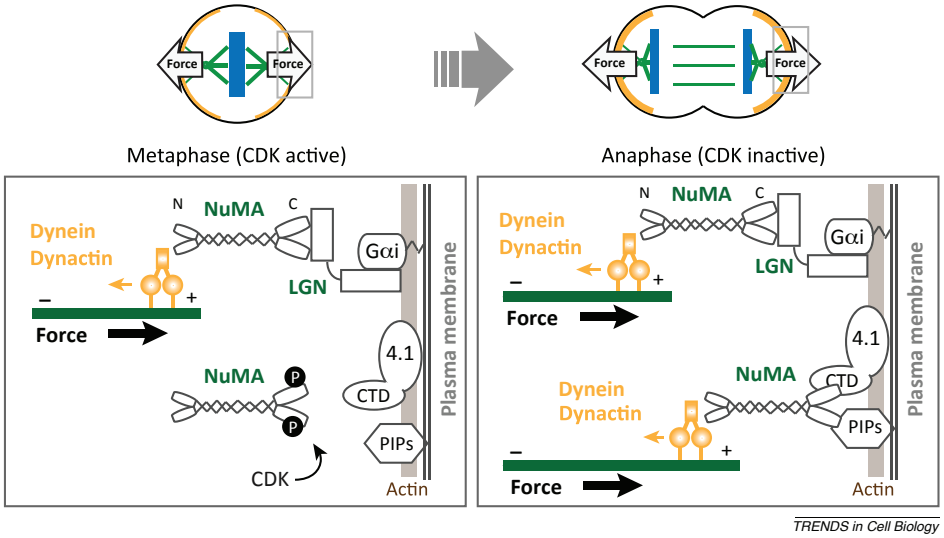

Adapted from Kiyomitsu, T., Trends in cell biology, 2015

Figure 8 - Cortical NuMA is regulates by CDK1 activity. The cortical recruitment of NuMA is finely tuned during mitosis. In metaphase, NuMA cortical localization is dependent on Gαi:LGN complexes and it is inhibited by the CDK1 phosphorylation on Thr-2055 (on the left). In anaphase, the dephosphorylation of Thr-2055 NuMA via PPP2CA and the inactivation of CDK1 increase the cortical recruitment of NuMA at the cortex. Two different interaction surfaces of NuMA target dephosphoryted NuMA at the cortex in anaphase: the membrane-associated proteins 4.1R/G and the direct phospholipid-binding domains of NuMA (Kiyomitsu, 2015).

Interestingly, direct interaction between residues 1788-1810 of NuMA and the cortical associated protein 4.1R/G had also been implicated in the cortical enrichment of NuMA observed in anaphase (Figures 8 and 9). More specifically, Kiyomitsu and co-workers

showed that ablation of 4.1R/G in HeLa cells reduces cortical recruitment of NuMA in anaphase (Kiyomitsu and Cheeseman, 2013). However, later studies by the Gonczy lab revealed that 4.1R/G is in fact required for cortical integrity, implying that the impairment of NuMA localization observed upon 4.1R/G knock-down is likely due to indirect effects of cortical disruption (Kotak et al., 2013). Insights into the function of the interaction between NuMA and 4.1R/G came from studies in murine keratinocytes conducted in the Lechler's group, which used Fluorescence-Recovery-After-Photobleaching (FRAP) experiments to demonstrate that binding of NuMA to 4.1R/G is required to stabilize NuMA at the cortex in metaphase (Seldin et al., 2013).

Collectively, these pieces of evidence demonstrate that the cortical localization of NuMA is finely regulated throughout mitosis by post-translational events, which sustain correct spindle positioning in metaphase, and proper elongation in anaphase.

1.4.2 The domain structure of NuMA

NuMA is a 2115–residue protein, whose domain structure consists of a poorly characterized N-terminal globular domain followed by an extended coiled-coil, and a C-terminal unstructured tail region (Figure 9).

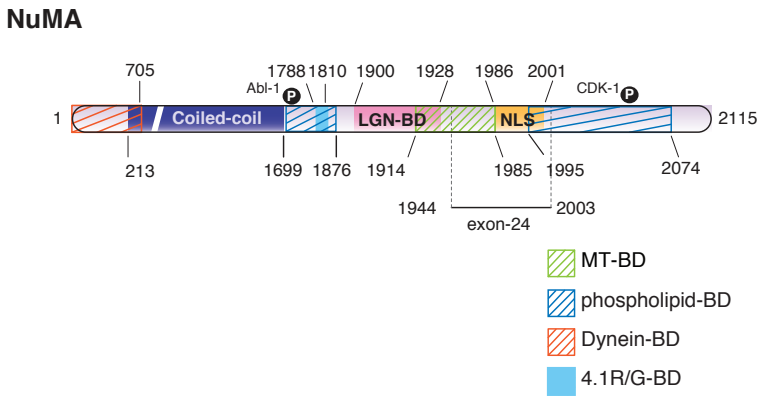

Figure 9 - Domain structure of human NuMA. Schematic representation of NuMA, with a central coiled-coil domain in blue, enlarged on the C-terminal region. The regions of interaction with Dynein, LGN, MTs, phospholipids and 4.1R/G; the nuclear localization signal (NLS) and the phosphorylation sites of CDK1 (Thr-2055) and Abl-1 (Tyr-1774) are also illustrated (for references see the main text).

For all mitotic activities, NuMA works in association with Dynein/Dynactin. Co-immunoprecipitation experiments in mitotic HeLa extracts revealed that the N-terminal portion of NuMA encompassing residues 1–705 interacts with Dynein (Kotak et al., 2012) (Figure 9). Consistently, over-expression or cortical targeting of this domain in HeLa cells impaired the localization of Dynein in a dominat-negative fashion (Kotak et al., 2012). The central parallel coiled-coil region of NuMA (213-1699) mediates homodimerization, while the C-terminus contains the interaction domains with LGN, phospholipids and MTs, as well as a nuclear localization signal (NLS) required for nuclear targeting of the protein during interphase (Gueth-Hallonet et al., 1996) (Figure 9).

Pull-down assays with a series of truncation mutants have shown that the region of NuMA required for the interaction with the N-terminal TPR domain of LGN encompasses residues 1892-1924 (numbering here and in the following refers to the long isoform of human NuMA, 2115 residue long)(Du et al., 2002). More recently the crystallographic

structure of the NuMA:LGN complex revealed that the 27-residue fragment of NuMA spanning residues 1900-1928 is sufficient to bind the inner surface of TPR1-7 of LGN in an extended conformation, and defined precisely the molecular determinant of the interaction surface (Zhu et al., 2011b) (Figure 9).

Several lines of evidence showed that the C-terminal portion of NuMA associates directly with MTs. In Xenopus extracts the C-terminus of NuMA induces the formation of MT-bundles (Merdes et al., 1996). Cosedimentation experiments with purified NuMA C-terminus and taxol-stabilized MTs, and the observation that overexpression of GFP-NuMA C-terminus in HeLa cells induces MT bundles revealed that NuMA binds directly MTs. In particular these experiments defined the fragment of NuMA encompassing residues 1914-1985 as the minimal domain necessary for MT binding and bundling (Du et al., 2002; Haren and Merdes, 2002) (Figure 9). The evidence that the MT-association domain of NuMA overlaps with the LGN-binding domain suggested that LGN and MTs are competitive ligands of NuMA, and implied that LGN could inhibit the interaction of NuMA with MTs. Indeed, in co-sedimentation experiments performed with *in vitro* translated NuMA-1580-2115 and MTs, the TPR domain of LGN (which binds to NuMA) seems to inhibit the sedimentation of NuMA with MTs (Du et al., 2002). In the same study, the ability of GST-NuMA-1914-1985 to induce MT polymerization was prevented by LGN-TPR, supporting the idea of the mutually exclusive binding of NuMA to LGN and MTs (Du et al., 2002).

The functional role of the NuMA region harbouring the MT-binding domain was examined in mitotic cells derived from mice carrying an heterozygous conditional mutation in the NuMA gene which results in exon-22 deletion (generating a NuMA protein lacking the residues corresponding to the region 1944-2003 of human NuMA) (Figure 9). Murine NuMA-Δexon22 is unable to localize at the spindle poles, and to maintain attachment of K-fibers to centrosomes, with subsequent defocusing of MTs (Silk et al., 2009). These results seemed to indicate that the MT-binding activity of NuMA is important to tether

MTs to the spindle poles.

Recent studies revealed that the C-terminal region of NuMA contains also phospholipid-binding domains necessary for the direct targeting of the protein at the cortex during anaphase (Kotak et al., 2013; Zheng et al., 2014). Initial localization experiments in Cos7 and HeLa cells mapped the phospholipid binding domain of NuMA in the fragment spanning residues 1995-2074, which contains the CDK1-phosphoryled site Thr-2055 (Zheng et al., 2014) (Figure 9). Until metaphase phosphorylation of Thr-2055 by active CDK1 would prevent direct binding of NuMA to the plasma membrane by charge repulsion, and allow its cortical enrichment only in anaphase when CDK1 is inactivated by cyclin-B degradation (Figure 8). Intriguingly, later studies by Kotak and colleagues revealed that also the region comprising residues 1699-1876 can target NuMA at the cortex, and is able to bind phospholipids *in vitro* (Kotak et al., 2013) (Figure 9), implying that several domains of NuMA contribute to its membrane localization during anaphase.

All these data showed that the C-terminal portion of NuMA constitutes a key element mediating different interactions important for mitotic activities of the protein.

1.4.3 NuMA in interphase

NuMA contains a nuclear localization signal (NLS) at residues 1988-2005, which it is recognized by importin-β to mediate import into the nucleus (Gueth-Hallonet et al., 1996) (Figure 9). During mitosis, dissociation of the interaction between NuMA and importin-β allows spindle assembly ((Nachury et al., 2001); **see also paragraph 1.1.2**). Electron microscopy studies suggest that in interphase NuMA could play a structural role the nucleus by forming multi-arm oligomers (Harborth et al., 1999). Moreover, NuMA has been involved in maintaining genome organization by binding DNA. Indeed, NuMA contains S/TPXX motifs in the end domain, which have been shown to bind specific DNA domains called MARs (matrix attachment regions) (Luderus et al., 1994). Recently, it has been proposed that nuclear NuMA works in DNA damage response by repairing double

strand breaks in conjunction with the SWI/SNF chromatin remodelling complex (Vidi et al., 2012; Vidi et al., 2014). Although very interesting, these studies are still rather preliminary, and we can say that the molecular function of NuMA in the nucleus is still under debate.

1.5 Aurora-A

Aurora-A is a Ser/Thr kinase involved in different mitotic processes including centrosome maturation and separation, assembly of a bipolar spindle, alignment of chromosomes, and cytokinesis (Nikonova et al., 2013) (Figure 10). Aurora-A is regulated during the cell cycle, and its activity is confined in mitosis, when its functions are strictly correlated with its localization. From prometaphase to metaphase, Aurora-A accumulates at the centrosomes and along the spindle MTs, while in anaphase it is found at the central spindle (Nikonova et al., 2013)(Figure 10). The kinase catalytic activity is activated by several cofactors including TPX2, which is liberated from importin-β near the centrosome by the Ran-GTP gradient ((Gruss and Vernos, 2004) and **see paragraph 1.1.2**). Binding of TPX2 to Aurora-A promotes a conformational change allowing the auto-phospholylation of Aurora-A on Thr-288 in the activation loop (Zorba et al., 2014). Auto-phosphorylation displaces the activation loop from the ATP-binding pocket providing access to Aurora-A substrates (Littlepage et al., 2002; Walter et al., 2000). The TPX2 interaction is also required to target Aurora-A at the centrosomes (Kufer et al., 2002). At the end of mitosis, Aurora-A is ubiquitinated by the APC complex and degraded by the proteasome (Littlepage and Ruderman, 2002).

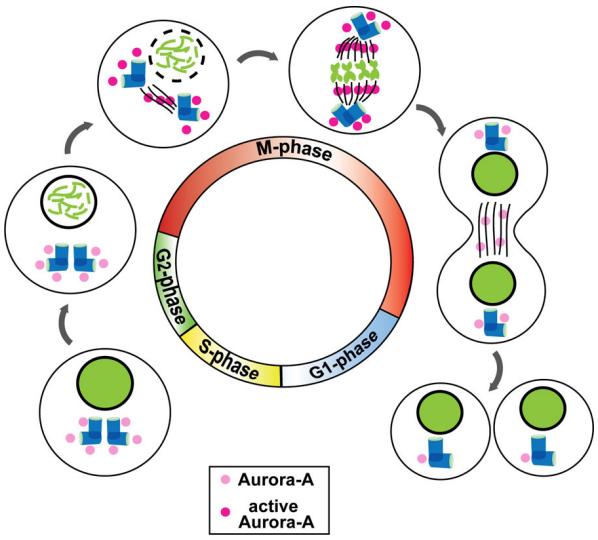

Figure 10 - Aurora-A orchestrates mitotic progression. Aurora-A accumulates at the centrosome in S-phase and it is activated in the transition between G2/M. From anaphase to telophase Aurora-A localizes also along the spindle MTs and at the midzone. At the end of the mitosis, Aurora-A is ubiquitinated and degraded (Nikonova et al., 2013).

Adapted from Nikonova, A. S. et al.., Cellular and molecular life sciences, 2013

1.5.1 The role of Aurora-A in spindle assembly

Aurora-A is recruited to the centrosomes right after their duplication in S phase, and it is activated at the G2/M transition. In mitosis Aurora-A promotes centrosome maturation by favouring the expansion of the PCM and MT-nucleation. Moreover, it is involved in centrosome separation and in bipolar spindle formation by phosphorylating Eg5 (Giet et al., 1999; Sardon et al., 2008). Consistent with its fundamental roles, Aurora-A depletion causes the formation of abnormal poles, monopolar spindles and short and sparse MTs (Giet et al., 2002).

The major Aurora-A activity is the assembly and the stabilization of the metaphase spindle by phosphorylation of MT-related proteins such as NEDD1, TACC3 and chTOG (De Luca et al., 2008; Peset et al., 2005; Peset and Vernos, 2008; Pinyol et al., 2013). However, recent studies showed that inhibition of Aurora-A in anaphase impairs the formation of a functional central spindle (Lioutas and Vernos, 2013). Molecularly, Aurora-A sustains central spindle assembly by phosphorylating TACC3 and the Dynactin subunit $p150^{Glued}$ on Ser-19, within the MT-binding domain (Lioutas and Vernos, 2013; Reboutier et al., 2013; Rome et al., 2010). Aurora-A inhibition or the expression of a non-phosphorylatable form of $p150^{Glued}$ (Ser-19-Ala) leads to Dynactin accumulation at the spindle poles and central spindle defects, which are rescued by the expression of the phosphomimic mutant

p150^{Glued} -Ser-19-Glu (Reboutier et al., 2013). Based on these findings, we can conclude that Aurora-A plays pivotal roles in mitosis by controlling the activity of multiple MT-associated proteins.

Recently, phosphoproteomic studies in HeLa cells showed that also NuMA is a substrate of Aurora-A (Kettenbach et al., 2011; Sardon et al., 2010; Toughiri et al., 2012). More specifically, Kettenbach and colleagues identified several phosphosites on the C-terminal portion of the protein, and investigated the function of phospho-Ser-1969 by localization experiments in mitotic HeLa cells transfected with GFP-NuMA-Ser-1969-Ala/Glu mutants. These experiments showed that Ser-1969-Ala mutant localize poorly at the spindle poles, while the Ser-1969-Glu mutant is recruited at the poles as the wild-type protein (Kettenbach et al., 2011). Altogether, these results demonstrate the NuMA is a substrate of Aurora-A, and that the Aurora-A kinase activity affects the localization of NuMA at the spindle poles.

1.5.2 Aurora-A in spindle orientation

In *Drosophila* NBs, Aurora-A has been implicated in regulating stem cell self-renewal by controlling the orientation of the mitotic spindle. More specifically in NBs, Aurora-A contributes to place the mitotic spindle parallel to the apico-basal polarity axis, this way determining the specific segregation of Numb in the basal ganglion mother cells (Lee et al., 2006a). A parallel study showed that symmetric misoriented NB divisions caused by Aurora-A inhibition compromise neuronal differentiation and result in uncontrolled NB expansion (Wang et al., 2006). Thus, in this system, Aurora-A acts as a tumour suppressor whose loss causes a tumour-like phenotype. The role of Aurora-A in orienting asymmetric divisions in vertebrate is less characterized. Aurora-A overexpression has been suggested to regulate cells fate and spindle orientation in human mammary gland (Regan et al., 2013). Interestingly, chemical inhibition of Aurora-A by MLN8237 (Alisertib) in U2OS cells in culture has also been shown to induce orientation defects (Asteriti et al., 2014).

Thus, this evidence indicates that Aurora-A works in spindle orientation, and that this function is conserved from invertebrate to mammals.

Studies in *Drosophila* S2 cell doublets, a so-called "induced polarization system", have suggested a possible molecular mechanism by which Aurora-A influences mitotic spindle orientation (Johnston et al., 2009). This mechanism relies on the phosphorylation of Pins on Ser-436 by Aurora-A, which allows binding of Pins to cortical Dlg. In the same study, Dlg was also shown to interact with the kinesin Khc-73, which would capture the plus-end of astral MTs in a Pins-independent manner. To confirm the role of Aurora-A/Pins^{LINKER} pathway for proper spindle alignment, Johnston and colleagues showed that the expression of a Pins phosphomimetic mutant rescues spindle misorientation in Aurora-A depleted NBs (Johnston et al., 2009). Studies in vertebrates revealed that the phosphorylation of LGN on the Ser-401, corresponding to Ser-436 of Pins, is important for orientation (Hao et al., 2010; Saadaoui et al., 2014). However, in MDCK cysts, the phosphorylation of Ser-401^{LGN} by apical aPKC has been proposed to prevent association of LGN to Gαi at the apical site, this way confining LGN at the lateral cortex (Hao et al., 2010).

1.6 Cortical cues to instructing spindle orientation

In 1884, Hertwig discovered that sea urchin embryos orient the mitotic spindle along their long axis (the "Hertwig rule") (Hertwig et al., 1884). These observations suggested that cells can sense shape changes in response to external forces, and coordinate the spindle orientation accordingly. In the last decade, this scenario has become much more complicated. Several cell-specific extrinsic and intrinsic molecular signals that provide molecular links between the cell cortex and the astral MTs have emerged (Figure 11). In asymmetric cell division, a polarity axis is created by the segregation of polarity proteins or fate determinates at opposite side of cortex. Localization of NuMA:LGN:Gαi at the apical site aligns the spindle parallel to the polarity axis allowing the unequal segregation of the fate determinates (Betschinger and Knoblich, 2004). In addition to intrinsic cortical

polarity cues, extrinsic cortical signals such as cell-to-cell and cell-to-extracellular matrix (ECM) interactions have been shown to play a role in orientation. In polarized epithelia, adhesion molecules are required to orient the spindle planar to the epithelial layer (Figure 11). In MDCK monolayer, cadherin knockdown causes spindle misorientation perturbing the cortical localization of the MT-binding protein APC (den Elzen et al., 2009; Nakajima et al., 2013). In mouse epithelial skin, loss of the junctional component α-catenin or β1-intergin causes spindle randomization (Lechler and Fuchs, 2005). Cell-adhesion to ECM determines spindle orientation also in non-polarized system. In HeLa cells grown on fibronectin-coated slides, the spindle aligns parallel to the substratum in a β1-integrin manner (Toyoshima and Nishida 2007 and Thery et al. 2005). Recent studies have also suggested that the actomyosin cortex is involved in spindle positioning, with mechanisms that are not fully clear (Fink et al., 2011; Kunda and Baum, 2009; Thery et al., 2005; Toyoshima and Nishida, 2007; Zheng et al., 2013).

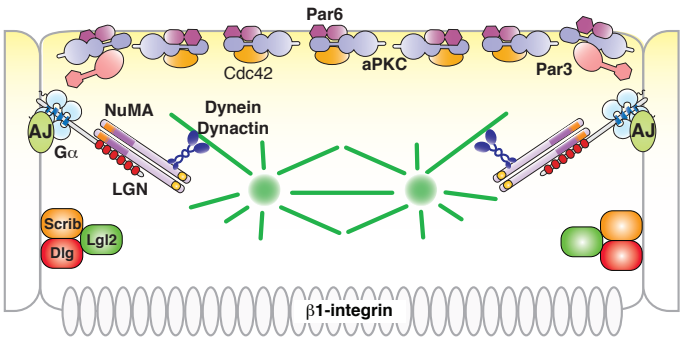

Figure 11 - Coupling of spindle orientation and cellular polarity in epithelia. In epithelial cells cortical polarization is established by apical distribution of the evolutionary conserved Par3:Par6:aPKC complex, which in turn defines the baso-lateral localization of the Scribble complex (Scribble (Scrib), Disc large (Dlg) and Lethal giant larvae (Lgl2)) by mutual antagonism between Lgl2 and aPKC (Bergstralh et al., 2013a). Polarity proteins are required for the proper localization of NuMA:LGN:Gαi complexes at the lateral cell cortex. Recently, extrinsic cortical signals such as junctional proteins and cell-to-extracellular matrix (ECM) interactions (β1-integrin) have been shown to play a role in orientation (Toyoshima and Nishida, 2007). However how intrinsic and extrinsic cortical cues are coupled to spindle orientation is still under debate.

1.6.1 Polarity proteins

As already mentioned, several polarity proteins play a role in spindle orientation including the tumour suppressors Dlg (discs large) and Lgl (lethal giant larvae), which in polarized epithelia localize baso-laterally. In the following paragraph, I will review what it is known on the molecular contribution of these two proteins to orientation mechanisms.

1.6.1.1 Dlg

Drosophila SOP cells form a monolayered polarized epithelium. In this system, Dlg acts as a scaffold molecule maintaining Pins at the anterior cortex asymmetrically (Bellaiche et al., 2001). Also in the *Drosophila* follicular epithelium, Dlg recruits Pins laterally to ensure planar cell divisions. Interestingly, ablation of Dlg in this system misorients the spindle and causes cell delamination, which is corrected right after cytokinesis by reintegration of the misplaced post-mitotic cell into the monolayer (Bergstralh et al., 2013b). As mentioned **in paragraph 1.5.2**, molecularly Dlg recognises the phosphorylated form of Pins, and kinesin Khc73. The LGN:Dlg:Khc-73 interactions, and their role in orientation, are conserved in vertebrate epithelia (Sans et al., 2005; Zhu et al., 2011a). Saadaoui and colleagues showed that depletion of Dlg1 in chick neuroepithelium and HeLa cells causes spindle misorientation, and reduction of LGN cortical levels (Saadaoui et al., 2014). This phenotype depends on the phosphorylation of Ser-401^{LGN}, although it is not clear in this system, which is the kinase responsible for LGN phosphorylation. Therefore, Dlg provides a conserved mechanism that couples spindle orientation with polarity by recruiting LGN at the cortex in metaphase.

1.6.1.2 Lgl2

Lgl was originally identified as a tumour suppressor protein in *Drosophila* NBs and epithelia (Bilder et al., 2000; Mechler et al., 1985; Ohshiro et al., 2000). *Drosophila* Lgl (D-Lgl) has two mammalian homologs with highly conserved functions, Lgl1 and Lgl2, which differ for a few residues at the C-terminal region (Cao et al., 2015). Studies in flies and mammals demonstrated that D-Lgl and Lgl2 are essential for establishment and

maintenance of apical-basal epithelial cell polarity (Cao et al., 2015; Humbert et al., 2008). In polarized epithelia, D-Lgl co-localize with the Par6:aPKC complex at the cell-to-cell contact regions. Upon cellular contact-induced polarization D-Lgl is phosphorylated by aPKC, and dissociates from the Par6:aPKC complex to localize at the basolateral membrane (Bilder et al., 2000; Hutterer et al., 2004; Tanentzapf and Tepass, 2003). A similar mechanism underlies polarization in vertebrate epithelia (Chalmers et al., 2005; Musch et al., 2002; Plant et al., 2003; Yamanaka et al., 2003). In *Drosophila* NBs, D-Lgl is essential for asymmetric localization at the basal site of the fate determinants Numb, Prospero, Brat, and of their adaptor proteins Pon and Miranda (Betschinger et al., 2003; Lee et al., 2006b; Ohshiro et al., 2000; Peng et al., 2000). Molecularly, at the beginning of mitosis, Aurora-A phosphorylates Par6, which in turn activates aPKC. aPKC then phosphorylates D-Lgl which is released form cortical Par6:aPKC:D-Lgl complexes. Subsequently, Bazooka enters the Par6:aPKC complexes thus allowing the phosphorylation of Numb, which is liberated form the cell cortex and confined in a cortical crescent on the opposite side respect to the Par complex (Wirtz-Peitz et al., 2008). Recent studies have also identified a role of Aurora-A phosphorylation in controlling the relocalization of D-Lgl from the cortex to the cytoplasm during mitosis in *Drosophila* imaginal disc and in follicular epithelia (Bell et al., 2014; Carvalho et al., 2014). Based on these studies, Aurora-A phosphorylation of D-Lgl is necessary for spindle orientation because D-Lgl cortical release allows the interaction of Dlg with Pins at the lateral cortex (see also **paragraph 1.6.1.1**), this way synchronising spindle orientation with cell cycle progression (Zhu et al., 2014). Intriguingly, biochemical evidence has suggested that in vertebrate cells Lgl2 could favour orientation by direct interaction with LGN^{TPR} (Yasumi et al., 2005). In summary, D-Lgl and its orthologue Lgl2 provide a conserved mechanism for establishment and maintenance of epithelia cell polarity, and participate to spindle orientation with a molecular mechanism that is still not fully clear.

1.7 Afadin and spindle orientation

Actin-associated proteins organising the mitotic cortex have been recently shown to be involved in spindle positioning. More specifically, in fly NBs the actin-binding protein Canoe has been shown to direct spindle orientation by binding to Pins (Carmena et al., 2011; Speicher et al., 2008; Wee et al., 2011). Whether its human counterpart Afadin is endowed with similar properties is an interesting open question.

1.7.1 Canoe

Drosophila Canoe is an actin-binding protein involved in cytoskeletal organization and adhesion. In *Drosophila* embryonic epithelia, it localizes at adherens junctions (AJs) through its PDZ domain, where it regulates cell-to-cell adhesion (Sawyer et al., 2011; Sawyer et al., 2009). In NBs, Canoe is involved in asymmetric cells division. In this system, it colocalizes apically with Baz:Par6:aPKC, and contributes to the alignment of the spindle along the apico-basal polarity axis and to the distribution of fate determinants such as Numb (Speicher et al., 2008). Genetic studies revealed that Canoe forms a complex with Pins by direct interaction of its C-terminus with Pins-TPR, and is required for apical recruitment of Mud (Carmena et al., 2011; Speicher et al., 2008; Wee et al., 2011). In flies the function of Canoe in asymmetric cells division is conserved in muscle and heart progenitors (Speicher et al., 2008). Interestingly, Wee and colleagues showed that in the S2 induced-polarization model system, the two Ras-association domains of Canoe interact directly with Ran-GTP, and this interaction is essential for recruitment of Mud to cortical Pins and for spindle orientation, for unclear molecular reasons (Wee et al., 2011). A further mechanisms impinging on the spindle orientation functions of Canoe has recently been reported in *Drosophila* S2 cells, in which the very C-terminus of Dishevelled has been shown to interact with the PDZ domain of Canoe (Johnston et al., 2013) suggesting that Canoe could act in the accessory pathway Fz:Dsh:Mud to orient the spindle (see also (Segalen et al., 2010); **and paragraph 1.4.1**).

1.7.2 Afadin

The vertebrate ortholog of Canoe is Afadin (or AF-6), which has 6 differently spliced isoforms (Lorger and Moelling, 2006; Saito et al., 1998). The longest splicing variants differ from the shortest for the presence of an additional C-terminal domain (Figure 35B), and are expressed ubiquitously (Mandai et al., 1997). In epithelia, Afadin localizes at AJs where it plays a prominent role in the organization of the apical junctional complex together with a plethora of junctional constituents including nectins, α-catenin, p120, LMO7, occludin and claudin (Niessen and Gottardi, 2008; Ooshio et al., 2007). Consistent with its functions in adhesion and in epithelia integrity, the Afadin knock-out is embryonically lethal in mice (Zhadanov et al., 1999), whereas tissue specific ablation of the gene have been reported to cause severe morphogenetic defects in the brain (Yamamoto et al., 2013), nephrons (Yang et al., 2013), and lymphatic system (Tawa et al., 2010). Studies in mouse small intestine have shown that Afadin is required to restrict Paneth cells (the niche of intestinal stem cells) at the base of the crypt by a cell adhesion-dependent mechanism. In Afadin-depleted small intestine, the length of the crypt-villus axis and the proliferation rate of the crypt basal columnar cells increase, suggesting a possible role of Afadin in regulating the stem cell fate (Tanaka-Okamoto et al., 2014). Recently, Afadin-loss has been reported in severe pancreatic cancers, where it correlates with bad prognosis. Molecularly, loss of AF-6 permits the interaction between Dishevelled 2 (Dvl2) and the transcription factor FOXE1 into the nucleus, increasing *Snail* expression. High levels of *Snail* transcription promote proliferation and metastasis in pancreatic cancer (Xu et al., 2015). Intriguingly, aberrant expression of the AF-6 gene has also been found in multiple cancer types (Letessier et al., 2007; Sun et al., 2013).

The domain structure of Afadin suggests a scaffolding role due to its binding domains for cytoskeletal components and cell adhesion molecules. Afadin contains a couple of Ras-association domains, followed by a Fork-Head (FHA) domain, a dilute domain (DIL), and a PDZ domain responsible for the interaction with nectins (Kobayashi et al., 2014) (Figure

35A). The C-terminal region present only in the long isoforms of Afadin binds to F-actin. Thus, long isoforms of Afadin may provide a link between nectin-based AJs and actin (Mandai et al., 1997; Sawyer et al., 2009). The localization of Afadin at AJs, its actin-binding properties, and the fact that the fly orthologue Canoe has been involved in spindle orientation, raise the question as to whether Afadin can be the molecular connection between lateral junctions and spindle motors in polarized vertebrate epithelia.

1.8 Aim of the project

Great progresses have been made over the past years in revealing conserved pathways underlying spindle positioning, and in identifying proteins involved in the process. In this context, my PhD project aimed at providing a better understanding of the molecular events underlying spindle orientation. In order to do so, I focused on some factors (Afadin and Lgl2) and activities (Aurora-A), which have been related to orientation but whose molecular function was still poorly understood.

Increasing evidence points at a key role of mitotic kinases including Plk1 and CDK1 in synchronizing spindle alignment with mitotic progression. Accordingly, it has recently been shown that inhibition of Aurora-A causes spindle misorientation (Asteriti et al., 2014). Given that NuMA is a substrate of Aurora-A (Kettenbach et al., 2011; Sardon et al., 2010; Toughiri et al., 2012), and the two proteins colocalize at the spindle poles, it is possible that the kinase activity of Aurora-A controls the mitotic functions of NuMA. Thus, the first aim of my PhD project was to investigate the effects of Aurora-A on spindle orientation, and to understand the molecular mechanism by which its activity maintains the correct functions of spindle motors.

Polarity proteins and actin-associated proteins have been implicated in spindle alignment. In this context, the second aim of my project was to understand if the actin-binding protein Afadin and the polarity protein Lgl2 have a role in spindle orientation, and to determine how they affect the localization and the activity of Gαi:LGN:NuMA:Dynein complexes.

2. MATERIALS AND METHODS

2.1 Cell cultures

2.1.1 HeLa, hTERT-RPE-1 and HEK293t cell lines

HeLa, HEK293t and hTERT-RPE1 cells were grown at 37°C in a 5% CO_2 atmosphere, in Dulbecco's Modified Eagle's Medium (DMEM) or MEM with Earle's Salts/Ham's F12 (1:1) respectively, complemented with 10% of fetal bovine serum, 2 mM L-glutamine, 50 μg/ml penicillin/streptomycin. For all experiments with HeLa and hTERT-RPE cells in culture, cells were plated on fibronectin-coated coverslip (5 μg/ml, Roche).

2.1.2 Caco-2 cysts

Caco-2 cells were cultured in DMEM medium supplemented with 20% fetal bovine serum, 2 mM L-glutamine, 0.1% $NaHCO_3$, and 0.1% non-essential amino acids. To produce cysts, 8-well chamber slides (ibidi) were coated with 10 mg/ml native Matrigel (BD) and solidified for 30 minutes at 37°C. Then, Caco-2 cells were diluted in complete medium supplemented with 2.5% Matrigel, and 400 μl of the suspension were plated in each well on solidified Matrigel at a dilution of 6000 cells/well. To allow the swelling of the central lumen, after 5 days 0.1 μg/ml of cholera toxin were added at each well, as reported by Jaffe (Jaffe et al., 2008). Cholera toxin-mediated activation of cAMP signaling favors lumen formation. After 6 days, cysts were fixed and immunostained.

2.2 Plasmids and RNAi

2.2.1 Aurora-A and NuMA project

For FRAP analysis and rescue experiments, a synthetic gene encoding full-length human NuMA (NCBI Reference Sequence: NM_006185) was subcloned into a pCDH lentiviral vector with an N-terminal GFP-tag (System Biosciences). I decided to express NuMA proteins under the control of a weak Ubc promoter in order to avoid misorientation effects caused by exceedingly high levels of NuMA overexpression. For the construction of

pCDH-GFP-NuMA-GoLoco, the GoLoco domain of human LGN encompassing residues 359-677 was first amplified by PCR, and then subcloned into the pCDH-GFP-NuMA vector at the C-terminus of NuMA. For cell biology studies, NuMA C-terminal fragments encompassing residues 1821-2115 (referred to as $NuMA^{Cter}$ in the text), residues 1821-2002, and the $NuMA^{Cter}$-Δ1944-2003 ($NuMA^{Cter}$-Δexon24 in the text) were inserted into the pCDH lentiviral vector in frame with a mCherry-tag. All point mutations of $NuMA^{Cter}$ were generated with the QuikChange mutagenesis kit (Stratagene) according to the manufacture guidelines. Prior to use, all constructs were sequence verified. The pEGFP-C1 vector (Clontech) containing GFP-Aurora-A-Asp274Ala (kinase dead, KD) was a generous gift from Prof. Erich Nigg. GFP-H2B was expressed from a pCDNA3 vector (Invitrogen).

For interfering Aurora-A and luciferase (GL2), small-interfering RNA oligos (siRNAs) with the following sense sequences 5'AUGCCCUGUCUUACUGUCAdTdT3' and 5'CGUACGCGGAAUACUUCGAdTdT3' were used (Applied Biosystems/Ambion).

2.2.2 Lgl2 project

For Lgl2 ablation, an On-target plus Human LLGL2 siRNA – SMART Pool (Thermo Scientific Dharmacon) was employed. For interfering LGN, I used siRNA with the following sense sequence: 5'CCAUGGAUGUAGUGGGAAAUU3' (Thermo Scientific - Dharmacon). As a control, I used a scrambled siRNA with the following sequence: 5'AGACGAACAAGUCACCGACUU3'. To monitor cellular localizations and for immunoprecipitation experiments, HA-tagged and GFP-tagged Lgl2 (NCBI Reference Sequence: NM_001031803) were cloned into a modified version of pCDNA5 vector (Invitrogen).

2.2.3 Afadin project

For knocking down human Afadin, four unique 29-mer short-hairpin RNAs (shRNAs) constructs cloned in lentiviral vectors carrying a GFP reporter and puromycin selection

(catalogue number TL311457; OriGene Technologies) were tested in HeLa cells. The two most effective hairpins (referred to as Afadin shRNA-1: GCAGUCGUCAACAAGAUGGUGAGCAUGAU, and Afadin shRNA-2: CUCUGUGGUGACACUGGAAGUAGCAAAGC in the text) were further used to generate cell lines stably interfered to study the effect of Afadin ablation in mitotic HeLa cells. To the same end, Caco-2 cells were infected with the Afadin shRNA-2 expressing lentivirus to generate a cell line stably lacking Afadin. To perform rescue experiments, the mCherry-tagged version of long rat Afadin (generous gift of Prof. Takai) was inserted into pCDH vector. To generate a sh-RNA-2 Afadin resistant gene, four silent base substitutions were introduced into the region of the cDNA of rat Afadin targeted by the shRNA-2 hairpin by QuikChange mutagenesis. To obtain the Afadin-ΔLGN variant unable to interact with LGN, the construct was further engineered by deletion of residues 1714-1751 of rat long Afadin, corresponding to the LGN-binding stretch encoded by residues 1709-1747 of human Afadin isoform-4. Both mCherry-Afadin-wild-type and mCherry-Afadin-ΔLGN were subcloned into pCDH vector.

2.3 Cell treatments and Transfections

2.3.1 Aurora-A and NuMA project

Aurora-A and CDK1 kinases inhibition were performed in mitotic cells with 20-50-100 nM MLN8237 (Selleck Chemicals) for 4 hours, and RO3306 (Calbiochem) at 9 μM for 10 minutes, respectively. The proteasome inhibitor MG132 (Cayman chemical company) was used at 25 μM for 30 minutes after nocodazole wash-out (more details are reported in the synchronization protocols of **paragraph 2.4**).

Transfections were conducted following the manufacture's instruction using Lipofectamine for plasmids or Oligofectamine and RNAiMAX (Invitrogen) for siRNA. More specifically, transfections were carried out using a Lipofectamine:DNA ratio of 1:1 with 1 μg of DNA per each well of a 12-well plate, or 2 μg of DNA per well of a 6-well

plate. siRNAs were used at 80 nM with 1.5 µl Oligofectamine for GL2 and Aurora-A interference per each well of a 12-well plate.

The mCherry-NuMA^{Cter} containing pCDH vectors were either used to generate stable cell lines by infection or transiently transfected (see **paragraphs 3.1.4.2-4** for the description of specific experiments).

For the viral production, HEK293t cell lines were transiently transfected with the vector of interest and the viral packaging system composed of three distinct vectors coding: Gag, Pol and Rev. After media change and 24 hours of incubation, the cell supernatant containing the virus was used to transduce the HeLa target cells.

Fluorescently-labeled NuMA proteins and constructs used in live cell imaging and for FRAP experiments (**paragraph 2.9**) were transiently transfected 48 hours before the experiments. For these experiments, I then selected the cells expressing exogenous proteins at lower levels to avoid the risk of observing unspecific mitotic defects caused by overexpression of spindle orientation genes (Kotak et al., 2012). More specifically, for the spindle orientation rescue experiments described in **paragraph 2.10**, I defined a total GFP fluorescence intensity threshold based on the GFP-NuMA signal tolerated by untreated HeLa cells and avoiding apoptosis or misalignment. I then filmed cells with GFP-fluorescent levels below that threshold to analyze the effect of MLN8237 treatment and ectopic targeting of the NuMA-GoLoco construct.

2.3.2 Lgl2 project

Transfections of GFP-Lgl2 were conducted following the manufacture's instruction using Lipofectamine (Invitrogen), with the same protocol detailed in **paragraph 2.3.1**. siRNAs were used at 50 nM with 5 µl RNAiMAX for Lgl2, scrambled and LGN interference per each well of a 12-well plate.

2.3.3 Afadin project

To assess the role of cortical filamentous actin (F-actin) in the localization of Afadin, LGN, and NuMA, mitotic HeLa cells synchronized by single thymidine block were treated with 1 μM of Latrunculin-A (Sigma, L5163) for 30 minutes (**paragraph 3.3.5.2**)

Transfections of mCherry-Afadin and mCherry-Afadin-ΔLGN for the rescue experiment of **paragraph 3.3.4** were conducted following the manufacture's instruction using Lipofectamine (Invitrogen) similarly to what outlined in **paragraph 2.3.1**. Short-hairpin based silencing of human Afadin is described in **paragraph 2.3.1**.

2.4 Synchronization protocols

2.4.1 Thymidine block

This synchronization protocol was applied in all the three projects to obtain a substantial pool of mitotic cells. HeLa cells were synchronized by single thymidine block using 2.5 mM of thymidine (Sigma, T1895) for 24 hours, and released from the G1/S arrest by washing away thymidine and adding fresh medium containing 30 μM deoxycytidine. MLN8237 (20-50 nM; Selleck Chemicals) was added to the medium 6 hours after release and cells were fixed after 9 hours from release (Figure 12A).

2.4.2 STLC and monastrol treatments

This synchronization procedure was adopted in the Aurora-A and NuMA project. Synchronization of HeLa cells in prometaphase was performed by adding 5 μM STLC (S-trityl-L-cysteine, Sigma) for 16 hours (Figure 27B). hTERT-RPE1 cells were synchronized in prometaphase by 5 μM STLC for 16 hours, with the addition of MLN8237 during the last 2 hours of treatment; then STLC was washed away and cells grown in complete medium plus MLN8237 were harvested after 2 hours (Figure 12B). For video-recording, hTERT-RPE1 cells were synchronized in prometaphase by monastrol (100 μM, Biomol International) for 16 hours, with the addition of MLN8237 during the last 2 hours of treatment; then monastrol was washed away and cells grown in complete medium plus

MLN8237. Control-treated cultures were incubated with dimethyl sulfoxide (DMSO).

2.4.3 Synchronization protocol to check mitotic phosphorylation by Phos-TAG SDS-PAGE

In Figures 23 A and B, HeLa cells were released from single thymidine block and treated with 3.3 μM nocodazole (Sigma) for 14 hours. The cells in prometaphase were harvested by shake-off and treated with 25 μM MG132 for 30 minutes. To inhibit CDK1 cells were incubated with 9 μM RO3306 together with MG132 for the last 10 minutes, and then harvested. To inhibit Aurora-A cells are treated with 50 nM MLN8237 starting from the last 3 hours and half of nocodazole incubation.

2.5 Immunofluorescence staining

2.5.1 HeLa and TERT-RPE-1 cell lines

Cells grown on coverslips were fixed as follow: **a**) −20 °C absolute methanol for 10 min to visualize NuMA, Afadin and $p150^{Glued}$ at the cortex; **b**) 4% paraformaldehyde (PFA) for 10 minutes at room temperature, followed by permeabilization with PBS 1X and 0.3% Triton X-100 for 5 minutes, to detect NuMA staining at poles, LGN and phospho-Thr288-Aurora-A; **c**) pre-extraction with PHEM buffer (60 mM Pipes pH 6.9; 25 mM Hepes pH 6.9; 5 mM EGTA and 2 mM $MgCl_2$) containing 0.1% Triton X-100 for 4 minutes, followed by 10 minutes in 4% PFA in PBS and 5 minutes in 0.3% Triton X-100 (all at room temperature) for NuMA staining in hTERT-RPE1 cells. Fixed cells were blocked with PBS containing 0.05% Tween 20 and 3% bovine serum albumin (BSA) for one hour, and incubated 2 hours with primary antibodies at room temperature. Secondary antibody incubation (donkey-anti-rabbit, and anti-mouse Alexafluor488 and Alexafluor647 (Life Technologies)) was carried out for 1 hour at room temperature.

Depending on the experiment, cells were stained with a monoclonal mouse antibody anti-LGN (Mapelli lab; 1:5), a monoclonal mouse antibody anti-NuMA (Mapelli lab; 1:3000), anti-$p150^{Glued}$ (BD, 610473, 1:1000), anti-phospho-Thr288-Aurora-A (Cell Signalling,

3079; 1:250), anti-α-tubulin (Abcam, ab4074; 1:50), a polyclonal rabbit anti-Afadin (polyclonal antibody, raised with fragment 1514-1824 of human Afadin isoform-4; working dilution 1:500, Mapelli lab) and TRITC-conjugated Phalloidin (diluted 1:10, Sigma).

2.5.2 Caco-2 cysts

After 6 days of culture, Caco-2 cysts were fixed for 30 min in 4% PFA, and permeabilized for 30 minutes with 0.5% Triton X-100. After two washes of 5 minutes with PBS 1X and Glycine 1%, and one wash of 5 minutes with IF buffer (PBS 1X, 0.2% Triton X-100, 0.01% BSA and 0.05% Tween 20), cysts were blocked with IF buffer containing 5% BSA for 90 minutes. F-actin was visualized with TRITC-conjugated Phalloidin (diluted 1:50, Sigma) incubated for 1 hour in IF buffer. DNA was stained with DAPI (0.1 mg/ml).

2.6 Microscopy on fixed samples

For Figure 13 wide-field microscopy was performed using a Nikon Eclipse 90i microscope equipped with an oil immersion Plan Fluor 100x objective (N.A. 1.3; Nikon) and a Qicam Fast 1394 CCD camera (QImaging). Image acquisition, deconvolution and Extended Depth of Focus on z-serial optical sections were performed using Nis-Elements AR 4.2 (Nikon). Images were further processed with Adobe Photoshop CS 8.0 and Adobe Illustrator.

Confocal microscopy was performed on a Leica TCS SP2 AOBS confocal microscope controlled by Leica Confocal Software. For all analysis, a 63x oil-immersion objective lens (HCX Plan-Apochromat 63× N.A. 1.4 Lbd Bl; Leica) was used. Image acquisition conditions were set to remove channel crosstalk, optimizing spectral detection bands, and scanning modalities. Images were processed with the Fiji software (Schindelin et al., 2012), Adobe Photoshop CS 8.0 and Adobe Illustrator.

2.7 Spindle orientation analysis

Spindle orientation was monitored using cells grown on fibronectin-coated coverslip, which under normal conditions divide with the spindle axis parallel to the substratum (Thery et al., 2005; Toyoshima and Nishida, 2007). To quantify the spindle tilt, metaphase cells were stained with anti-NuMA antibody and DAPI. Cells were imaged in x-z optical sections passing through the spindle poles. Spindle axis angles with respect to the substratum were measured with the angle tool of Fiji. Statistical analysis of spindle angle distributions were performed with Prism (GraphPad Software), and plotted in angular histograms using a custom-written macro for MatLab. Statistical analysis of the data was performed in Prism applying the Mann-Whitney test (Figures 16C and 34C) or Kruskal-Wallis test (Figure 36C), or a one-way ANOVA Tukey's test (Figure 43C) (see **paragraph 2.16** for statistical analysis).

2.8 Measurements of the fluorescence intensity at the spindle poles and at the cortex

2.8.1 Quantification of NuMA at the spindle poles

To evaluate the amounts of NuMA at the spindle poles, cells were fixed with 4% PFA to preserve the total level of the protein. To quantify the fluorescence intensity of endogenous NuMA at the spindle poles, the α-tubulin signal was used to draw a mask around the spindle-pole region using the Fiji software, and the fluorescence signal of NuMA inside the mask was integrated (Figure 18A-B-C).

To quantify endogenous NuMA at the spindle poles in cells transiently transfected with GFP-Aurora-A-Asp274Ala or GFP-H2B, a circular area around the spindle pole was draw with the Fiji software and the fluorescence signal of NuMA inside this area was integrated. The α-tubulin mask was not used because mCherry and GFP signals were already present in cells, and another fluorophore was not available (Figure 18D).

To quantify the levels of mCherry-NuMA^{Cter} at the spindle poles, the mCherry signals were integrated within an α-tubulin mask, while the amount of mCherry-NuMA^{Cter} in the cytosol was measured by integrating the mCherry signal of the same α-tubulin mask positioned in the cytoplasm area. To compare the spindle-pole accumulation of the diverse NuMA^{Cter} constructs among each other and upon MLN8237 treatment, the polar versus cytoplasmic ratio was computed. I decided to consider the pole-to-cytosol ratio to account for the variability in the expression levels of mCherry-NuMA^{Cter} constructs within the cell population (Figure 25B). Statistical evaluation of the quantified signals was conducted with the Mann-Whitney test as described in **paragraph 2.16**.

2.8.2 Quantification of NuMA, LGN and Dynactin at the cortex

For the assessment of NuMA, LGN and p150^{Glued} cortical levels, cells were fixed with absolute MetOH. Quantification of cortical signals were conducted on confocal sections of metaphase cells in Fiji with the following procedure. To obtain the intensity profile of the immunostained proteins, a 2.7 μm-wide line was manually drawn from the spindle pole to the nearest cellular cortex, perpendicularly to the metaphase plate. The amount of "protein at the cortex" was calculated by integrating the profile on a 1.35 μm-large area centered at the peak of the profile, whereas the level of 'protein in the cytosol' was quantified by integrating the same area 1.35 μm-away from the peak towards the DNA. Statistical analyses of the ratio between the signal at the cortex and the one in the cytosol were performed in Prism with the Mann-Whitney test (see **paragraph 2.16** for details).

2.9 FRAP analysis

HeLa cells were plated on 28 mm glasses coated with fibronectin. Cells were transfected with full length GFP-NuMA. After 24 hours, cells were synchronized with a single thymidine block and analysed 8 hours after the release. To evaluate the effect of Aurora-A inhibition, 50 nM MLN8237 were added 5 hours after thymidine release. FRAP was performed on an UltraVIEW-VoX spinning-disk confocal system (PerkinElmer) equipped

with an EclipseTi inverted microscope (Nikon) provided with a Nikon Perfect Focus System, an integrated FRAP PhotoKinesis unit (PerkinElmer), and a Hamamatsu CCD camera (C9100-50) and driven by Volocity software (Improvision; Perkin Elmer). All images were acquired through a 60x oil-immersion objective (Nikon Plan Apo VC, N.A. 1.4). GFP signal was excited with a 488 nm 50mW diode laser. Photobleaching was performed on a 5 μm diameter circular region around one of the spindle poles. After defining the region of interest, the laser was used at the maximum power for 30 bleaching cycles to bleach GFP signal. After bleaching, images were acquired every 2 seconds for 5 minutes for GFP-NuMA. The time of acquisition depends on the time required to reach the plateau of intensity after the bleaching. Analyses of the recovery curves were conducted using a custom macro in Fiji. Briefly, the mean intensity value in the bleached area was measured, corrected for the background and for the acquisition photobleaching, and the curves were then normalized to the prebleaching mean intensity values. Recovery rates were quantified by fitting normalized fluorescence intensities of bleached areas to a one-phase exponential association by a custom-software of MatLab (Figure 19A).

The fluorescence recovery of GFP-NuMA full length was fitted to a single exponential function: I(t)=A(1-exp(-b*t)) with a custom software of MatLab. The half-time of recovery ($t_{1/2}$) was calculated as follows $t_{1/2}$ = ln(0.5/-b), and the mobile fraction (Fm) as $Fm=(I\varepsilon-I_0)/(I_i-I_0)$ where Iε was the final intensity at the end of the experiment (plateau), I_0 was the intensity after bleaching and I_i was the initial intensity before bleaching (Figure 19B). Statistical analyses of the FRAP data were performed in Prism with the Student's *t*-test (see **paragraph 2.16** for statistical analysis).

2.10 Live cell imaging

To monitor misoriented cell divisions of HeLa and hTERT-RPE1 cells treated with MLN8237, cells were seeded in 4-well micro-slides (IbiTreat, cod.80426, Ibidi), and analysed in time-lapse experiments using an Eclipse Ti inverted microscope (Nikon) and a

40x (Plan Fluor, N.A. 0.60, DIC, Nikon) objective. For the entire observation period, cells were kept in a microscope stage incubator at 37°C and 5% CO_2. Differential interference contrast (DIC) frames were acquired every 7 minutes over 24/48 hours using a DS-Qi1Mc camera and the NIS-Elements AR 3.22 software (Nikon). HeLa cells were video-recorded from the moment of MLN8237 addition for 24 hours, while hTERT-RPE-1 cells were video-recorded for 24 hours from the time of monastrol wash-out (Figure 15).

For the misorientation rescue experiments of the **paragraph 3.1.6**, HeLa cells were plated on 28 mm glasses coated with fibronectin, and transfected with either GFP-NuMA or GFP-NuMA-GoLoco. After 24h, cells were thymidine-synchronized and treated with 50 nM MLN8237 as described above. Starting from MLN8237 addition, cells were filmed using a DeltaVision Elite imaging system (Applied Precision) driven by softWoRx software and equipped with a CoolSNAP HQ2 CCD camera (Photometrics), at the same environmental conditions described above. Images were acquired using an Olympus 60x/1.42 Plan Apo N oil immersion objective for 16 hours every 5 minutes as z-stacks. Nine optical section images were taken at 3 μm intervals. Then, the sections were processed by an iterative deconvolution method, and projected to single plane (Figure 32A).

2.11 Quantitative PCR analysis

To evaluate the Afadin-depletion, total RNA was isolated from HeLa and Caco-2 cells with the RNeasy kit method (QIAGEN). 1 μg of RNA was used for reverse transcription using ImProm-II™ Reverse Transcription System (Promega, Cat. n° A3800) according to manufacturer's instructions. Transcript depletion was checked by quantitative PCR (qPCR) using TaqMan assays (Life Technologies, catalogue number Hs00984486_m1 for human Afadin). Samples were amplified with primers and probes for human Afadin, and GAPDH as a housekeeping gene. The Ct values were normalized to the GAPDH curve. The relative changes in Afadin expression were quantified using the $2^{-\Delta\Delta Ct}$ method (Livak and Schmittgen, 2001)(Figures 37B and 38B).

2.12 Immunoblotting

For quantification of active Aurora-A (Figure 14), mitotic HeLa cells collected by shake-off were lysed in RIPA buffer (50 nM Tris-HCl pH 8.0, 150 nM NaCl, 1% NP40, 1 mM EGTA, 0.25% sodium deoxycholate), with the addition of protease and phosphatase inhibitors. The extracts were resolved by SDS-PAGE and transferred on a nitrocellulose membrane. 50 μg of extracts per lane were loaded. Blocking and antibody incubations were performed at room temperature in TBS containing 0.1% Tween 20 and 1% low-fat milk, or in TBS containing 0.1% Tween 20 and 5% BSA for anti-phospho-Aurora-A hybridization. The antibodies used were: mouse anti-Aurora-A (BD Transduction Laboratories; 1:250), rabbit anti-phospho-Thr288-Aurora-A (C39D8; Cell Signaling Technology; 1:500), goat anti-actin (I-19; SantaCruz Biotechnology; 0.4 mg/ml).

To check expression levels of mCherry-NuMA^{Cter} constructs, and for cosedimentation assays (Figures 24 and 27B), mitotic HeLa cells stably expressing FLAG-mCherry-NuMA^{Cter} were lysed in JS buffer (75 mM Hepes pH 7.5, 1.5 mM EGTA, 1.5 mM MgCl2, 0.15 M KCl, 0.1% NP40; glycerol 15%) supplemented with protease and phosphatase inhibitors. Cleared lysates were separated by SDS-PAGE, transferred onto nitrocellulose membrane, and analysed by immunoblotting using mouse monoclonal anti-NuMA antibody (Mapelli's lab, at 1:200 dilution) and anti-α-tubulin antibody (Abcam ab4074; 1:1500). Blocking and antibody incubation were performed at room temperature in TBS containing 0.1% Tween 20 and 5% low fat milk. The same procedure was used to check the level of Afadin, LGN and Lgl2 in Figures 33D, 37A, 38A and 42 by using rabbit polyclonal anti-Afadin antibody (Mapelli's lab, at 1:500 dilution), mouse monoclonal anti-LGN antibody (Mapelli's lab, at 1:500 dilution), anti-LLGL2 antibody (Abnova, at 1:500 dilution), mouse monoclonal antibody anti-actin (clone AC-40, Sigma; at 1:1000 dilution) and mouse monoclonal anti-vinculin (clone hVIN-1, Sigma; at 1:8000 dilution).

2.13 Phos-TAG SDS-PAGE

The Phos-TAG SDS-PAGE is a phosphate-affinity gel electrophoresis technique developed to detect different phosphorylation states of proteins by using a separating gel containing Phos-tag acrylamide (Wako Pure Chemical Industries Ltd.)(see **paragraph 3.1.4.1**). To analyse mitotic $NuMA^{Cter}$ phosphorylations, 50 μg of HeLa cellular lysate were separate with a 8% Phos-TAG acrylamide SDS-PAGE, transferred onto nitrocellulose membrane, and then analysed by immunoblotting with rabbit anti-FLAG antibody (SIGMA, F7425; 1:2000) (Figure 23B). To prevent excessive heating of the gel, Phos-TAG SDS-PAGEs were run at 80 volt for 5 hours. The same method was used to detect individual phosphorylations of purified mCherry-$NuMA^{Cter}$, as detailed below (Figure 24).

2.14 Immunoprecipitation

To test the interaction between Lgl2 and LGN, *human* Lgl2 (residues 1-1020) was cloned into a modified version of pCDNA5 with a N-terminal GFP-tag. Empty pEGFP-N1 (Clontech) was used as a specificity control. HeLa cells were transfected with the two vectors, and after 24 hours from transfection cells were synchronized with a single thymidine block. Cell lysates prepared in lysis buffer (75 mM HEPES pH 7.5, 150 mM KCl, 15% glycerol, 0.1% NP40, 1.5 mM $MgCl_2$, 1.5 mM EGTA and protease/phosphatase inhibitor cocktail) were incubated with 10 mg/ml of anti-GFP antibody (Mapelli's lab) overnight at 4 °C, and later with Protein-A for 2 hours. The incubation cycles were repeated twice. Proteins immunopreciptated on beads were then washed three times in 1 ml of lysis buffer, and analysed by SDS-PAGE and immunoblotting by using anti-GFP antibody (Mapelli's lab, at 1:2000 dilution), mouse monoclonal anti-LGN antibody (Mapelli's lab, at 1:500 dilution) and mouse monoclonal anti-NuMA antibody (Mapelli's lab, at 1:200 dilution)(Figure 33C).

2.15 Protocols for *in vitro* assays with purified proteins

Most of the *in vitro* assays conducted with purified proteins were performed collaboratively by Manuel Carminati, one of our group's members. Thus, they will be summarized briefly in the following paragraphs.

2.15.1 Protein expression and purification

Fragments of human NuMA spanning residues 1821-2115, 1821-2001 and 2002-2115 were cloned into a pETM14 vector (Novagen) in frame with a hexa-histidine tag, and expressed in BL21 Rosetta E. *coli* cells. The overexpressed proteins were purified by Nickel-affinity and cation-exchange chromatography. For MT forming assays of **paragraph 3.1.5.2**, the same NuMA fragments were cloned into a pGEX-6PI vector (GE Healthcare), and expressed as above. GST fusion proteins were purified by affinity on gluthatione beads, and eluted with 10 mM glutathione. The TPR domain of human LGN encompassing residues 1-409 (LGN^{TPR} in the text) and GST-$NuMA^{1861-1928}$ were cloned in pGEX-6P1. They were purified on glutathione sepharose (GSH) beads, followed by ion-exchange chromatography performed after proteolytic GST-tag removal.

2.15.2 *In vitro* kinase assays

Kinase assays were carried out using 1 ng of the purified kinase domain of Aurora-A (generous gift of Prof. Richard Bayliss) incubated with 2 μM of the $NuMA^{Cter}$ fragments. The reagents were incubated for 30 minutes at 30° C in kinase buffer consisting of 20 mM Hepes pH 7.5, 5 mM $MgCl_2$, 0.2 M KCl, 0.5 mM EGTA, 2 mM DTT, 0.25 mM $NaVO_4$, and 1 mM ATP. To inhibit Aurora-A, 1 mM of MLN8237 was added to the reaction mix. To discriminate the phospho-proteins from their non-phosphorylated counterparts, samples were separated by Phos-TAG SDS-PAGE (Wako Rure Chemical Industries,Ltd, AAL-107), and stained with Coomassie blue (Figure 22B).

2.15.3 Microtubule co-sedimentation assays

Microtubule cosedimentation assays were carried out as indicated in Ciferri (Ciferri et al., 2008). Briefly, MTs were diluted to a final concentration of 9 µM in general tubulin (GT) buffer (80 mM PIPES pH 6.8, 1 mM $MgCl_2$, 1 mM EGTA) supplemented with 1 mM GTP, 50 µM Paclitaxel, and 60 mM NaCl. 1 µM $NuMA^{Cter}$ fragments were added to a final volume of 50 µl. Reactions were incubated at room temperature for 15 minutes, and ultracentrifuged for 15 minutes at 400,000 g at 25 °C. Pellets and supernatants were analysed by SDS-PAGE and visualized by Coomassie staining (Figures 27A and 28C). To assess whether NuMA could associate simultaneously with MTs and with LGN, the cosedimentation assays were repeated in the presence of 1 µM LGN^{TPR} (Figure 30A).

To perform MT cosedimentation experiments with cell extracts, HeLa cells stably expressing mCherry-$NuMA^{Cter}$ and synchronized with STLC in prometaphase, with or without MLN8237, were lysed in JS buffer supplemented with protease and phosphatase inhibitors. Cleared lysates were subjected to ultracentrifugation at 400,000 *g* with previously polymerized MTs at 25°C for 15 minutes. Pellet and supernatant fractions were separated by SDS-PAGE, transferred onto nitrocellulose membrane, and analysed by immunoblotting (Figure 27B and **see paragraph 2.12**).

2.15.4 *In vitro* microtubule bundling assays

Microtubule bundling assays of Figure 28B were performed according to Du et al. (Du et al., 2002). Briefly, rhodamine-labeled and unlabeled tubulin were mixed at a 1:10 ratio at a final concentration of 36 µM in GT buffer supplemented with 1 mM GTP, and incubated with 25 µM GST-$NuMA^{Cter}$ fragments. 5 µl of the reactions were kept at 37 °C for 4 minutes, and later fixed for 3 minutes at room temperature with 45 µl GT complemented with 1% glutaraldehyde. Fixed samples were diluted to 200 µl with GT buffer containing 50% glycerol, spotted onto poly-lysine slides, and visualized by wide-field microscopy using a 60x oil immersion objective.

2.15.5 Actin co-sedimentation assays

Actin co-sedimentation assays of Figure 44 were conducted according to (Scita et al., 2001). In brief, purified rabbit G-actin was allowed to polymerize into F-actin for 20 minutes at room temperature in F-buffer (5 mM Tris-HCl pH 7.8, 0.2 mM ATP, 1 mM DTT, 0.1 mM $CaCl_2$, 1 mM MgCl2 and 0.1 M KCl). Polymeric F-actin (1 μM) was incubated with 15 μM of His-Afadin^{Cter} and LGN^{TPR} for 15 minutes at room temperature, and subsequently ultracentrifuged for 25 minutes at 400,000 g at 4°C. Pellet and supernatant fractions were separated by SDS-PAGE, and visualized by Coomassie staining.

2.15.6 *In vitro* GST Pull-Down

For the pull-down assay in Figure 30B, 1μM of GST-LGN^{TPR} was immobilized on GSH-beads, and incubated with 2 μM NuMA^{Cter}. After washes, proteins bound to beads were separated by SDS-PAGE, and detected by Coomassie staining.

For the pull-down assays in Figure 41D, 1 μM of GST-Afadin fragments were immobilized on GSH-beads, and incubated with 5 μM of LGN^{TPR}. After washes, proteins bound to beads were separated by SDS-PAGE, and detected by Coomassie staining.

For the pull-down assays in Figure 33B, 5 μM of GST-LGN^{TPR} immobilized on GSH-beads were incubated with 2 mg/ml of cellular lysate of HEK293t transiently transfected with HA-Lgl2 and treated with 3.3 μM of nocodazole. Equal amounts of GST were used as a negative control. After washes with JS buffer, proteins bound to beads were separated by SDS-PAGE, and detected by immunoblotting with an HA-antibody (1:2000).

2.16 Statistical analysis

Data were tested for normality using D'Agostino-Pearson omnibus normality test. The significance of differences between means values was tested by Student's *t*-test for Gaussian-distributed data (Figure 19B), while non-normal data were analysed by Mann-Whitney test. Multiple comparisons were carried out with Kruskal-Wallis test or a one-way

ANOVA Tukey's test. The Kruskal-Wallis test is the one-way analysis of variance (ANOVA) used to compare two or more means of independent samples to a control mean, as reported in Figures 29 and 36. Instead, the Turkey's test is used to compare every mean with other means of independent samples, such as in the rescue experiment of Figure 43C. For the contingency tables relative to time-lapse experiments and for comparisons of cortical mCherry-NuMA, the Fisher's exact test was applied. The Fisher's exact test is used to evaluate categorical data such as cortical/not-cortical localization (Figure 26B) or oriented/misoriented divisions (Figures 15 and 32).

All statistical analyses were conducted using the GraphPad Prism 6.0 software, with the criterion for statistical significance set to $P < 0.05$.

3. RESULTS

3.1 Aurora-A and NuMA

3.1.1 Experimental setting to studying Aurora-A function in mitosis

Multiple mitotic processes are governed by Aurora-A functions: separation and maturation of centrosomes at mitotic entry, mitotic microtubule nucleation, and integrity of the spindle poles (Nikonova et al., 2013). Consistent with key roles of Aurora-A in mitosis, complete inhibition of Aurora-A causes a strong delay in prometaphase with highly disorganized spindle, thus precluding studies of mitotic division and spindle orientation (Asteriti et al., 2014). Therefore, to address the contribution of Aurora-A to orientation mechanisms, I set out to define conditions to partially inactivate its kinase activity, and allow a subpopulation of mitotic cells to form a correct metaphase plate and a normal bipolar spindle.

Historically mechanisms underlying spindle dynamics have been investigated in HeLa cells plated on fibronectin-coated coverslips, which divide with the spindle axis aligned to the substratum (Thery et al., 2005; Toyoshima and Nishida, 2007). Therefore, I decided to adopt this cellular system for my spindle orientation analyses. In addition, to exclude cell-type specific effects of Aurora-A inhibition, which could be relevant only in transformed cells, I repeated part of the experiments in non-transformed hTERT-RPE-1 cells.

I first developed synchronization protocols to increase mitotic populations. HeLa cells were synchronized in G1/S phase through a single thymidine block treatment, while hTERT-RPE-1 cells were synchronized in prometaphase using STLC (Figure 12A-B). STLC is a specific chemical inhibitor of the kinesin Eg5, which has been shown to play an essential role in centrosome separation and in bipolar spindle formation (Mayer et al., 1999; Ogo et al., 2007). To understand the molecular mechanism underlying the spindle orientation function of Aurora-A, two different strategies were applied. The first one was to transiently ablate Aurora-A by using small interfering RNA oligos. The second one was to treat cells with the selective Aurora-A chemical inhibitor MLN8237 (Alisertib).

MLN8237 is a second-generation Aurora-A inhibitor, acting as an ATP competitor, with high specificity for Aurora-A (Asteriti et al., 2014; Manfredi et al., 2011). To test the Aurora-A inactivating conditions in mitotic cells, I coupled the synchronization protocols described above with Aurora-A RNAi transfection or MLN8237 treatment as shown in Figure 12C.

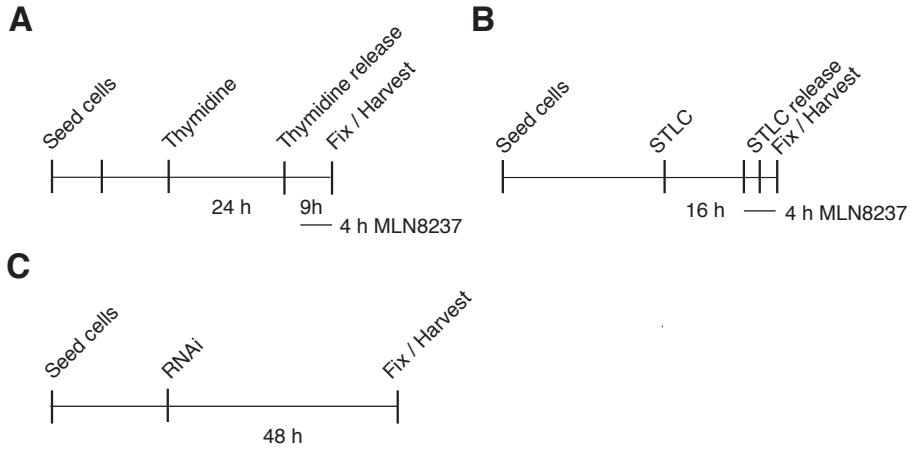

Figure 12 - Synchronization protocols. Schematic representation of the synchronisation protocols used to study spindle orientation in Aurora-A inhibited conditions. (**A**) HeLa cells were synchronized in G1/S phase through a single thymidine block treatment for 24 hours. After a five hours release of cells into mitosis, MLN8237 or DMSO (negative control) were added for additional four hours, prior to fixation or harvesting. (**B**) hTERT-RPE-1 cells were synchronized in prometaphase using 5 μM of the Eg5 inhibitor STLC for 24 hours. MLN8237 or DMSO was added two hours before STLC wash-out, and maintained for additional two hours, before fixation. (**C**) Aurora-A was interfered in HeLa cells by a transient transfection of specific siRNA (Aurora-Ai). GL2-siRNA (GL2i) oligos targeting the luciferase gene were used as specificity control. 48 hours post-transfection, asynchronous HeLa cells were analysed.

It is known that the kinase activity of Aurora-A is enhanced by autocatalytic phosphorylation of Thr-288 in its activation T-loop (Littlepage et al., 2002; Walter et al., 2000). Therefore, to assess to which extent Aurora-A was inactivated by the treatments, the residual activity of the kinase was monitored by immunofluorescence and immunoblotting with a specific anti-phospho-Thr288-Aurora-A antibody. Setting-up experiments indicated that 50 nM MLN8237 were sufficient to abolish the signal of phospho-Thr288-Aurora-A at the spindle poles in HeLa cells in metaphase (Figure 13A),

whereas 100 nM of MLN8237 were required to obtain the same inhibition in hTERT-RPE1 mitotic cells (Figure 13B). RNA-interference (RNAi)-mediated inactivation of Aurora-A in HeLa cells decreased the overall Aurora-A protein levels resulting in the reduction of the active Aurora-A fraction (Figure 14). Most importantly, under all tested conditions, I could observed by α-tubulin staining that cells could still form a bipolar spindle, which is a strict requirement to study spindle misorientation defects (Figure 13A-B).

To analyse the effect on spindle orientation of Aurora-A inhibition, a substantial number of cells in metaphase had to be imaged. To ensure that a significant proportion of cells undergoing Aurora-A inhibitory treatments could reach metaphase, I examined the effect of Aurora-A inactivation on mitotic progression. About 30% of synchronized HeLa cells treated with 50 nM MLN8237 or interfered for Aurora-A were found in metaphase (Figure 13A), This fraction decrease to about 10% in the case of hTERT-RPE-1 cells treated with 100 nM MLN8237 (Figure 13B). Collectively these results provided the experimental conditions that I used to address the role of Aurora-A in spindle orientation.

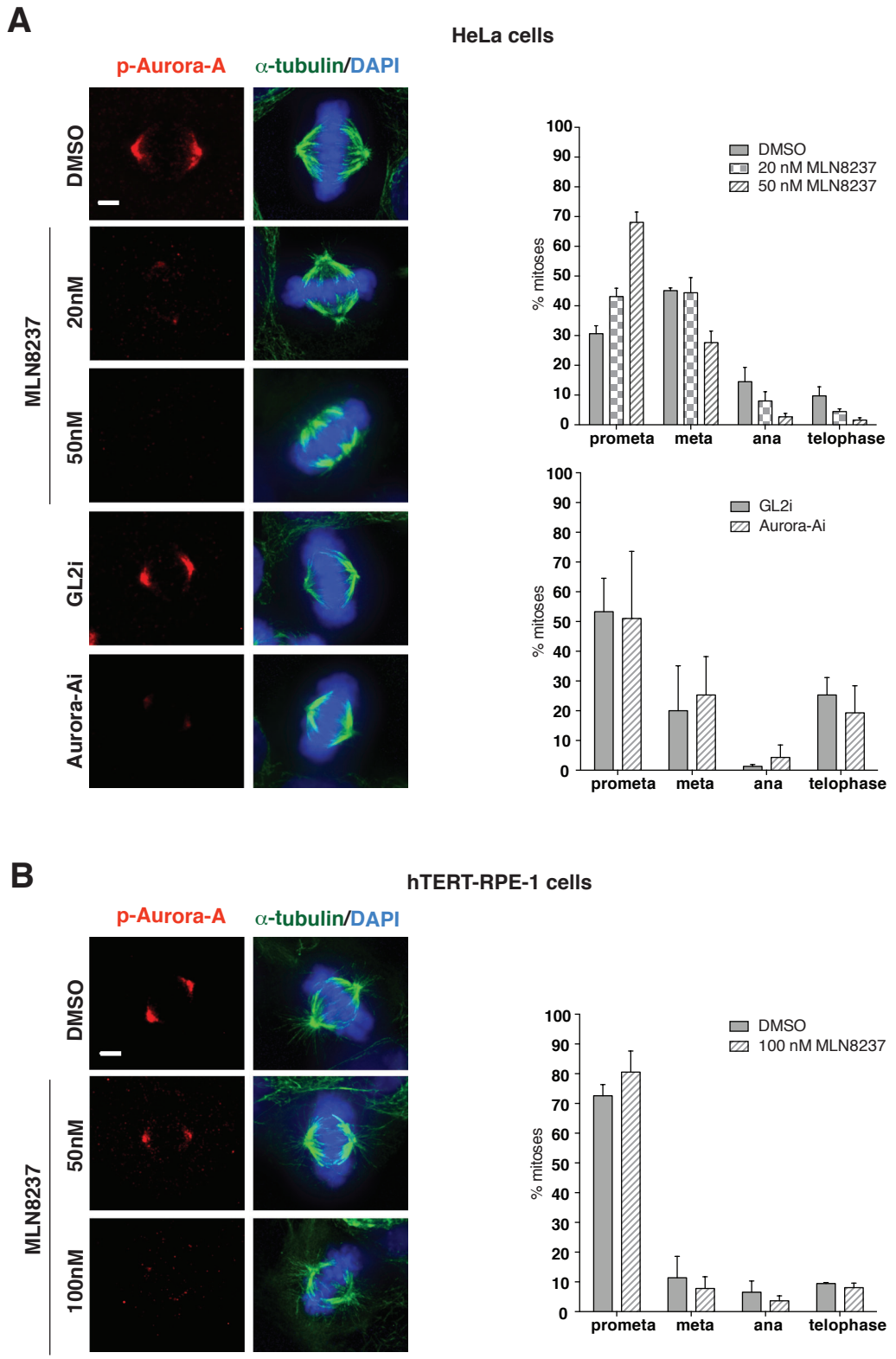

Figure 13 - Establishment of protocols for partial Aurora-A inhibition in mitotic HeLa and hTERT-RPE-1 cells. (**A**) Immunofluorescence analysis with anti phospho-Thr288-Aurora-A (p-Aurora-A, red) of HeLa cells treated with DMSO or MLN8237 (20 and 50 nM), or interfered for Aurora-A (Aurora-Ai; GL2i used as control). The mitotic spindle is visualized with anti-α-tubulin antibody (green), and the DNA is stained with DAPI (blue). Histograms (means ± SD) represent the distribution of cells in different mitotic phases under the conditions described above; n > 300

from 3 independent experiments. (B) Analysis of Aurora-A inhibition in hTERT-RPE-1 cells treated with DMSO or MLN8237 (50 nM and 100 nM). Immunofluorescence staining and histograms are as in (A); n > 400, from 2 independent experiments. Scale bars: 5 μm.

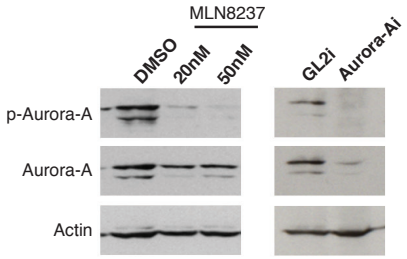

Figure 14 - Monitoring of Aurora-A inhibition levels in HeLa cells by immunoblotting. Left: Immunoblotting of phospho-Thr-288-Aurora-A (p-Aurora-A) and Aurora-A in mitotic extracts of HeLa cells treated with DMSO or MLN8237 (20 and 50 nM). Right: Immunoblotting as before of mitotic extracts from asynchronously growing HeLa cells interfered for luciferase (GL2i) or Aurora-A (Aurora-Ai). In all experiments, actin was used as loading control.

3.1.2 Aurora-A is required for the correct orientation of the mitotic spindle in HeLa and in hTERT-RPE-1 cells

The mitotic kinase Aurora-A has been implicated in spindle orientation in several cellular systems (Asteriti et al., 2014; Johnston et al., 2009; Lee et al., 2006a; Regan et al., 2013; Wang et al., 2006). To confirm the role of Aurora-A in orienting the spindle in HeLa and in hTERT-RPE-1 cells, we started performing time-lapse video-recording analysis in collaboration with Guarguaglini's group in Rome (see **paragraph 2.10** of Material and Methods for details).

In MLN8237-treated or Aurora-A-interfered conditions, a substantial proportion of cells did not divide parallel to the substratum and the two forming daughters were visualized in two different focal planes in telophase (Figure 15A). More specifically, these experiments revealed that between 15 and 25% of bipolar divisions of MLN8237-treated HeLa and hTERT-RPE-1 cells were misoriented in comparison with the 5% and 2% of DMSO-treated control cells (Figure 15A-B). In addition, we noticed that in both cell lines the reduced Aurora-A activity induced a substantial mitotic delay (Figure 15A), in line with what previously reported (Asteriti et al., 2014; Marumoto et al., 2003). A potential

explanation for this phenotype is that the spindle assembly checkpoint is activated by improper formation of mitotic spindle or by unattached kinetochores of misaligned chromosomes present in Aurora-A inhibited cells (Marumoto et al., 2003). Although interesting, I decided not to pursue this experiments further.

To measure more accurately the extent of spindle orientation defects, I quantified the spindle axis angles with respect to the substratum in fixed cells in metaphase using a method proposed by Thery et al. (2005) and Toyoshima and Nishida (2007)(Figure 16). Non-polarized cultured cells grown on fibronectin align the mitotic spindle parallel to the substratum by β1-integrin-mediated cell-substrate adhesion (Thery et al., 2005; Toyoshima and Nishida, 2007). Therefore, I plated cells on a fibronectin-coated coverslip, and I performed immunofluorescence analyses on fixed samples stained with DAPI to visualize the DNA, and with our monoclonal antibody against NuMA to visualize the spindle poles (Figure 16A). For these spindle orientation analyses, cells were optically sectioned with a line passing through the spindle poles, and the angle between the pole-to-pole axis and the substratum was evaluated in a confocal x-z section containing this line (Figure 16A). In both cell lines, the majority of control cells displayed spindles oriented parallel to the substratum, as expected, but misorientation occurred in Aurora-A inhibited conditions (Figure 16B). Accordingly, spindle angular distributions of Aurora-A inhibited cells shifted towards greater values as compared to control cells (Figure 16C). Collectively, these results indicate that either depleting or chemically inactivating of Aurora-A in cultured cells alters the orientation of the mitotic spindle, and results in misaligned divisions.

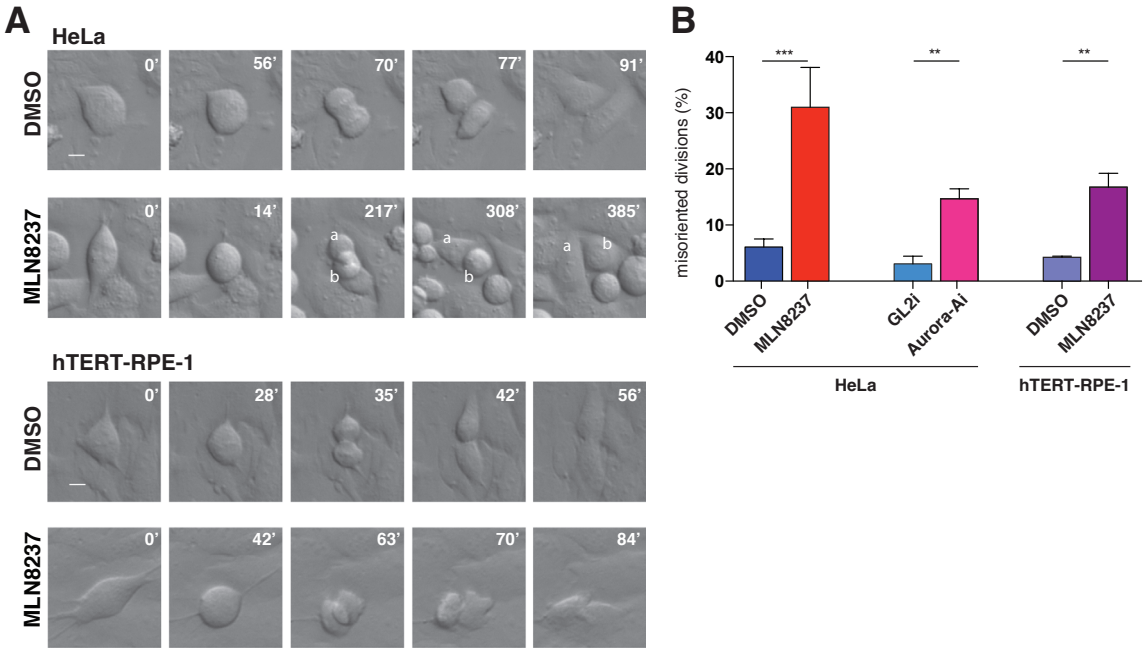

Figure 15 - Aurora-A is required for the correct orientation of the mitotic spindle. (**A**) Still frames from time-lapse video-recording of HeLa and hTERT-RPE-1 cells dividing parallel to the substrate when treated with DMSO (top rows), or misoriented in presence of MLN8237 (bottom rows). Minutes from the round-up are indicated on top right corner of each frame. a and b mark daughters derived from the filmed division. Scale bars: 10 μm. (**B**) Quantification (%) of the occurrence of the phenotype shown in A in HeLa (DMSO or 50 nM MLN8237; GL2i or Aurora-Ai) and hTERT-RPE-1 (DMSO or 100 nM MLN8237) cells. For all conditions, more than 80 bipolar mitoses from two independent experiments were analysed. **: $P < 0.01$ and ***: $P < 0.001$.

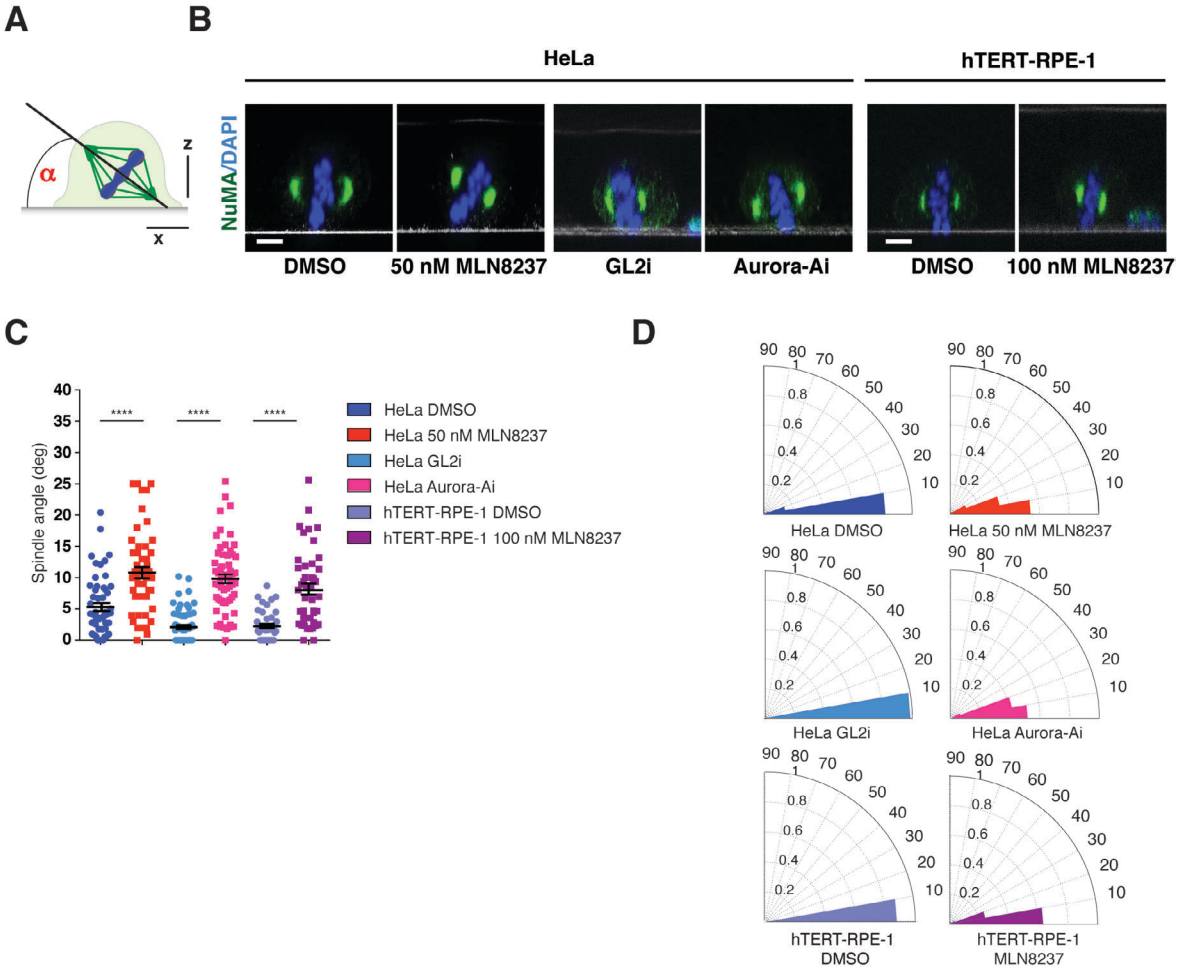

Figure 16 - The alignment of the mitotic spindle with the substratum requires Aurora-A activity. (**A**) Representative confocal z-sections of metaphase HeLa and hTERT-RPE-1 cells treated with DMSO or MLN8237, and HeLa cells interfered with Aurora-Ai or GL2i. Cells were stained with anti-NuMA antibody (green) and DAPI (blue). In all x-z sections, the plane of the coverslip is visible as a white line. Scale bar: 5 μm. A schematic representation of the measured mitotic spindle angle is shown in the cartoon on the right. (**B**) Scatter plots illustrating the distribution of spindle angles in HeLa cells (DMSO or 50 nM MLN8237; GL2i or Aurora-Ai) and hTERT-RPE-1 cells (DMSO or 100 nM MLN8237). For all conditions, means ± SEM are shown; n > 40 from three independent experiments. ****: $P < 0.0001$. (**C**) Radial histograms illustrating the distributions of the spindle axis angles in HeLa cells (DMSO or 50 nM MLN8237; GL2i or Aurora-Ai) and hTERT-RPE-1 cells (DMSO or 100 nM MLN8237).

3.1.3 Inhibition of Aurora-A activity impairs NuMA localization in metaphase

Spindle orientation depends on the polarized localization of force generators linking astral MTs to the cell cortex. The best-characterized players of this machinery are LGN, NuMA and the microtubule motors Dynein/Dynactin (Du and Macara, 2004; Kotak et al., 2012; Woodard et al., 2011). To investigate whether the spindle orientation defects observed

upon Aurora-A inactivation were due to a perturbed localization of the main players of the spindle orientation pathway, I analysed the distribution of LGN, NuMA and the $p150^{Glued}$ subunit of Dynactin in Aurora-A inhibited mitotic cells.

3.1.3.1 Aurora-A does not regulate the localization of LGN

To check if Aurora-A affects the polar enrichment of LGN in metaphase, I performed immunofluorescence analyses. The effect of Aurora-A inhibition on the localization of cortical LGN was quantified using an intensity line-scan including cortex and cytoplasmic signals (see **paragraph 2.8.2** of Material and Methods for details). The ratio between LGN cortical and cytoplasmic fluorescence intensities revealed that no significant impairment of the cortical distribution of LGN occurred upon MLN8237 treatment (Figure 17). Several studies seem to suggest that LGN phosphorylation is required in spindle orientation. However, the identity of the kinase responsible for this LGN phosphorylation is still controversial. In fact, studies in *Drosophila* S2 cells revealed that Aurora-A phosphorylates Pins on Ser-436 (Johnston et al., 2009), while in MDCK cells, LGN has reported to be phosphorylated on Ser-401 (corresponding to Ser-436 of Pins) by aPKC. In MDCK cells, the phosphorylation of LGN is required to exclude the protein from the apical surface (Hao et al., 2010). Recent studies on neuroepithelial cells revealed the phosphorylation of LGN on the same Ser-401 impairs the cortical localization of LGN through Dlg and caused spindle misorientation. However the authors did not investigated which is the kinase responsible of this phenotype (Saadaoui et al., 2014). Our studies indicate that partial Aurora-A inhibition does not alter LGN cortical recruitment in HeLa cells.

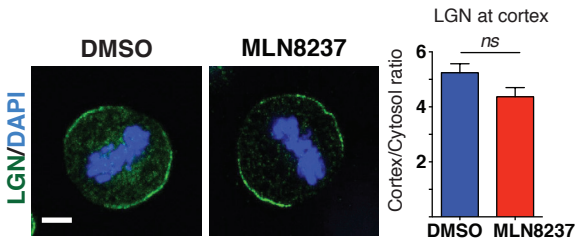

Figure 17 - Aurora-A does not regulate the localization of LGN. Immunofluorescence analysis of endogenous LGN (green) in HeLa cells treated with DMSO or MLN8237. Histograms represent the LGN cortical-to-cytosol fluorescence ratio (means ± SEM; n > 30 from three independent experiments). *ns*: non-significant statistical difference.

3.1.3.2 Inhibition of Aurora-A alters NuMA localization

In mitosis NuMA plays dual functions: at the spindle poles it contributes to focus MTs and to maintain centrosome-spindle coupling, while at the cortex it mediates cortical recruitment of Dynein in conjunction with LGN:Gαi in order to position the mitotic spindle (Kotak et al., 2012; Silk et al., 2009). The experiments described in the previous paragraph demonstrated that the cortical localization of LGN is not affected by Aurora-A inhibition. Therefore, I checked whether Aurora-A inactivation could perturb the localization of NuMA.

Quantitative image analysis (see **paragraph 2.8** of Material and Methods for details) showed that MLN8237-treatment in HeLa cells induces a 6-fold enrichment of NuMA at the spindle poles, and abrogate the cortical NuMA signal (Figure 18A). Similar results were obtained in Aurora-A interfered cells (Figure 18B). In MLN8237-treated hTERT-RPE-1 cells, the spindle pole signal increased about 4-fold and the cortical signal was abolished (Figure 18C). Altogether these results indicate that Aurora-A activity has a major role in establishing the correct localization of NuMA in metaphase cells. To further corroborate this idea, I investigated the effects of transient expression of an Aurora-A kinase-dead mutant on NuMA localization (indicated as Aurora-A-KD in the following). For these analyses I used an Aurora-A mutant protein carrying the Asp-274-Ala mutation in the catalytic domain. The Asp-274 residue is required to carry out phosphoryl-transfer

on Aurora-A substrates (Crane et al., 2004). I reasoned that expression of a KD-version of the kinase could have a dominant-negative effect, thus mimicking the phenotype observed upon Aurora-A inhibition. The distribution of NuMA in HeLa cells expressing GFP-tagged Aurora-A-KD was compared to the one of cells transfected with GFP-tagged histone H2B, that I used as negative control. Quantification of NuMA signals at the spindle poles and at the cortex showed that the transient overexpression of a kinase inactive Aurora-A induced a partial relocation of NuMA from the cell cortex to spindle poles, consistent with the expected dominant negative effect (Figure 18D). The effect on NuMA localization was partial compared to Aurora-A-inhibited conditions, likely because in HeLa cells expressing GFP-tagged Aurora-A-KD, endogenous Aurora-A is still active and could phosphorylate NuMA.

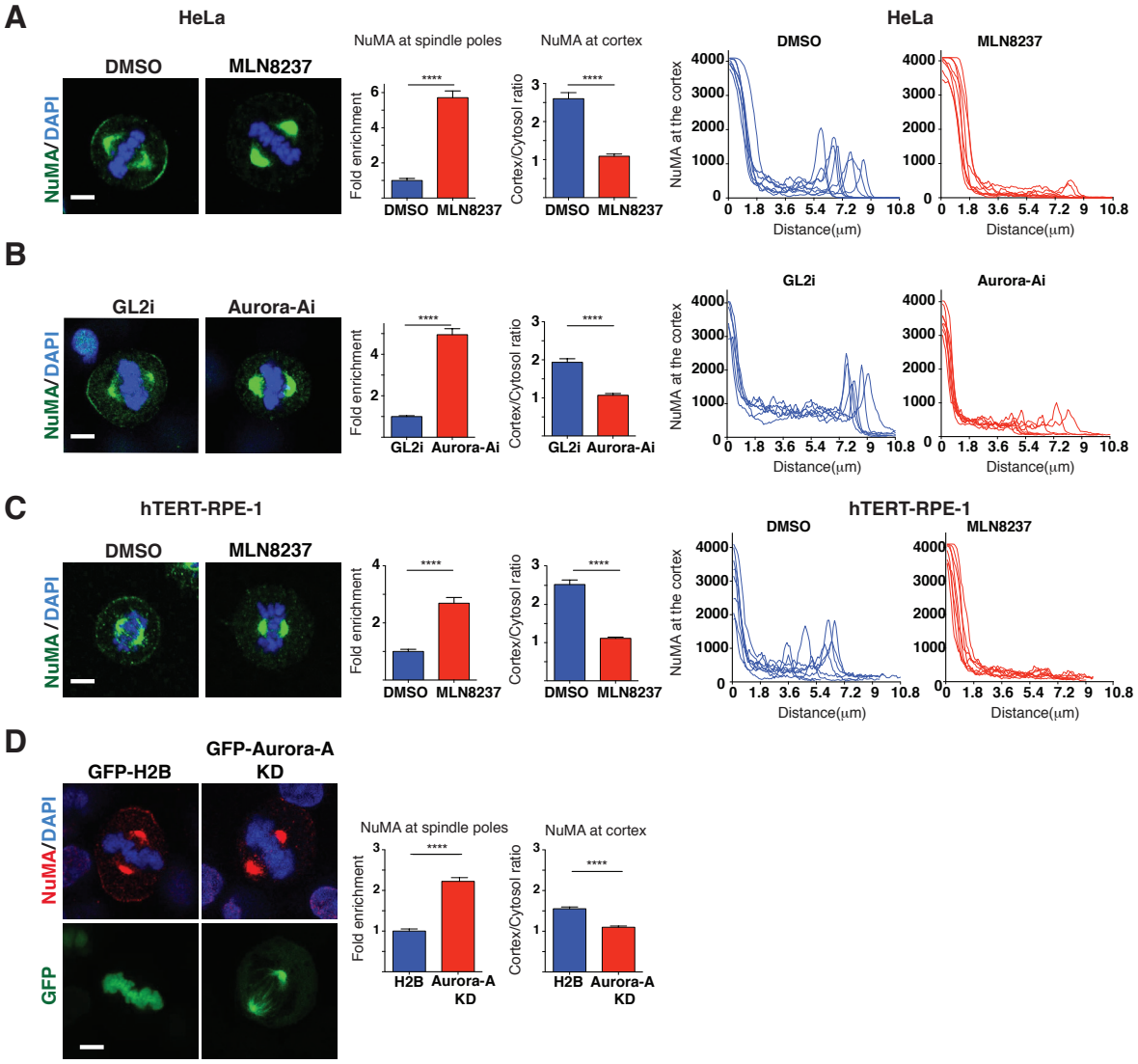

Figure 18 - Inhibition of Aurora-A impairs NuMA localization. (**A**) Immunofluorescence analysis of endogenous NuMA (green) in HeLa cells treated with DMSO or MLN8237. Histograms show the quantification of the signal intensity of NuMA at the spindle poles as fold-change relative to control (means ± SEM; n > 40 from three independent experiments), and the cortex-to-cytosol fluorescence ratio (means ± SEM; n > 30 from three independent experiments). Right: Representative line-scan profiles of NuMA signal along a line drawn from the spindle pole to cell cortex in metaphase. (**B**) Immunofluorescence analysis of endogenous NuMA in control GL2- (GL2i) or Aurora-A-interfered (Aurora-Ai) HeLa cells. Levels of NuMA at the spindle poles and at the cortex are quantified as in panel (A). Quantifications summarize three independent experiments with n > 50 for polar NuMA, and n > 40 for cortical NuMA. Right: Representative line-scan profiles of NuMA signal measured and in (A). (**C**) Immunofluorescence analysis of endogenous NuMA in hTERT-RPE-1 cells treated with DMSO or MLN8237. Levels of NuMA at the spindle poles and at the cortex are quantified as in panel (A) from three independent experiments. (**D**) Immunofluorescence analysis of endogenous NuMA (red) in HeLa cells transiently transfected with GFP-Aurora-A-KD or GFP-H2B as control. Histograms represent the quantification of the signal intensity of NuMA at the spindle poles compared to control (means ±

SEM; n > 30 from three independent experiments), and the cortex-to-cytosol fluorescence ratio (means ± SEM; n > 45 from three independent experiments). ****: P < 0.0001.

3.1.3.3 Aurora-A controls the mobility of NuMA at the spindle poles

Based on the change in NuMA distribution caused by Aurora-A inhibition, I considered that in the absence of Aurora-A activity NuMA could be trapped at the spindle poles, this way depleting the cytosolic fraction able to reach the cortex. To test this hypothesis, I set out to perform FRAP experiments in mitotic HeLa cells transiently transfected with GFP-NuMA. In metaphase HeLa cells, exogenously expressed GFP-NuMA localizes at the spindle poles (Figure 31B). To evaluate the effect of Aurora-A inhibition on the mobility of GFP-NuMA, I photobleached the GFP-NuMA signal at one of the two spindle poles in DMSO- or MLN8237-treated cells in metaphase, and I monitored the dynamics of FRAP recovery. The half-time of the recovery and the mobile fraction of bleached GFP-NuMA were determined by FRAP measurements on individual cells fitted with a single exponential curve (Figure 19A and **paragraph 2.9** of Material and Methods). The half-time of the recovery ($t_{1/2}$) is the time at which the half of the fluorescence signal has recovered compared to fluorescence intensity level at the plateau. In turn, the fluorescence intensity at the plateau compared to the pre-bleached intensity signal reflects the mobile fraction within the localized fluorophore population. In unperturbed conditions, the $t_{1/2}$ of the GFP-NuMA signal after photobleaching was about 53 seconds compared to 95 seconds of $t_{1/2}$ in Aurora-A-inhibited cells. This evidence indicates that the turnover of NuMA at the spindle poles is significantly slower in MLN8237-treated cells (Figure 19B). Concomitantly, in the same inhibited conditions, the GFP-NuMA fluorescence intensity at the plateau diminished compared to control cells indicating a reduction of the mobile fraction of NuMA at the spindle poles from 60% of control cells to about 40% (Figure 19B). Most notably, I observed that the recovered GFP signal did not reach 100% of the pre-bleached intensity. This result is consistent with the existence of two different populations of NuMA at the spindle poles, one stably bound and the other dynamically

cycling, and it is fully in line with previous reports (Kisurina-Evgenieva et al., 2004; Seldin et al., 2013).

Taken together, the FRAP results showed that the continuous exchange between the cytoplasmic and spindle-pole-associated pools of NuMA is finely tuned by the activity of Aurora-A. In particular, Aurora-A prevents aberrant accumulation of NuMA at the spindle poles, and allows its recruitment at the polar sites of the membrane. Inhibition of its kinase activity shifts the steady-state distribution of NuMA to being predominately spindle-pole associated.

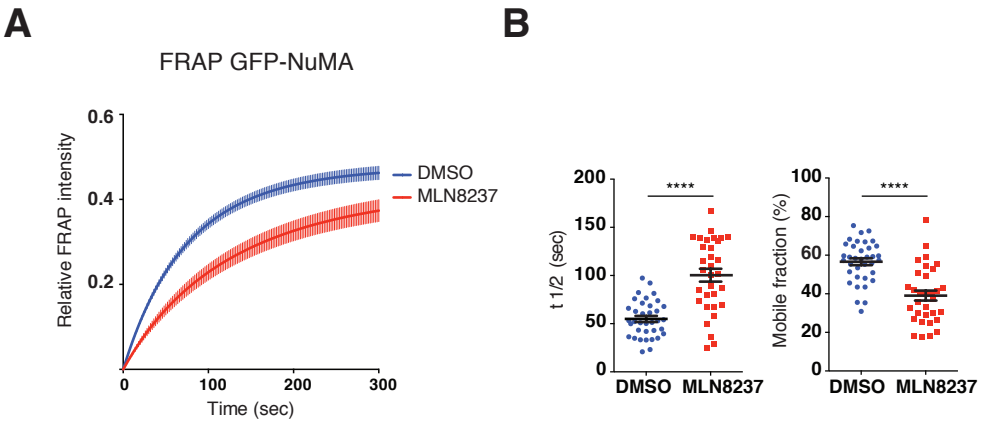

Figure 19 - Aurora-A controls the mobility of NuMA at the spindle poles. FRAP analysis of full-length GFP-NuMA transiently transfected into HeLa cells treated with DMSO or MLN8237. (**A**) Recovery curve of the bleached GFP-signal at the spindle poles over 5 minutes. (**B**) Dot-plots (bottom) showing the distribution of $t_{1/2}$ (seconds) and the mobile fraction (%) of GFP-NuMA at the spindle poles in cells treated with DMSO or MLN8237 (means ± SEM; n > 40 from three independent experiments). The mean value of the $t_{1/2}$ for DMSO-treated cells was 53.5 seconds, and for MLN8237-treated cells was 95.3 seconds. The mean values of the GFP-NuMA mobile fraction were about 61% and 40% in cells treated with DMSO or MLN8237, respectively. In all statistical analyses, ****: $P < 0.0001$.

3.1.3.4 Incomplete inhibition of Aurora-A leaves nuclear localization of NuMA unperturbed

In interphase, NuMA localizes in the nucleus, where its role is still largely unclear. A few reports suggested that it participates in various aspects of chromatin structure and function, possibly due to its nucleotide-binding activities (Harborth et al., 1999; Merdes and Cleveland, 1998; Vidi et al., 2012; Vidi et al., 2014). To investigate whether Aurora-A could affect the distribution of NuMA in non-mitotic cells, I checked the interphase localization of NuMA in MLN8237-treated cells, and found that nuclear-targeting of NuMA was unaltered (Figure 20). This result is somehow expected based on the notion that the activity of Aurora-A peaks in mitosis.

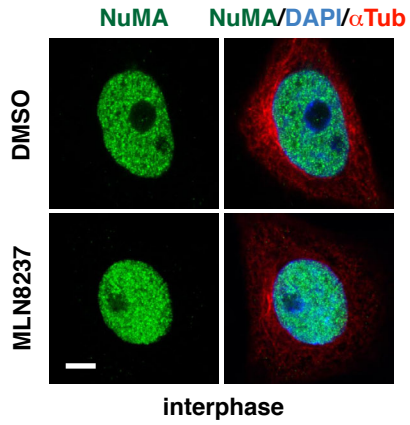

Figure 20 - Partial inhibition of Aurora-A does not perturb NuMA localization in interphase. Confocal images of HeLa cells in interphase treated with DMSO or 50 nM MLN8237, and stained with anti-NuMA (green), anti-α-tubulin (red) and DAPI (blue). Scale bars: 5 μm.

3.1.3.5 Inhibition of Aurora-A impairs Dynactin localization

In symmetrically dividing HeLa cells, NuMA is required to recruit Dynein/Dynactin to the cell cortex via interactions with its own amino-terminal domain (Kotak et al., 2012; Seldin et al., 2013). Therefore, I checked if the loss of cortical NuMA observed upon Aurora-A inactivation could affect cortical targeting of Dynein/Dynactin. To this end, I imaged the cellular localization of the Dynactin subunit $p150^{Glued}$ in MLN-treated cells, and compared it to control cells. Quantitative image analysis (see **paragraph 2.8.2** of Material and Methods for details) showed that MLN8237-treatment in HeLa cells abrogates the

p150^{Glued} cortical signal (Figure 21). Although I cannot exclude a direct effect of Aurora-A on Dynactin, this result strongly suggests that the Aurora-A–dependent absence of NuMA from the cortex results in the inability of Dynactin to reach the cortex.

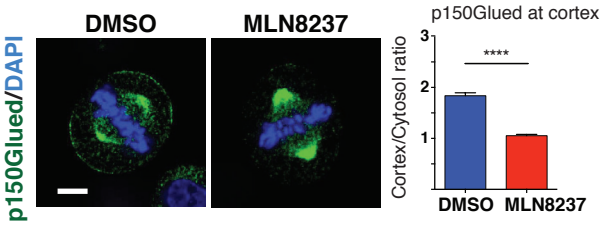

Figure 21 - Inhibition of Aurora-A impairs Dynactin localization. Immunostaining of p150^{Glued} (green) in mitotic HeLa cells treated with DMSO or MLN8237. Histograms represent the p150^{Glued} cortical-to-cytosol fluorescence ratio (means ± SEM; n > 45 from three independent experiments). ****: P < 0.0001. Scale bars: 5 μm.

3.1.4 Aurora-A phosphorylates NuMA on the C-terminus

The experiments reported so far demonstrated that the activity of Aurora-A is required for spindle positioning, and for correct NuMA distribution. The region of NuMA involved in LGN and MT binding is the C-terminal domain (Du et al., 2001; Du et al., 2002; Haren and Merdes, 2002). Therefore, I reasoned that this domain was the best candidate for the Aurora-A regulatory functions. First hints into the possibility that the C-terminal region of NuMA could be a direct substrate of Aurora-A came from analysis of its primary sequence, by which it was possible to identify three putative sites (namely Ser-1969, Ser-1991 and Ser-2047) conforming to the Aurora-A consensus site R/K-x-S/T-ϕ (where ϕ stands for a hydrophobic residue) (Cheeseman et al., 2002; Ferrari et al., 2005). These analyses *in silico* were performed by using PHOSIDA web sites (http://www.phosida.com/). Interestingly, two of the predicted phosphosites fall in previously characterized domains of NuMA: Ser-1969 is in the mapped MT-binding domain (Du et al., 2002; Haren and Merdes, 2002), while Ser-1991 lies in the nuclear-localization-signal (NLS) (Gueth-Hallonet et al., 1996) (Figure 22A). Importantly, Ser-1969, Ser-1991 and Ser-2047 were recently found among the sites phosphorylated in mitotic HeLa cells by Aurora–A in a large-scale proteomic study performed by Kettenbach

and colleagues (Kettenbach et al., 2011; Sardon et al., 2010).

3.1.4.1 Aurora-A directly phosphorylates NuMA C-terminus in vitro

To assess whether the three predicted phospho-sites could be phosphorylated directly by Aurora-A *in vitro*, a kinase assay was performed with the purified kinase domain of Aurora-A (generous gift of Prof. Richard Bayliss) and a C-terminal fragment of NuMA encompassing residues 1821-2115 (referred to as $NuMA^{Cter}$ hereon) (Figure 22A). To design the $NuMA^{Cter}$ construct we considered that NuMA consists of two N- and C-terminal domains and a central coiled-coil region (213-1699) responsible for dimerization (Harborth et al., 1995; Yang et al., 1992). Therefore, the C-terminal construct to be used in the experiments with Aurora-A was designed to start after the coiled-coil to avoid association with endogenous NuMA (Figure 22A). The construct of $NuMA^{Cter}$ was cloned into a vector for bacterial expression, and purified to homogeneity. To detect phosphorylated proteins, the samples of the *in vitro* kinase assay were separated on Phos-TAG SDS-PAGE. This technique allows monitoring the phosphorylated proteins as gel-shifted bands. The phosphorylated proteins migrate more slowly due to the presence of the phosphate-binding molecule "Phos-tag" in the separating gel. The Phos-tag is a dinuclear metal complex (1,3-bis[bis(pyridin-2-ylmethyl)amino]propan-2-olato manganese(II) complex) which, acts as a phosphate-binding tag molecule in an aqueous solution. Coomassie-stained Phos-TAG^{TM} SDS-PAGE showed that wild-type $NuMA^{Cter}$ incubated with Aurora-A displays three retarded bands (Figure 22B; *lane 2*) compared to unmodified $NuMA^{Cter}$ (Figure 22B; *lane 1*). To ensure that the observed shifts were due to the activity of Aurora-A, the kinase assay was repeated in the presence of MLN8237. As expected, under this condition the shift of wild-type $NuMA^{Cter}$ was completely abolished (Figure 22B; *lane 3*). In line with previous finding, mass spectrometry analysis of the phosphorylated bands established that the phosphorylation occurred on the three serine-residues of $NuMA^{Cter}$ previously identified by primary sequence inspection. To further confirm that only Ser-1969, Ser-1991 and Ser-2047 are phosphorylated *in vitro*, we

repeated the kinase assay with a variant of NuMA^{Cter} with the three phospho-sites replaced by alanines (NuMA^{3Ala}). The NuMA^{3Ala} incubated with Aurora-A did not shift significantly (Figure 22B; *lane 4 and 5*), indicating that under our experimental conditions the three phospho-sites Ser-1969, Ser-1991 and Ser-2047 are the only ones phosphorylated by Aurora-A *in vitro*.

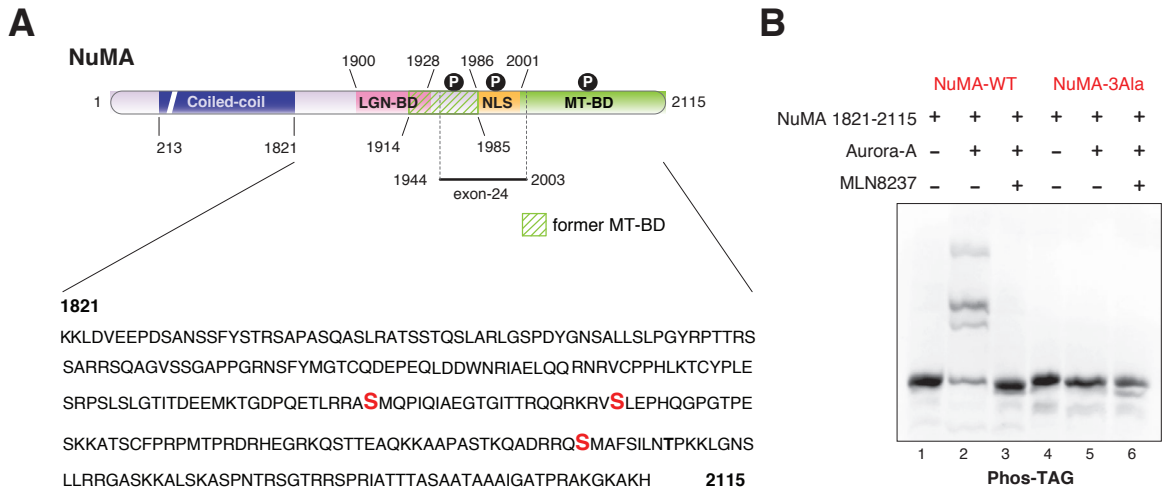

Figure 22 - Aurora-A directly phosphorylates NuMA^{Cter} *in vitro*. (**A**) Schematic representation of the domain structure of NuMA, enlarged on the C-terminal portion spanning residues 1821-2115 (NuMA^{Cter} in the text and below). Fragments with known functions are highlighted with different colours including the LGN-binding domain (residues 1900-1928, pink), the *old* MT-binding domain (residues 1914-1985, dashed green) and the nuclear localization signal (NLS, residues 1986-2001, orange). The MT-binding domain identified in this study encompassing residues 2002-2115 is coloured in green. A black line highlights the exon 24 of human NuMA corresponding to exon 22 of mouse NuMA (Silk et al., 2009). In the primary sequence of NuMA^{Cter}, the Aurora-A phospho-serine sites Ser-1969, Ser-1991 and Ser-2047 are coloured in red. (**B**) Coomassie blue-stained Phos-TAG SDS-PAGE of the *in vitro* kinase assay performed with the purified kinase domain of Aurora-A and NuMA^{Cter} wild-type (NuMA-WT), or Ser-1969-Ala, Ser-1991-Ala and Ser-2047-Ala mutant (NuMA-3Ala). Samples loaded in lane 3 and 6 contained 1 mM MLN8237 in the reaction buffer. The purified NuMA^{Cter} samples used as substrates are loaded in lane 1 and 4 as controls.

3.1.4.2 NuMA phosphorylation by Aurora-A in vivo

To confirm that NuMA is phosphorylated by Aurora-A *in vivo* on the same residues, I generated HeLa cell lines stably expressing the same $NuMA^{Cter}$ and $NuMA^{3Ala}$ constructs used for the studies *in vitro*, fused to FLAG-mCherry-Tag. The constructs were cloned in a pCDH lentiviral vector with an Ubc promoter, which ensured that the expression levels were similar to the ones of endogenous NuMA.

First, to test whether the three serine-phosphosites identified *in vitro* were inhibited by MLN8237 treatment *in vivo*, I run a Phos-TAG SDS-PAGE using mitotic lysates of cells expressing $NuMA^{Cter}$ constructs, treated or not with 50 nM MLN8237. Previous reports showed that NuMA is phosphorylated on Thr-2055 by the kinase CDK1, and that this phosphorylation negatively regulates the cortical localization of NuMA in metaphase (Kotak et al., 2013; Seldin et al., 2013; Zheng et al., 2014). To distinguish between the Aurora-A-mediated phosphorylation of NuMA and the one of CDK1, I decided to compare cells treated with 50 nM MLN8237 or with 9 μM RO3306, an ATP-competitive inhibitor of CDK1 (Vassilev et al., 2006). To obtain a sufficient amount of mitotic lysates for the Phos-TAG SDS-PAGE under CDK1-inhibited conditions, cells were arrested in metaphase by a synchronization protocol adapted form McCloy and colleagues (McCloy et al., 2015) (see **paragraph 2.4.3** of Material and Methods for details) (Figure 23A). Mitotic cells treated with MLN8237, RO3306 or DMSO were compared. In the assay, the lysate from untreated interphase cells was also added as negative control of mitotic phosphorylation (Figure 23B; *lanes 1* and *5*). Equal amounts of all the samples were separated by Phos-TAG SDS-PAGE. To visualize $NuMA^{Cter}$ wild-type and $NuMA^{3Ala}$, I transferred the species separated by Phos-TAG SDS-PAGE on a nitrocellulose membrane and performed an immunoblotting with antibodies against the FLAG-tag. In untreated mitotic samples, a major band is visible in the upper part of the blot together with several minor bands, that correspond to various phosphorylated forms of $NuMA^{Cter}$ (Figure 23B; *lane 2*). In the interphase samples, only one band was present, confirming that the differential shifts

observed in the mitotic lysates represent mitotic phosphorylations of NuMA^{Cter} (Figure 23B; *lane 1*). Unfortunately, I could not observe any difference between the MLN8237-treated lysates and the untreated mitotic lysate (Figure 23B; *lanes 2 and 3*). Conversely, the major top band visible in the blot of mitotic lysate disappeared upon RO3306 treatment indicating that it reflects the CDK1 phosphorylation of NuMA^{Cter} in mitosis (Figure 23B; *lane 4*). In line with this interpretation, similar results were obtained for NuMA^{3Ala} construct (Figure 23B; *lanes 5-8*). I concluded that Phos-TAG separation of NuMA^{Cter}-expressing mitotic lysates was not able to detect the Aurora-A activity on NuMA^{Cter} *in vivo*. A possible explanation for the difficulty of visualizing the Aurora-A related band-shift by Phos-TAG SDS-PAGE is that a number of target sites for different kinases are present in the NuMA C-terminal domain, including the ones of Abl1 (Matsumura et al., 2011), and Plk1 (Kiyomitsu and Cheeseman, 2012), and these could mask Aurora-A phosphorylations.

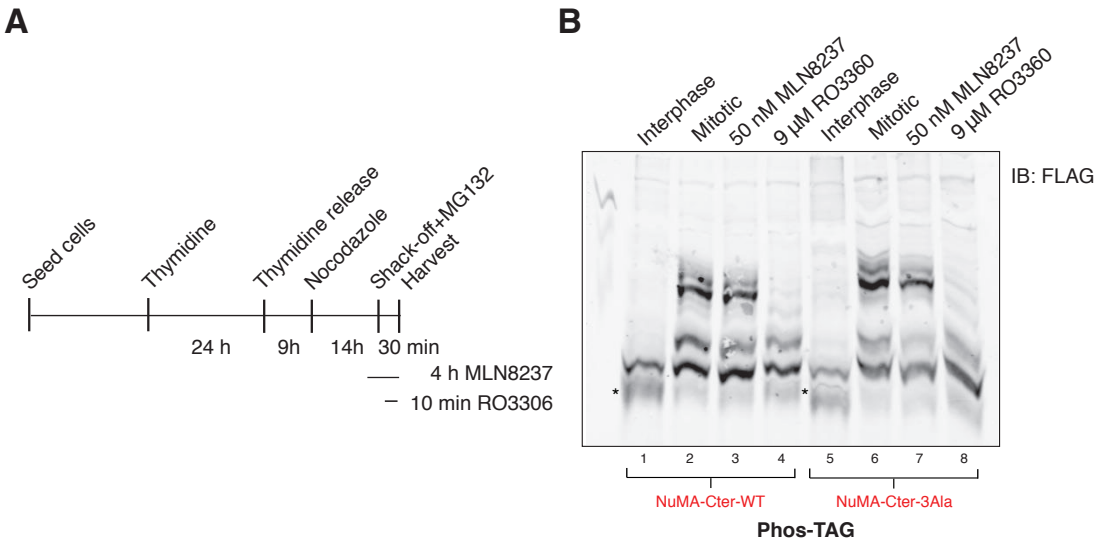

Figure 23 - NuMA phosphorylation by Aurora-A *in vivo*. (**A**) Schematic representation of the synchronisation protocol used for mitotic CDK1 and Aurora-A inhibitions. HeLa cells were synchronized in G1/S phase through a single thymidine block treatment for 24 hours. After nine hours release of cells into mitosis, 3.3 µM nocodazole was added for additional 14 hours to arrest cells in prometaphase. In the last 3 hours of nocodazole incubation, the culture medium was supplemented with 50 nM MLN8237. After shake-off, mitotic cells were further incubated for 30 minutes with nocodazole, MLN8237 and the proteasome inhibitor MG132 to arrest cells in metaphase. After 15 minutes of incubation with 25 µM MG132, 9 µM of the CDK1 inhibitor

RO3306 were added for 10 minutes prior to harvesting. (**B**) Immunoblotting anti-FLAG of a Phos-TAG SDS-PAGE separating mitotic lysates of cells stabling expressing NuMA^{Cter} wild-type (NuMA-Cter-WT), or with Ser-1969, Ser-1991 and Ser-2047 mutated into alanine (NuMA-Cter-3Ala). Samples loaded in lanes 1 and 5 are lysates of cells in interphase, which I used as negative controls of mitotic phosphorylations. Lanes 2 and 6 are mitotic lysate unperturbed. Lanes 3 and 7 are mitotic lysates of cells treated with 50 nM MLN8237. Lanes 4 and 8 are mitotic lysates of cells treated with 9 μM RO3306. *: indicates protein degradation.

3.1.4.3 Phosphorylation of Ser-1969 of NuMA by Aurora-A regulates its polar localization

To explore the physiological relevance of the phosphosites identified *in vitro*, I generated additional HeLa cell lines stably expressing the mCherry-tagged NuMA^{Cter} construct singularly or triple mutated either to alanines or to aspartic acid in the three serine phosphosites. Importantly, previous reports revealed that Aurora-A influences the mitotic localization of Dynactin (Reboutier et al., 2013; Rome et al., 2010), implying that the altered NuMA localization that I observed upon Aurora-A inhibition could be an indirect effect of Dynactin redistribution. It is known that the region mediating the interaction between NuMA and Dynein/Dynactin resides in the N-terminal domain of NuMA spanning residues 1-705 (Kotak et al., 2012). This evidence, coupled to the fact that NuMA^{Cter} starts after the coiled-coil region and cannot dimerize with endogenous NuMA, implies that the behaviour of the NuMA^{Cter} constructs used in the cell biology studies in Aurora-A inhibited cells is independent from Dynein/Dynactin.

Western blot analysis of lysates expressing the different NuMA^{Cter} mutants confirmed that all cell lines expressed comparable levels of NuMA^{Cter}, and that the overexpression levels of the C-terminal fragments driven by Ubc promoter was about 3-fold higher than endogenous NuMA (Figure 24).

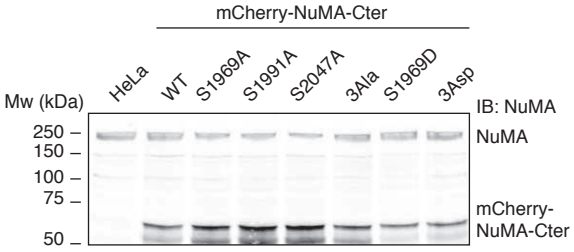

Figure 24 – Generation of stable cell lines expressing NuMA^{Cter} wild-type or mutated. Anti-NuMA immunoblotting of mitotic lysates of HeLa cells wild-type, or stably expressing mCherry-NuMA^{Cter} constructs. The expression levels of mCherry-NuMA^{Cter} constructs were compared to endogenous NuMA as normalizing signal.

I then analysed the mitotic distribution of mCherry-NuMA^{Cter} mutants in the cell lines expressing the various constructs. Quantification of the amount of each construct at the spindle poles was achieved by comparing the mCherry signal at the spindle poles relative to the cytoplasm (see **paragraph 2.8.1** of Material and Methods for details). In metaphase, wild-type NuMA^{Cter} localized at the spindle poles, where it accumulated abnormally upon Aurora-A inhibition, mimicking the effect observed for endogenous NuMA. A similar phenotype was detected with the single Ser-1991-Ala and Ser-2047-Ala mutants. Conversely, the NuMA^{Cter}-Ser-1969-Ala and the 3Ala mutants strongly enriched at the spindle poles even in untreated cells, and became insensitive to MLN8237 treatment (Figure 25A-B). In both the NuMA^{Cter} constructs carrying serine to glutamic acid substitutions on Ser-1969 or all three serine-phosphosites, NuMA^{Cter} localized to the spindle poles to the same extent of the wild-type construct, but in MLN8237-treated conditions I could not observe any enrichment (Figure 25A-B). Collectively, these results indicate that Ser-1969 of NuMA plays a pivotal role in determining the levels of NuMA at the spindle poles.

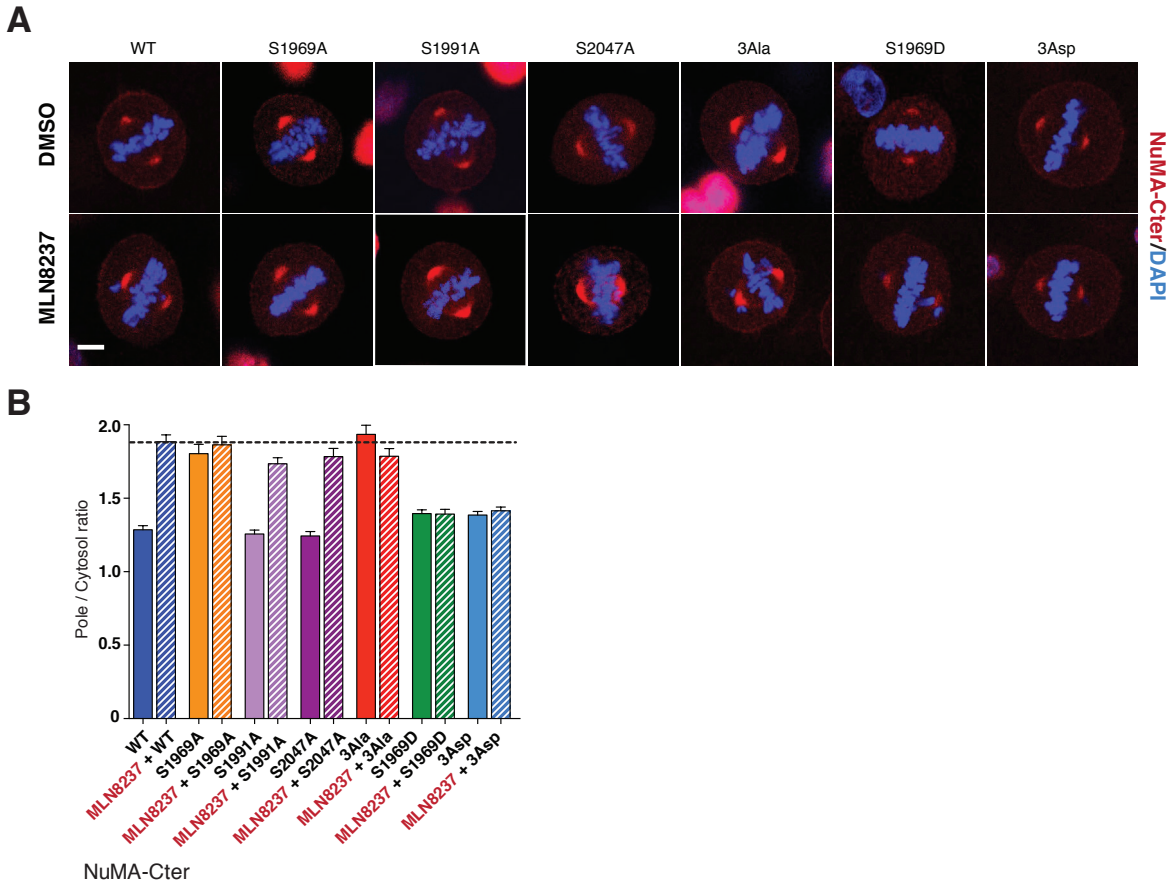

Figure 25 - Aurora-A-phosphorylation on Ser-1969 regulates polar NuMA localization. (**A**) Confocal images of metaphase HeLa cells stably expressing mCherry-NuMA^{Cter} mutants. Mutant proteins compared are: wild-type, S1969A/D, S1991A, S2047A, and S1969-S1991-S2047 mutated into alanine (3Ala) or aspartic acid (3Asp). Representative images of HeLa cells treated with DMSO (top row) or 50 nM MLN8237 (bottom row) are shown. (**B**) Quantification of the mCherry fluorescence ratio between poles and cytosol in the cell lines visualized in (A) (means ± SEM; n > 20 from three independent experiments).

3.1.4.4 Phosphorylations of Ser-1969 and Ser-2047 of NuMA by Aurora-A regulate its cortical localization

Beside accumulation at the spindle poles, inhibition of Aurora-A prevents cortical targeting of NuMA. To investigate the importance of the phosphorylation of NuMA on its cortical localization, I set out to monitor the mCherry signal at the cortex of the mCherry-NuMA^{Cter} mutated proteins. In a first attempt, I tried to analyse cortical mCherry in the HeLa cell lines stably expressing the NuMA^{Cter} constructs. However, I soon realized that the expression levels were too low and the cortical recruitment of the smaller NuMA fragments too weak to allow a reliable evaluation of cortical signals. Therefore, to obtain

higher expression levels, I resorted to transiently transfect the same constructs in HeLa cells. Because also under these conditions, the levels of cortical NuMA^{Cter} were much lower than for endogenous NuMA, to compare the diverse mutants, I decided to simply count the percentage of cells with visible cortical mCherry signal rather than using a line-scan quantification. In metaphase, wild-type mCherry-NuMA^{Cter} localizes uniformly at the cortex (Figure 26A, left panel), suggesting that restricting its cortical localization to cortical crescents above the spindle poles requires the N-terminal domain. In the majority of cells, single substitution of Ser-1969 to alanine reduced the localization of NuMA^{Cter} at the cell cortex to the same extent observed for the NuMA^{3Ala}. Conversely, NuMA^{Cter} phosphomimetic mutants of Ser-1969 alone or together with Ser-1991 and Ser-2047 localized at the cortex (Figure 26A-B). Furthermore, I noticed that the NuMA^{Cter} phosphomutant for Ser-2047-Ala did not localize at the cells cortex (Figure 26A-B). Intriguingly, this residue resides in the region of NuMA (encompassing residues 1995-2074) sufficient for membrane localization when expressed in HeLa cells (Zheng et al., 2013)(Figure 9). Thus, this observation seems to suggest an additional Aurora-A-mediated mechanism regulating targeting of NuMA at the plasma membrane in metaphase.

Overall, these data suggested that in metaphase the activity of Aurora-A prevents the accumulation of NuMA at spindle poles by phosphorylation of Ser-1969, and this allows NuMA recruitment at the cortex together with the phosphorylation on Ser-2047.

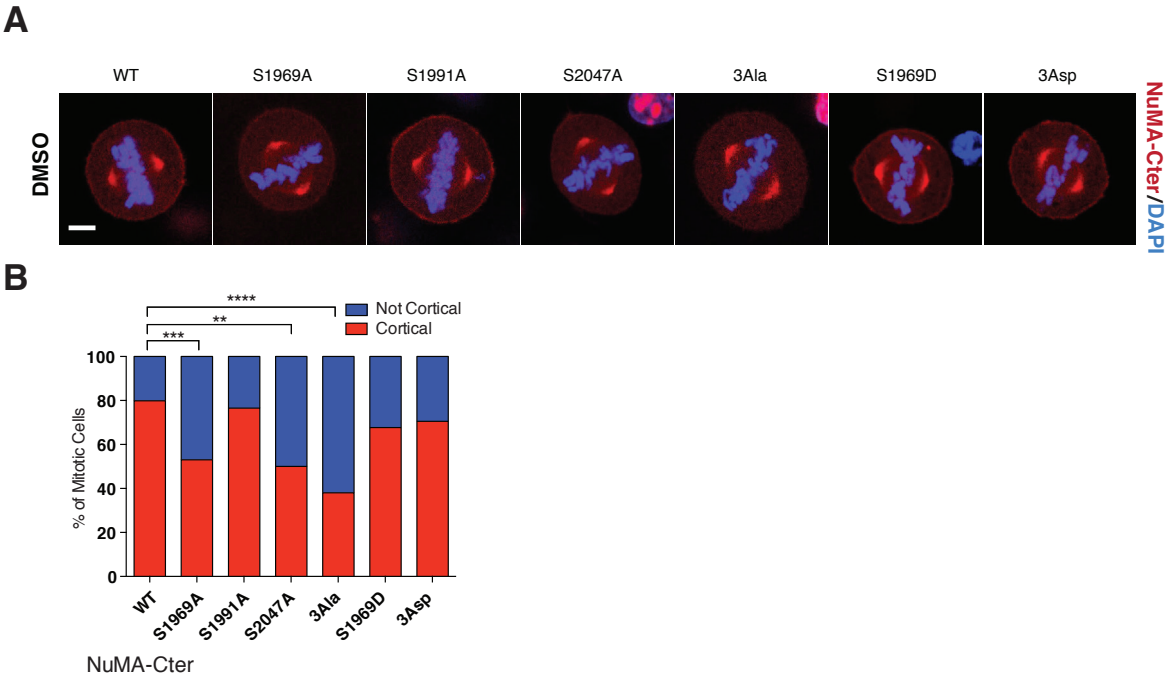

Figure 26 - The Aurora-A-phosphorylations on Ser-1969 and on Ser-2047 regulate cortical NuMA localization. (**A**) Confocal images of metaphase HeLa cells transiently expressing mCherry-NuMA^{Cter} mutants treated with DMSO. The mutants analysed are the same of the HeLa cell lines imaged in (Figure 25 A). (**B**) Analysis of the mCherry signal at the cortex in metaphase HeLa cells transiently expressing mCherry-NuMA^{Cter} mutants. The proportion of cell displaying cortical mCherry signal is plotted in red (% of cortical and not cortical signal; n > 40). ****, *** and ** indicate a statistical difference of $P < 0.0001$, $P < 0.001$ and $P < 0.01$ respectively.

3.1.5 NuMA and microtubules interaction

3.1.5.1 Binding of NuMA to microtubule is independent of Aurora-A

The evidence that Aurora-A inhibition triggers the accumulation of NuMA at the spindle poles indicates that at the spindle poles a receptor of NuMA exists, whose affinity is modulated by Aurora-A. Intriguingly, the phosphosite involved in the enrichment of NuMA at the spindle poles, Ser-1969, lies in the protein region harbouring the previously identified MT-binding domain (Du et al., 2002; Haren and Merdes, 2002). Therefore, we checked whether the phosphorylation of NuMA could affect its affinity for MTs. These experiments were performed by Manuel Carminati, a member of our group. Cosedimentation assays of purified NuMA^{Cter} with taxol-stabilized MTs revealed that Aurora-A phosphorylation or the replacement of the three serine-phosphosites with aspartic acid (3Asp) did not affect the binding affinity of NuMA^{Cter} for MTs *in vitro*

(Figure 27A). Moreover, a cosedimentation assay performed with mitotic lysates of HeLa cells stably expressing mCherry-NuMA^{Cter} and treated with STLC in the presence of increasing concentrations of MTs confirmed that Aurora-A inhibition did not change the affinity of NuMA^{Cter} for MTs under the same conditions by which NuMA^{Cter} accumulates at the spindle poles (Figure 27B).

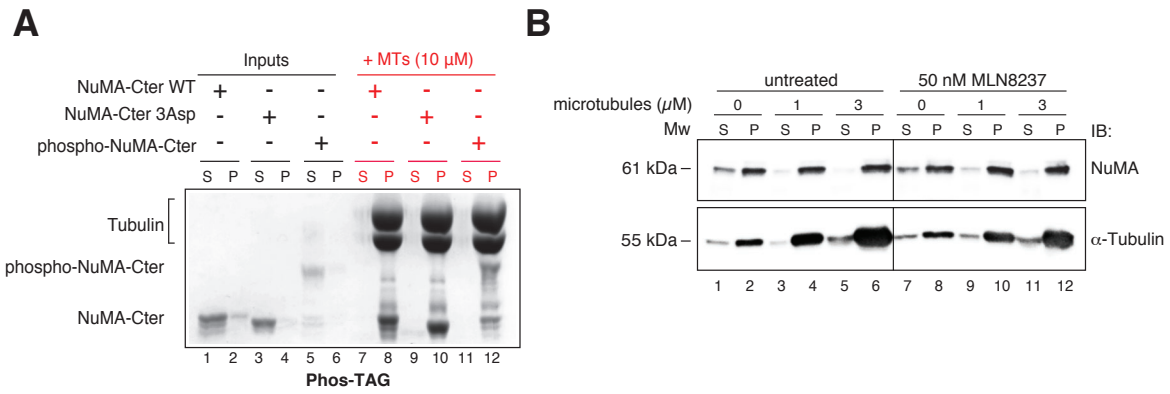

Figure 27 - Binding of NuMA to MTs is independent of Aurora-A. (**A**) Cosedimentation of 2 µM NuMA^{Cter} with 10 µM polymeric tubulin (MTs). Wild-type NuMA^{Cter} unmodified or phosphorylated by Aurora-A, and NuMA^{Cter}-3Asp (Ser-1969/Ser-1991/Ser-2047 replaced with Asp) were analysed in the assay. After cosedimentation, the supernatant (S) and pellet (P) fractions were analysed on a Phos-TAG SDS-PAGE followed by Coomassie staining (*lanes 7-12*). The solubility of NuMA^{Cter} in the absence of MTs was tested as a specificity control (*lanes 1-6*). (**B**) Lysates of mCherry-NuMA^{Cter}–expressing HeLa cells arrested in prometaphase by 5 µM STLC treatment were cosedimented with increasing amounts of exogenous MTs previously polymerized *in vitro*. The MT-binding ability of mCherry-NuMA^{Cter} present in the lysates was assessed in untreated (*lanes 1-6*) and 50 nM MLN8237-treated (*lanes 7-12*) conditions. The presence of NuMA^{Cter} in the pellet (P) and supernatant (S) fractions was monitored by immunoblotting using anti-NuMA antibodies. MTs were visualized by anti-α-tubulin.

3.1.5.2 Aurora-A activity does not impair the MT-bundling activity of NuMA

Dimeric constructs of NuMA encompassing the MT-binding domain have been recently shown to bundle MTs (Forth et al., 2014). To assess whether this activity could be perturbed by Aurora-A, we generated dimeric GST-fusion proteins of NuMA^{Cter} and two complementary subdomains encompassing residues 1821-2001 and 2002-2115, respectively (Figure 28A). The ability of the unmodified or phosphorylated fusion proteins to stabilize and bundle MTs was tested in a MT formation assays (Figure 28B).

Rhodamine-labeled tubulin was incubated in GT buffer supplemented with GTP (see **paragraph 2.15.4** of Material and Methods for details) in the presence of purified GST-tagged NuMA constructs, and the effect on MT formation was visualized by wide-field microscope. $NuMA^{Cter}$ and $NuMA^{2002-2115}$ constructs bundled efficiently MTs in presence and in absence of Aurora-A phosphorylation, whereas on $NuMA^{1821-2001}$ did not, similarly to the GST control (Figure 28B).

Altogether these results confirmed that Aurora-A does not affect the MT binding ability of NuMA nor its capacity to bundle MTs.

3.1.5.3 Identification of a new MT-binding domain

In the MT formation assays described in the previous paragraph, we observed that the NuMA fragment 1821-2001 containing the previously mapped MT-binding domain did not promote MT bundling. To further investigate this unexpected result, we repeated the cosedimentation experiments of Figure 28C with the three C-terminal NuMA fragments used in the MT bundling assay, and found that $NuMA^{2002-2115}$ cosedimented with MTs as the entire $NuMA^{Cter}$, while $NuMA^{1821-2001}$ did not (Figure 28C). We concluded that the MT-binding domain of NuMA lies within the C-terminal region 2002-2115.

I then set out to test whether the newly identified MT-binding domain was implicated in the localization of NuMA at the spindle poles, Previous studies by the Cleveland's laboratory revealed that exon-22 of the murine NuMA gene, corresponding to amino acids 1926-1985 of mouse NuMA and encompassing the mapped MT-binding domain (Du et al., 2002; Haren and Merdes, 2002), is essential to connect the mitotic centrosome to the spindle aster (Silk et al., 2009). Thus I decided to compare the localization at the spindle poles of three constructs: the entire $NuMA^{Cter}$, $NuMA^{1821-2002}$ and $NuMA^{Cter}$ deleted for residues 1944-2003 of human NuMA corresponding to exon-22 of mouse NuMA (NuMA-Δexon-24) (Figure 22). These construct were fused to mCherry, and transiently transfected in HeLa cells.

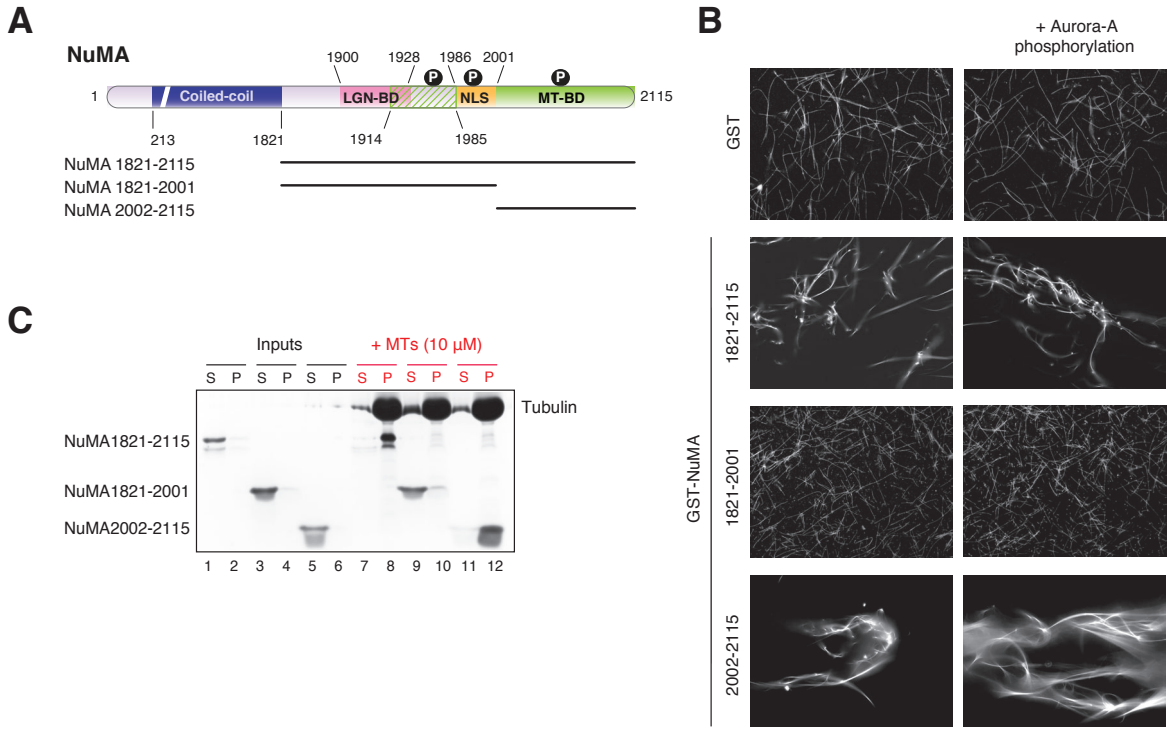

Figure 28 - Aurora-A activity does not impair the MT-bundling activity of NuMA and the identification of a new MT-binding domain of NuMA. (A) Schematic representation of the C-terminal fragments of NuMA (NuMA$^{1821-2115}$, NuMA$^{1821-2001}$ and NuMA$^{2002-2115}$) used in the *in vitro* MT-bundling assay and *in vitro* MT-cosedimentation assay. Domains with known functions are highlighted with different colors including the LGN-binding domain (residues 1900-1928, pink), the *old* MT-binding domain (residues 1914-1985, dashed green) and the nuclear localization signal (NLS, residues 1986-2001, orange). The MT-binding domain identified in this study encompassing residues 2002-2115 is colored in green. P indicates the phospho-serines target of Aurora-A. **(B)** Representative images of *in vitro* MT bundling assay performed with rhodamine labelled tubulin in the presence of GST-NuMA$^{1821-2115}$, GST-NuMA$^{1821-2001}$ and GST-NuMA$^{2002-2115}$, or GST as control. Experiments were performed both with unmodified (left panels) and phosphorylated NuMA fragments (right panels). **(C)** Cosedimentation of 2 µM NuMA^{Cter} fragments with 10 µM polymeric tubulin (MTs). Supernatant (S) and pellet (P) fractions were separated by SDS-PAGE and Coomassie stained (*lanes 7-12*). The solubility of NuMA^{Cter} fragments was separately assessed in the absence of MTs (*lanes 1-6*).

Silk and colleagues showed that removal of exon-22 in the mouse NuMA gene generate a protein unable to localize at the spindle poles (Silk et al., 2009). I confirmed that the spindle poles localization of human NuMA-Δexon-24 (the counterpart of mouse exon-22) is severely compromised (Figure 22A and Figure 29A). NuMA$^{1821\text{-}2002}$, lacking the newly identified MT-binding domain, localized at the spindle poles almost to the same extent of NuMA^{Cter}, indicating that direct MT binding is not required for the recruitment of NuMA at the spindle poles (Figure 29A-B). I concluded that the region of NuMA encompassing residues 1944-2003 mediates spindle poles localization; although it is not involved in direct MT binding. This is fully consistent with our previous finding that the Ser-1969 phosphosite is the major determinant regulating the accumulation of NuMA at the spindle poles. Based on these findings, we propose that the complementary fragments of NuMA^{Cter} identified by our analysis spanning residues 1821-2001 and 2002-2115 contain separate functions: the former one is important for spindle pole localization and the latter for direct association of NuMA with MTs.

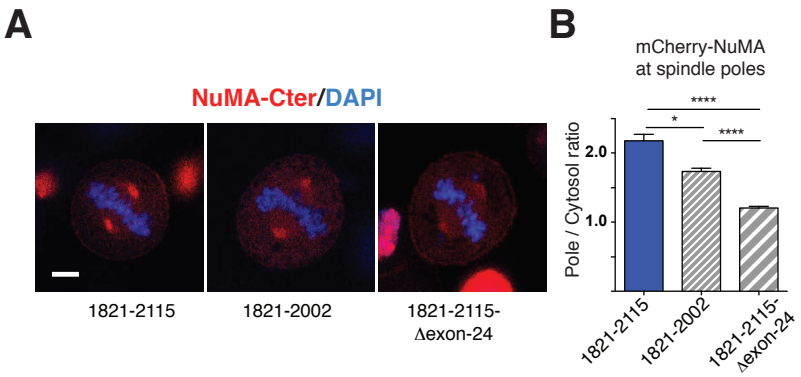

Figure 29 - The direct binding of NuMA to MTs is not required for its recruitment at the spindle poles. (**A**) Confocal sections of metaphase HeLa cells transiently expressing the entire mCherry-NuMA^{Cter} (residues 1821-2115), or its deletions Δ2003-2115 and Δ1944-2003 (Δexon-24). (**B**) Histograms show the quantification of the mCherry signal at the spindle poles with respect to cytoplasm (means ± SEM; n > 30 from three independent experiments). **** and * indicate a statistical difference of $P < 0.0001$ and $P < 0.05$ respectively.

3.1.5.4 The binding of NuMA with MTs does not interfere with its association with LGN

The newly identified MT-binding domain of NuMA lies downstream of the LGN-binding stretch, spanning residues 1900-1928 (Figure 22A)(Culurgioni et al., 2011; Du et al., 2002; Zhu et al., 2011b), rather than overlapping with it as previously reported. This result opens the possibility that a single molecule of NuMA could interact simultaneously with both LGN and MTs. To check this hypothesis, we cosedimented MTs with NuMA fragments containing only the LGN-binding region ($NuMA^{1821-2001}$), only the MT-binding domain ($NuMA^{2002-2115}$) or both ($NuMA^{Cter}$) in the presence of equimolar amounts of LGN^{TPR}. As expected, the entire $NuMA^{Cter}$ is found in the pellet fraction with LGN^{TPR}, $NuMA^{1821-2001}$ remains in the soluble fraction with LGN^{TPR}, and $NuMA^{2002-2115}$ went in the pellet but left LGN^{TPR} in the supernatant (Figure 30A). Thus, our analyses revealed that $NuMA^{Cter}$ could associate simultaneously with LGN and MTs.

3.1.5.5 Aurora-A does not affect the interaction of NuMA with LGN

Finally, we checked if the direct interaction between LGN and NuMA could be perturbed by Aurora-A phosphorylation. Impairment of the binding between LGN and NuMA could explain the reduction of cortical NuMA upon Aurora-A inhibition (**Paragraph 3.1.3.2**). It has been shown that LGN recognizes the C-terminal motif of NuMA encompassing residues 1900-1928 with its N-terminal TPR domain (Du et al., 2002; Zhu et al., 2011b), and that this interaction is indispensable for spindle orientation during metaphase (Du and Macara, 2004; Du et al., 2001; Seldin et al., 2013). To test the effect of Aurora-A on the LGN:NuMA binding we performed a pull-down assay with GST-LGN^{TPR} adsorbed on beads and phosphorylated $NuMA^{Cter}$ in solution. The amount of $NuMA^{Cter}$ retained on beads with LGN^{TPR} did not increase upon Aurora-A phosphorylation, indicating that Aurora-A phosphorylation did not affect the binding between the two proteins. The same pull-down performed with $NuMA^{Cter}$ 3Asp mutant confirmed these results (Figure 30B).

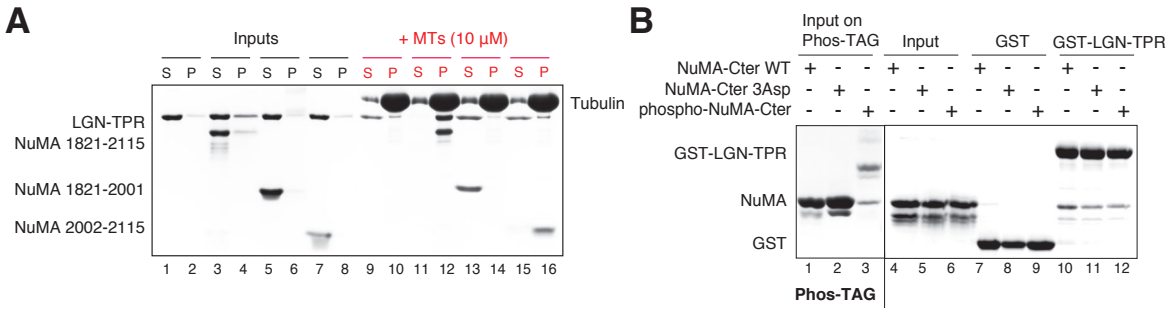

Figure 30 - The binding of NuMA to MTs does not interfere with the LGN:NuMA interaction, which in turn is not perturbed by Aurora-A phosphorylation. (**A**) MT cosedimentation assays conducted as in Figure 28C in the presence of 1 µM LGN^{TPR}. (**B**) *In vitro* pull-down assay performed with GST-LGN^{TPR} absorbed on glutathione beads and purified $NuMA^{Cter}$ in solution. After washes, species retained on beads were separated by SDS-PAGE and Coomassie-stained. The $NuMA^{Cter}$ samples used in the pull-down experiment were also separately loaded on a Phos-TAG SDS-PAGE to monitor their phosphorylation state (*lanes 1-3*).

In summary, our results revealed: (A) the binding of NuMA to MT and LGN is independent of Aurora-A activity; (B) The fragment of NuMA encompassing residues 2002-2115 contains the MT-binding domain, while residues 1821-2001 are involved in spindle pole association regulated by Aurora-A; (C) $NuMA^{Cter}$ could interact simultaneously with LGN and MTs.

3.1.6 Rescue of the spindle orientation phenotype by targeting NuMA at the cortex

To position the mitotic spindle properly, cortical NuMA:LGN:Gαi complexes exert pulling forces on astral MTs via the interaction between NuMA and the minus-end directed motor Dynein/Dynactin (Kotak et al., 2012; Seldin et al., 2013). Our previous experiments showed that Aurora-A inhibition prevents cortical enrichment of NuMA, leaving LGN unaltered, suggesting that Aurora-A could cause spindle misorientation by impairing the cortical localization of NuMA. To explore this possibility, I investigated whether ectopic targeting of NuMA at the membrane could bypass the requirement of Aurora-A activity for spindle orientation. Studies from the Cheeseman laboratory revealed that fusion of the GoLoco region of LGN to the C-terminal domain of NuMA suffice to target $NuMA^{Cter}$ at the plasma membrane (Kiyomitsu and Cheeseman, 2012). Therefore, for the rescue experiments, I generated a chimeric protein carrying the GoLoco region of LGN

encompassing residues 359-677 fused C-terminally to GFP-NuMA (GFP-NuMA-GoLoco hereon) (Figure 31A). As negative control of the rescue experiments, I used HeLa cells expressing GFP-NuMA full-length. First, I tested the localization in mitosis of the two constructs transiently transfected in HeLa cells. When expressed at low levels, GFP-NuMA recapitulated the mitotic localization of endogenous NuMA at the cortex and at the spindle poles. In MLN-treated cells, the GFP signal of GFP-NuMA increased at the spindle poles and was abrogated at the cortex, as expected (Figure 31B, left panel). In mitotic cells, the GFP-NuMA-GoLoco chimera localized uniformly at the plasma membrane at higher levels than GFP-NuMA, while it displayed a weaker localization at the spindle poles. This phenotype is likely due to the constitutive association of NuMA-GoLoco with membrane-bound Gαi moieties. Upon MLN8237 treatment, GFP-NuMA-GoLoco accumulated at the spindle poles similarly to GFP-NuMA, however part of the protein was still visible at the cortex (Figure 31B, right panel). Interestingly, preliminary observations of mitotic cells in the x-z projection revealed that in the GFP-NuMA-GoLoco expressing cells the spindle axis did not misalign upon 50 nM MLN8237 treatment as observed in the GFP-NuMA expressing cells (Figure 31B, right panel).

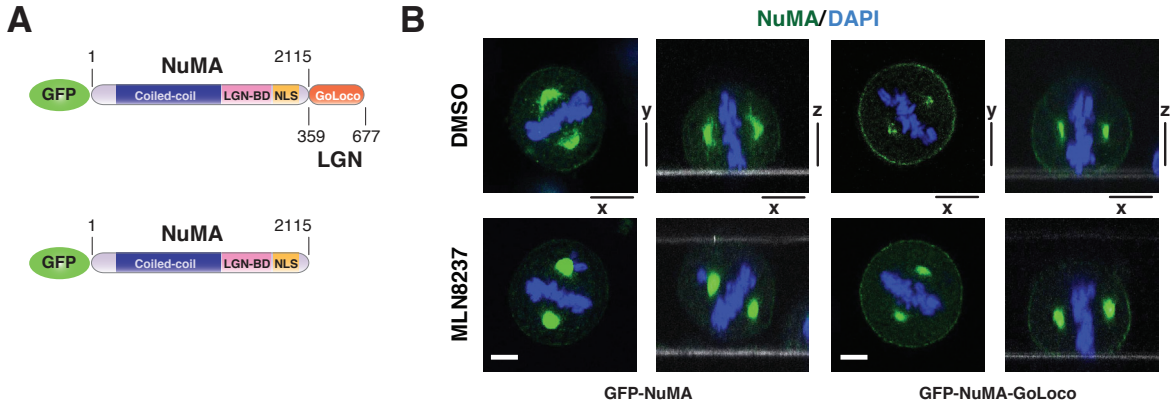

Figure 31 - Characterization of the GFP-NuMA-GoLoco chimera used in the rescue experiments. (**A**) Schematic representation of GFP-NuMA full length, and GFP-NuMA-GoLoco proteins used for the time-lapse rescue experiments. (**B**) Confocal x-y and x-z sections of HeLa cells transfected with GFP-NuMA-GoLoco and GFP-NuMA, and treated with DMSO (top) or 50 nM MLN8237 (bottom). The localization of exogenous NuMA proteins and DNA was visualized by GFP and DAPI, respectively. Scale bars correspond to 5 μm.

To better quantify the extent of spindle misalignment, I performed live-cell imaging experiments of cells transfected with GFP-NuMA and GFP-NuMA-GoLoco using the GFP signal and DIC to monitor the spindle poles and the position of the forming daughter cells, respectively (Figure 32). As expected, time-lapse video-recording of cells expressing GFP-NuMA treated with 50 nM MLN8237 showed misoriented spindles in 40% of divisions, whereas only 10% of unperturbed cells showed a similar phenotype (Figure 32A-B). Conversely, cells expressing GFP-NuMA-GoLoco underwent about 20% of misoriented divisions regardless of the MLN8237 treatment (Figure 32A-B). I also noticed an enhanced misorientation phenotype in unperturbed cells expressing GFP-NuMA-GoLoco compared to wild-type, which I think might be caused by the increased targeting of NuMA to the cell cortex by the LGN-GoLoco domain, which can induce abnormal oscillatory movements of the spindle (Figures 31B and 32A-B)(Kotak et al., 2012). Notably, the presence of GFP-NuMA-GoLoco also partly rescued the mitotic delay induced by MLN8237 treatment (Figure 32A). Altogether the results suggest that the misoriented phonotype that we observed upon Aurora-A inhibition is due to impairment in the cortical recruitment of NuMA.

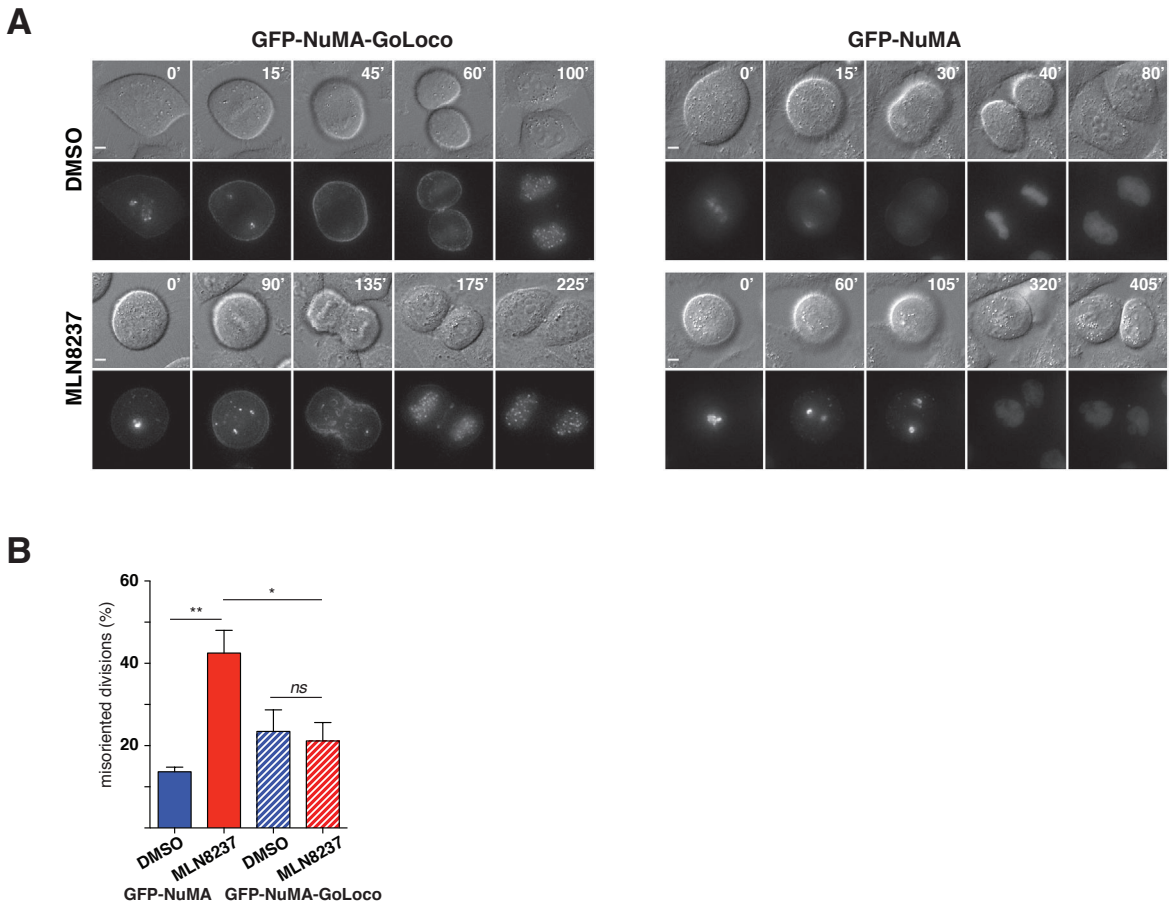

Figure 32 - Rescue of the spindle misorientation phenotype by ectopic cortical targeting of NuMA. (**A**) DIC and GFP-fluorescent frames from time-lapse video-recording of mitotic HeLa cells expressing GFP-NuMA-GoLoco or GFP-NuMA, and treated with DMSO or MLN8237. Minutes from the round-up are indicated at the top right corners. Scale bars: 5 μm. (**B**) Quantification (%) of misoriented bipolar divisions of HeLa cells treated as in (A) (means ± SEM; for all conditions n > 45 from three independent experiments). About 13% and 42% of GFP-NuMA expressing cells were misoriented in DMSO or in 50 nM MLN8237, respectively. GFP-NuMA-GoLoco expressing cells underwent 23% of misaligned divisions in DMSO, and 21% upon MLN8732 treatment. ** and * indicate a statistical difference of $P < 0.01$ and $P < 0.05$ respectively.

3.2 Lgl2

3.2.1 Lgl2, a putative new player in the spindle orientation

Biochemical evidence from Yasumi and co-workers suggested that the C-terminal region of human Lgl2 could associate directly with LGN^{TPR}, and that overexpression or knocking-down of Lgl2 in HEK293t cells could cause spindle disorganization and multiple micronuclei (Yasumi et al., 2005).

On these premises, I set out to study the putative role of Lgl2 in spindle orientation. First, I tried to reproduce the direct interaction between the C-terminal domain of Lgl2 and the TPR domain of LGN *in vitro*. The domain structure of Lgl2 consists of two N-terminal β-propellers followed by an unstructured C-terminal region (Figure 33A). Thus, I designed a few C-terminal constructs of Lgl2 based on literature (Yasumi et al., 2005), sequences alignment of Lgl orthologs from different species, and secondary structure prediction. I then tried to develop protocols to purify Lgl2 full-length or its C-terminal fragments from different recombinant sources, including *E. coli* BL21 and *High5* insect cells infected with recombinant baculoviruses. Unfortunately, under all tested conditions, the Lgl2 constructs were not soluble (data not shown). A possible explanation for these persistent insolubility problems is that post-translational modifications or specific chaperons are required for the correct folding of the protein.

I then tried to confirm the association between Lgl2 and LGN *ex vivo*. To this end, I performed a pull-down assays using GST-LGN^{TPR} adsorbed on GSH-beads and a HA-tagged Lgl2 construct encompassing residues 641-1020 expressed in HEK293t cells. By expressing the Lgl2 C-terminal domain in HEK293t cells I was hoping to overcome the insolubility problems observed upon bacterial expression. Mitotic phosphorylation of Lgl2 has been reported to control a conformational rearrangement required for association of the protein to the plasma membrane (Betschinger et al., 2005). Thus, to enrich for mitotic post-translational modifications possibly affecting the Lgl2:LGN interaction, I arrested HEK293t cells transfected with HA-Lgl2 by nocodazole treatment. However, under these

conditions, I could not detect binding between LGN and the C-terminal domain of Lgl2 (Figure 33B), suggesting that the low affinity or the transient nature of the interaction hampers its detection. Next, to assess whether the presence of the N-terminal region of Lgl2 could stabilize the protein and preserve its interaction potential, I performed a co-immunoprecipitation (Co-IP) experiment in mitotic cells expressing GFP-tagged full-length Lgl2. Also in this case, I could not score any interaction between Lgl2 and endogenous LGN (Figure 33B). Most interestingly, in the Co-IP experiments performed with full-length GFP-Lgl2, I noticed that Lgl2 interacted with NuMA (Figure 33C), thus suggesting an alternative molecular explanation underlying the spindle orientation functions of Lgl2.

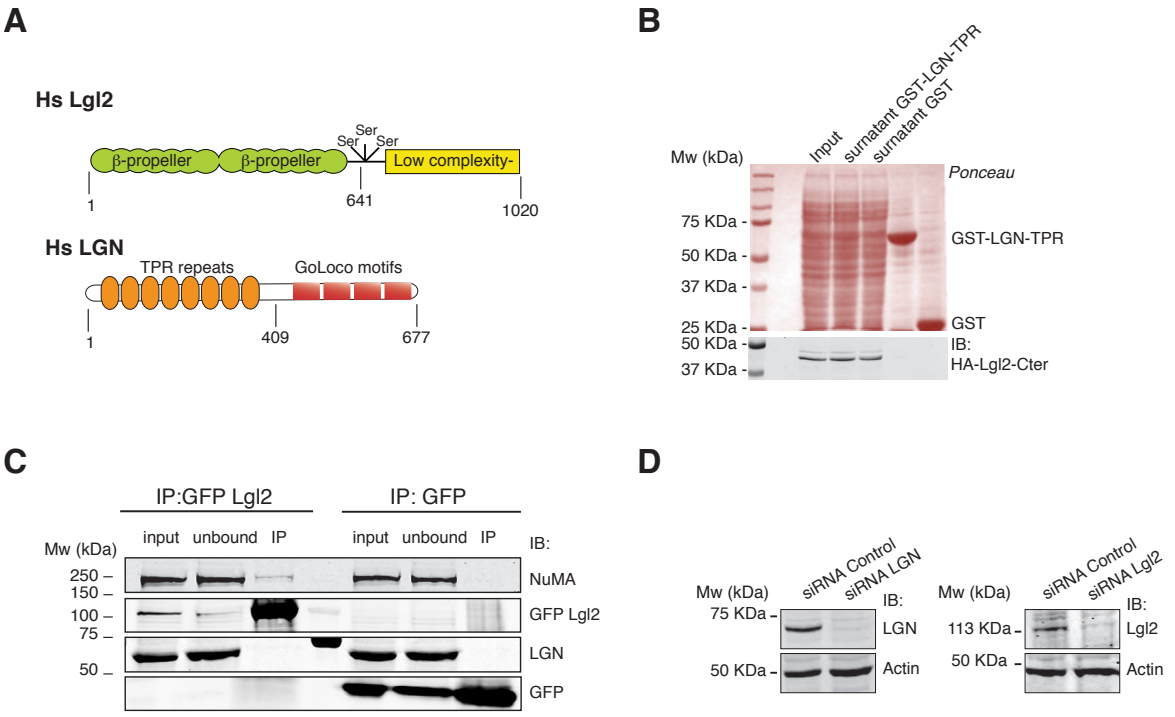

Figure 33 - Lgl2:LGN interaction was not reconstituted *in vitro* and *ex vivo*. Human Lgl2 interacted with NuMA. (**A**) Schematic diagrams of the domain organizations of LGN and Lgl2. Lgl2 consists of two β-propeller domains, followed by a C-terminal low complexity region. In the central parts are present three conserved phosphorylation sites target of the aPKC kinase (Ser-645, Ser-649 and Ser-653)(Zhu et al., 2014). LGN consist of eight TPR repeats at the N-terminus and four GoLoco motifs at the C-terminus. (**B**) *In vitro* pull-down assay performed with 5 μM of GST-LGN^{TPR} absorbed on glutathione beads and cellular lysate of mitotic HEK293t cells transiently expressing human HA-tagged Lgl2$^{641-1020}$. After washes, species retained on beads were separated by SDS-PAGE and blotted with anti-HA antibody. (**C**) Mitotic HeLa cells transiently expressing

GFP-Lgl2 or GFP-tag were lysated. Cell lysates were immunoprecipitated with an antibody against GFP then analysed by Western blotting with anti-NuMA and anti-LGN antibodies. The binding of NuMA to GFP-Lgl2 was scored in three independent experiments. (**D**) Immunoblotting of lysates of HeLa cell lines transiently interfered with LGN, Lgl2 and scrambled siRNAs showing the efficiency of the siRNA-based depletions. Actin was used as loading control.

To further investigate the issue, I decided to characterize the localization of Lgl2 in mitotic cells. By transient transfection of GFP-Lgl2 in HeLa cells synchronized with a single thymidine block, I found that Lgl2 localizes uniformly at the cortex from prometaphase to telophase (Figure 34A). Encouraged by these finding, I explored whether Lgl2 could be implicated in spindle orientation. To this end, I transfected HeLa cells with small-interfering RNA oligos (siRNAs) targeting Lgl2, LGN (as positive control) or scrambled oligos (as negative control). Immunoblotting from lysate of treated HeLa cells showed the efficiency of the siRNA-based depletion for both Lgl2 and LGN, which was about 90% of knock-down compared to scrambled siRNA (Figure 33D). Then I analysed the spindle orientation of Lgl2-depleted cells with the method previously described (see **paragraph 2.7** of Material and Methods for details). In cells interfered for Lgl2 or LGN, I observed a spindle randomization (Figure 34B-C). To quantify the misorientation phenotype, I measured the distribution of spindle axis angles. In cells silenced for both Lgl2 and LGN, the average spindle angles were 11.9° and 12.5° instead of 6.3° of control cells (Figure 34C). Accordingly, the spindle angular distribution shifted towards grater values in Lgl2- and LGN-depleted cells as compared to control conditions (Figure 34C). Altogether, these results demonstrate that Lgl2 regulates the spindle alignment in HeLa cells, and suggested that the molecular mechanism underlying this function is the interaction between Lgl2 and NuMA rather than with LGN as was previously reported.

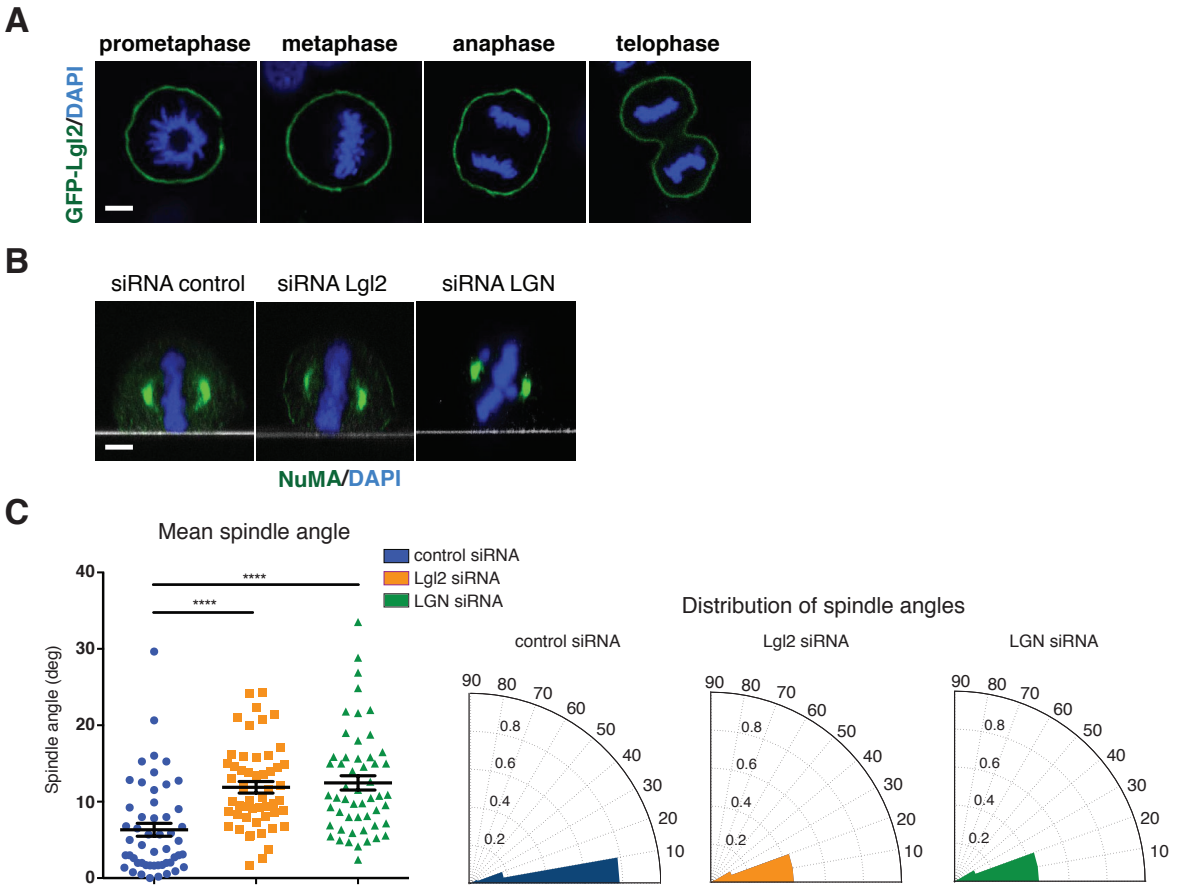

Figure 34 - Lgl2 is required for proper spindle orientation in HeLa cells. (**A**) Cortical localization of GFP-Lgl2 transfected in HeLa cells. Lgl2 distributes uniformly at the cortex throughout mitosis. (**B**) Representative confocal z-sections of mitotic HeLa cells expressing a control siRNA and siRNAs targeting Lgl2 and LGN, fixed and stained for NuMA and DNA (DAPI). The plane of the coverslip is visible as a white line. (**C**) Quantification of the mitotic spindle alignment to the plane of the coverslip of scrambled-, Lgl2- and LGN- interfered HeLa cells. Dot plots (with means ± SEM; n > 50) and radial histograms illustrate the distributions of the spindle axis angles for the three interfering conditions. **** indicates a statistical difference of $P < 0.0001$ between control cells and Lgl2 or LGN siRNA expressing cells from three independent experiments. All the scale bars correspond to 5 μm.

3.3 Afadin

3.3.1 Afadin promotes correct spindle orientation in HeLa cells and in polarized Caco-2 cells grown in cysts

Increasing evidence point at the relevance of the acto-myosin cortex and adhesion proteins in regulating the spindle orientation (den Elzen et al., 2009; Fink et al., 2011; Kunda and Baum, 2009; Machicoane et al., 2014; Nakajima et al., 2013; Sandquist et al., 2011; Thery et al., 2005; Toyoshima and Nishida, 2007). Thus, the actin-binding property of Afadin, its documented function in junctional organization, and the spindle orientation role reported for its fly ortholog make it an ideal candidate to play a pivotal role in F-actin-dependent spindle orientation pathways in vertebrates. In vertebrate epithelia, Afadin is involved in linking nectin-based AJs to the actin cytoskeleton (Ikeda et al., 1999; Lorger and Moelling, 2006; Mandai et al., 1997; Sawyer et al., 2009; Takai et al., 2008). In vertebrates, Afadin exists in two splicing variants differing in the C-terminal region (Mandai et al., 1997). Long splicing variants of Afadin contain two Ras-associating domains, a Forked-Head domain (FHA), a diluted domain (DIL), a PDZ domain and an F-actin binding domain at the C-terminus (Figure 35A). Thus, to investigate the spindle-orientation functions of Afadin we set out to study its long isoform.

3.3.1.1 Afadin co-localized with LGN and NuMA in HeLa cells

To start addressing the mitotic function of Afadin, I first characterized its localization in mitotic HeLa cells. To this aim, I employed a polyclonal antibody generated in the laboratory, which was raised against the fragment 1514-1824 of the isoform-4 of human Afadin (Figure 35B). Confocal microscopy showed that from prometaphase to anaphase Afadin localizes uniformly at the cortex, and in metaphase co-localizes with LGN and NuMA at the polar region of the cell cortex. In telophase, it enriches at the cortical region in proximity to the cleavage furrow (Figure 35C). In interphase, Afadin is enriched at the cell-to-cell contact in confluent cells; otherwise it is cytosolic (data not shown). The

cortical localization displayed by Afadin in mitosis encouraged us to further explore whether it could be implicated in spindle orientation.

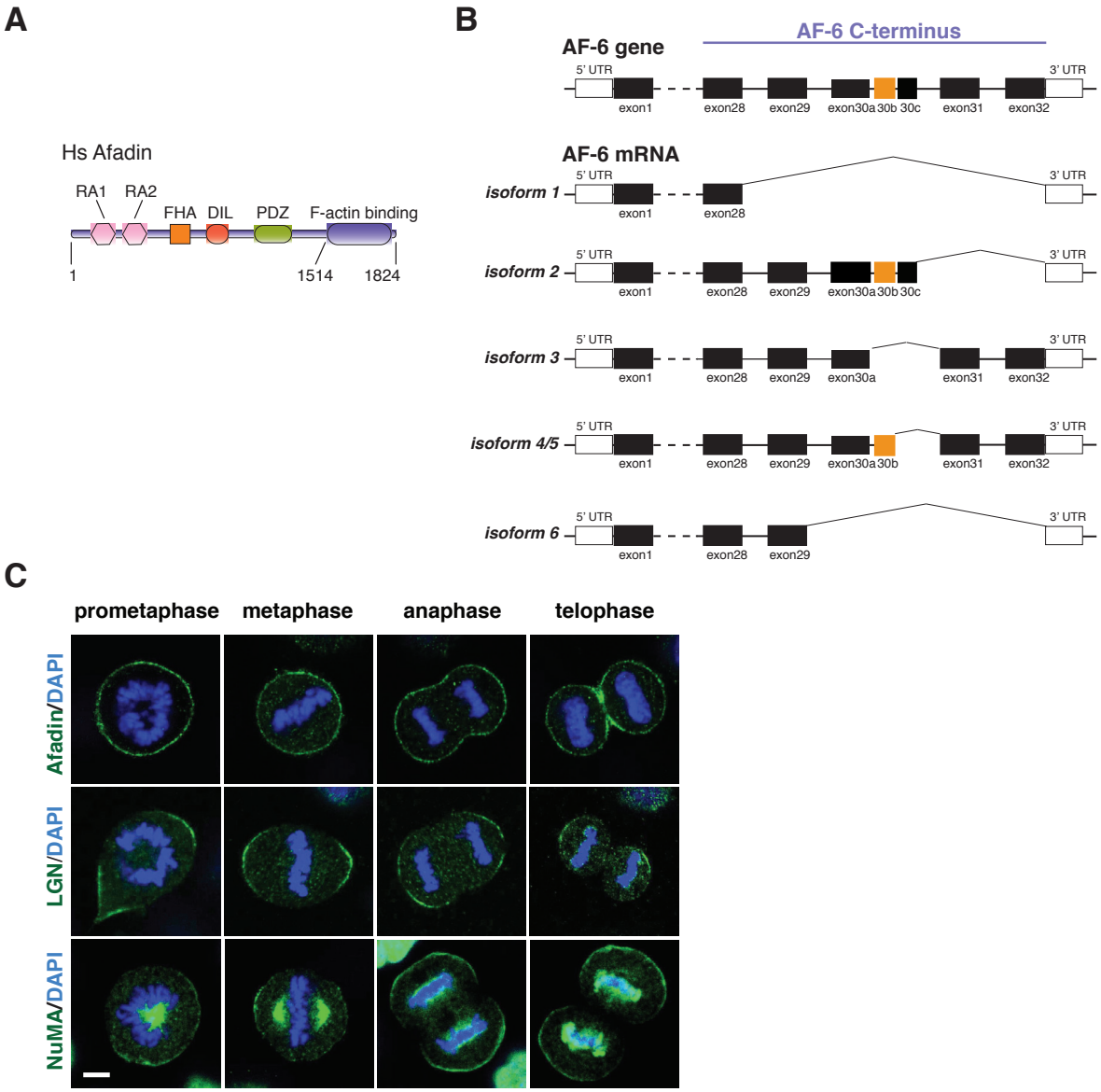

Figure 35 - In mitosis Afadin co-localizes with LGN and NuMA. (**A**) Schematic representation of the domain structure of long isoforms of human Afadin consisting of two Ras-association domains (RA1 and RA2), a Fork-Head domain (FHA), a Dilute domain (DIL) and a PDZ (PSD95/Dlg/ZO-1) domain, followed by a C-terminal F-actin binding region. **(B)** Scheme of human Afadin/AF-6/MLLT4 gene, and its splice variants. The AF-6 gene is located on human chromosome 6, and consists of 32 exons. Alternative splicing produces six transcripts differing in their C-terminal region. Human Afadin isoforms 1 and 6 stop at exons 28 and 29 respectively, and are similar to *short* variant of rat Afadin (also known as *s-Afadin*), which was reported to be unable to bind to F-actin. Human Afadin isoforms 2, 3, 4 and 5 are similar to *long* rat Afadin (*l*-Afadin), which binds to F-actin. Isoforms 4 and 5 differ for the presence of additional 11 residues between exon 28 and 29. The LGN-binding site of Afadin characterized in this study is coded by exon 30 (highlighted in orange), and is present in all human long isoforms except isoform-3. (**C**) Cortical

localization of endogenous Afadin in HeLa cells. Afadin distributes uniformly at the cortex throughout mitosis, and localizes with LGN and NuMA above the spindle poles from prometaphase to anaphase. In telophase Afadin enriches at the cortical region in proximity of the cleavage furrow.

3.1.1.2 Afadin and spindle orientation in HeLa cells

Previous studies had established that the ortholog of Afadin in *Drosophila*, known as Canoe, binds to LGN/Pins, and contributes to proper spindle positioning (Speicher et al., 2008; Wee et al., 2011). To start addressing the mitotic role of Afadin in vertebrate cells, I used two lentiviral short-hairpin RNA vectors (shRNA-1/2) targeting human Afadin to generate HeLa cell lines stably interfered for Afadin. I also produced a HeLa cell line expressing a scrambled shRNA oligo to be used as negative control. Immunofluorescence analysis (Figure 36A), immunoblotting from interfered lysates (Figure 37A) and qPCR analysis (Figure 37B) showed that for both hairpins shRNA-1/2 the efficiency of the shRNA-based depletion was about 80% as compared to control shRNA. I then analyse the spindle alignment of the interfered cell lines with the same protocols used for the Aurora-A project (see **paragraph 3.1.2** and **paragraph 2.7** of Material and Methods for details). Briefly, HeLa cell lines were grown on fibronectin-coated slides and synchronized by single thymidine block, and then imaged in the x-z plane. In wild-type HeLa cells, the mitotic spindles were aligned parallel to the substratum, while in both cells lines interfered for Afadin I observed a pronounced spindle randomization (Figure 37B). To quantify the misorientation defects, I measured the angles between the substratum and the pole-to-pole axis (see **paragraph 2.7** of Material and Methods for details). In the cell lines lacking Afadin, the average spindle angle were 13.9° and 15.4° instead of 7.6° of the control cells (Figure 37C). Accordingly, the spindle angular distribution of Afadin-depleted cells shifted towards grater values compared to wild-type HeLa (Figure 37C). Altogether, these results revealed that Afadin contributes to spindle alignment in adherent HeLa cells in culture.

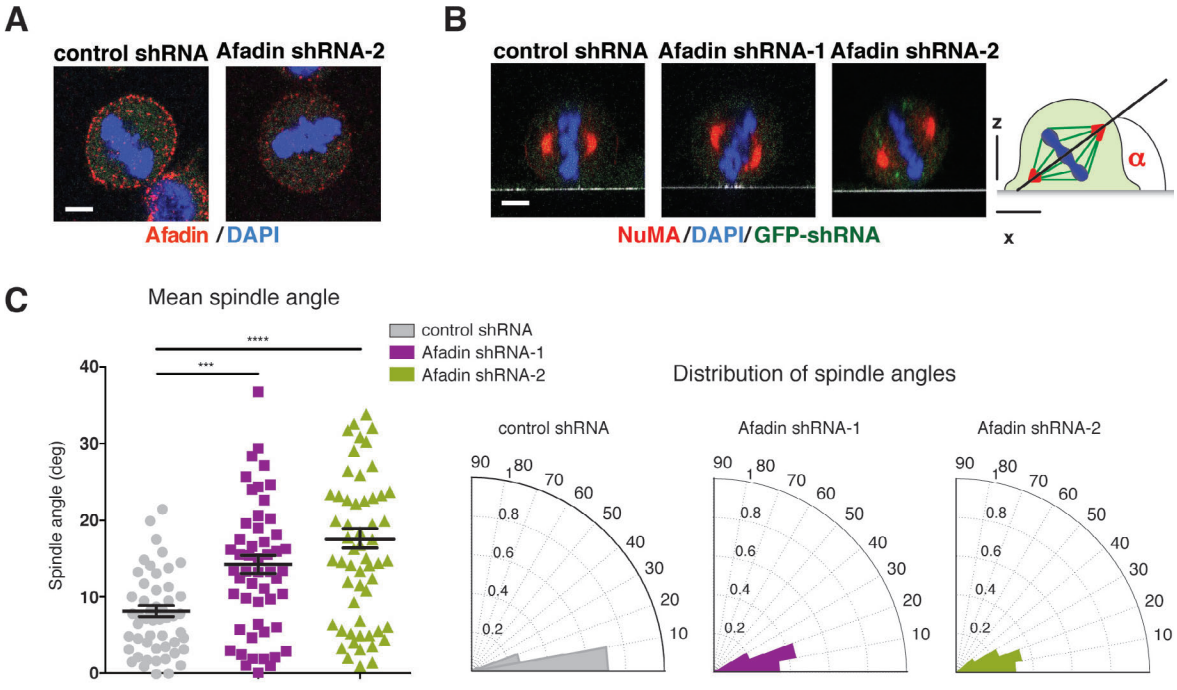

Figure 36 - Afadin is required for proper spindle orientation in HeLa cells. (**A**) Confocal sections of mitotic HeLa cells expressing a control shRNA and shRNA-2 targeting Afadin. Metaphase cells were fixed and stained for endogenous Afadin. Afadin staining was lost in Afadin shRNA-2 expressing cells. The scale bar corresponds to 5 μm. (**B**) Representative confocal z-sections of mitotic HeLa cells stably expressing control shRNA or two Afadin-targeting shRNAs (green GFP reporter). Cells were stained for NuMA (red) and DNA (DAPI, blue). The plane of the coverslip is visible as a white line. A schematic representation of the experimental setting is shown in the right panel. (**C**) Quantification of the mitotic spindle angles to the plane of the coverslip in wild-type and Afadin-interfered HeLa cells. Scatter plots (with means ± SEM) and radial histograms illustrate the distributions of the spindle axis angles for the three cell lines. **** indicates a statistical difference of $P < 0.0001$ between control cells and Afadin shRNA expressing cells from three independent experiments, *** indicates $P < 0.001$. Scale bars correspond to 5 μm.

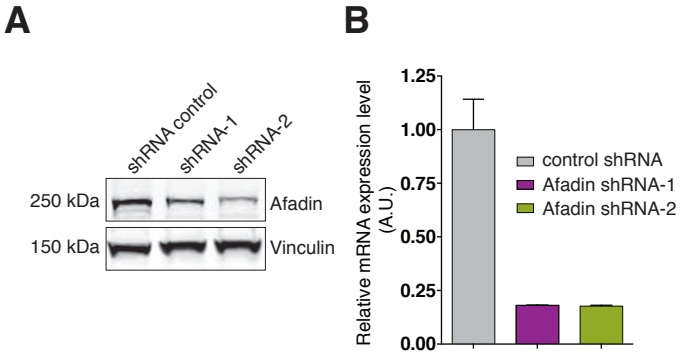

Figure 37 - Generation HeLa cell lines stably interfered for Afadin. (**A**) Immunoblotting of lysates of HeLa cell lines stably interfered for Afadin showing the efficiency of the shRNA-based depletions. Vinculin was used as loading control. (**B**) Analysis of Afadin expression levels by qPCR in lysates of HeLa cells wild-type or stably interfered for Afadin. Levels of the Afadin mRNA were normalized to the GAPDH internal control.

3.3.1.3 Role of Afadin in Caco-2 planar divisions and cystogenesis

Afadin is an adhesion protein required for the stabilization of the cell-cell junctions during epithelial formation (Ikeda et al., 1999; Mandai et al., 1997). To understand the functional relevance of the spindle orientation functions of Afadin in the morphogenesis of polarized epithelia, I analysed the growth of three-dimensional cysts of Caco-2 cells. When seeded in Matrigel, wild-type Caco-2 cells undergo planar divisions to form monolayer epithelial spheres with the apical side facing the inner lumen (Jaffe et al., 2008). I first generated a Caco-2 cell line expressing the same Afadin shRNA-2 hairpin, and verified that the Afadin protein levels were significantly reduced compared to wild-type Caco-2 by immunoblotting and qPCR (Figure 38A-B). Then I compared the cystogenesis of wild-type and Afadin-ablated Caco-2 cells (see **paragraph 2.1.2** of Material and Methods for details). As expected, the majority of wild-type cells form single-lumen cysts. Conversely, cysts grown from Caco-2 cells lacking Afadin fail to organize a single lumen, and grow as multi-lumen acini or cellular spheres (Figure 39A-B). The phenotype that we observed in the Afadin-ablated Caco-2 cells is compatible with spindle orientation defects, since it is similar to what reported for ablation of LGN (Zheng et al., 2010). Consistently, visualization of cell divisions in cysts formed by Afadin-depleted cells revealed that the mitotic spindle axis was not oriented parallel to the basal membrane, as observed in control cysts (Figure 39A). Nonetheless, it is not possible to rule out that also junctional defects caused by Afadin loss could contribute to the multiple lumen phenotype displayed by Caco-2 interfered cysts. Based on these findings, we conclude that Afadin is required for correct epithelial cystogenesis and planar cell divisions.

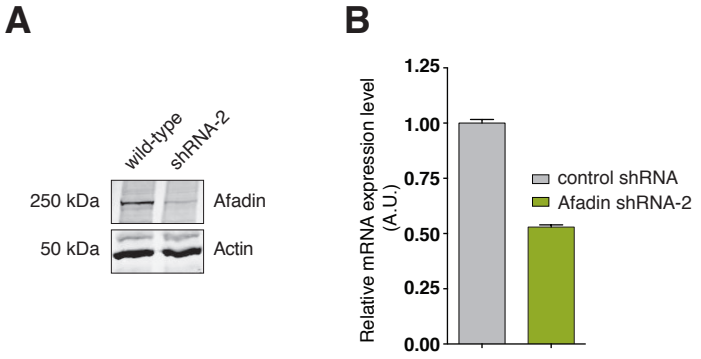

Figure 38 - Efficiency of the shRNA-2-based depletion of Afadin in Caco-2 cells. (**A-B**) Lysates of Caco-2 wild-type or stably-expressing the shRNA-2 targeting Afadin were analysed by immunoblotting (actin was used as loading control), and qPCR as in Figure 37.

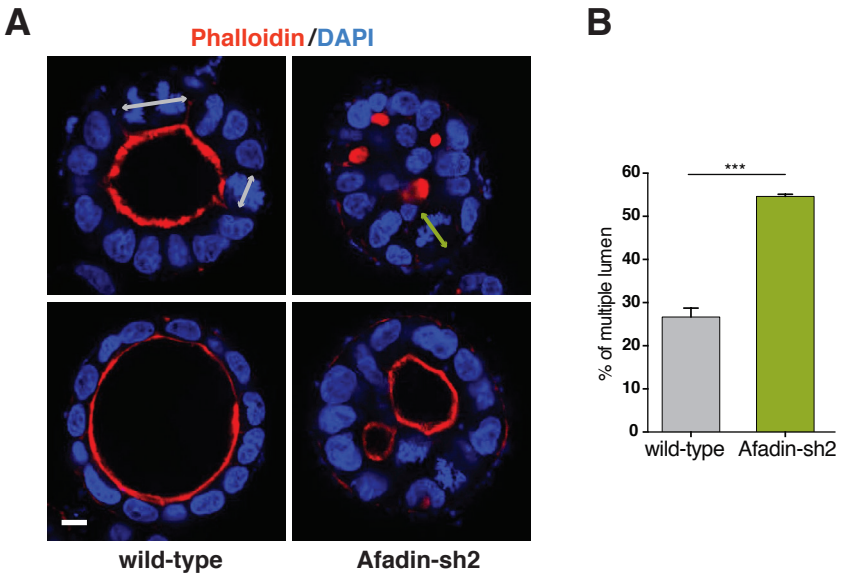

Figure 39 - Role of Afadin in Caco-2 planar divisions and cystogenesis. (**A**) Caco-2 cells wild-type or lacking Afadin were cultured as a single-cell in Matrigel, and after 6 days fixed and stained with TRITC-conjugated Phalloidin and DAPI. Confocal sections of the equatorial region of the cysts revealed that control Caco-2 cells form monolayered spheres with a single lumen, whereas most of the Caco-2 cells lacking Afadin grow as full or multi-lumen spheres. Top, left: mitotic cells form wild-type cysts align the spindle along the epithelial plane (visualized as a white arrowed line). Top right: Afadin-depleted Caco-2 cells undergo misoriented divisions with the spindle axis pointing toward the centre of the cyst (green arrowed line). (**B**) Quantification of defective cystogenesis as percentage of cysts with single lumen of Caco-2 cells wild-type or lacking Afadin (mean ± SD for about 100 cysts from 3 independent experiments). *** indicates a statistical difference of $P < 0.001$ between control cysts and Afadin shRNA-2 expressing cysts. Scale bar corresponds to 10 μm.

3.3.2 In mitosis Afadin is required for cortical recruitment of LGN, NuMA, and Dynein/Dynactin

According to the current model, oriented cell divisions require cortical targeting of Dynein/Dynactin via the NuMA:LGN:Gαi complex (Kotak et al., 2012). In order to explore the molecular mechanism by which Afadin contributes to oriented divisions, I analysed the effect of Afadin silencing on the localization of LGN, NuMA, and the Dynactin subunit $p150^{Glued}$ in mitotic HeLa cells. In control conditions, in metaphase LGN, NuMA and $p150^{Glued}$ enrich in crescents at a polar regions at the cortex above the spindle poles (Figure 40A). However, in Afadin knockdown cells, these proteins fail to localize at the cortex. (Figure 40A) Quantification of the cortical signals by line-scan (see **paragraph 2.8.2** of Material and Methods for details) showed that the levels of LGN at the cortex in Afadin-depleted cells were about 3-fold lower then in control cells, but still significantly higher compared to cytoplasmic levels (Figure 40A). This evidence seem to suggest that Afadin is only one of the anchoring mechanisms securing LGN at the cortex, and is fully in line with other evidence indicating that also Dlg and Gαi-GDP play essential functions in the cortical recruitment of LGN in metaphase (Du and Macara, 2004; Peyre et al., 2011; Saadaoui et al., 2014; Woodard et al., 2011; Zheng et al., 2010). Depletion of endogenous Afadin abrogates cortical localization of NuMA and $p150^{Glued}$ (Figure 40A). Most interestingly, I observed that the reduction of the cortical levels of LGN, NuMA and $p150^{Glued}$ of Afadin-ablated cells persisted in anaphase (Figure 40B), in spite of the fact that LGN is not essential for cortical targeting of NuMA at this later phase of mitosis (see **paragraph 1.4.1**). Collectively these results indicated that the spindle orientation defects of Afadin-depleted cells are accompanied by severe cortical reduction of the force generating proteins LGN, NuMA and $p150^{Glued}$.

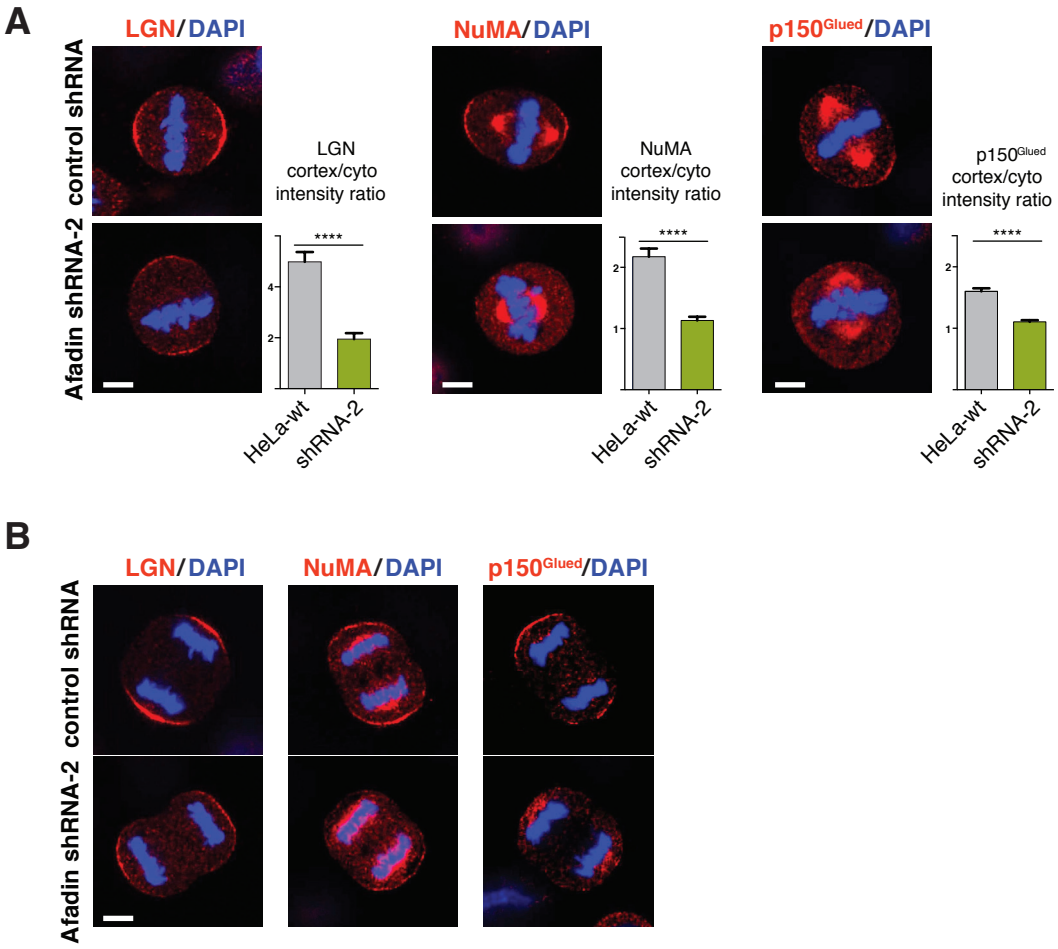

Figure 40 - In mitosis Afadin is required for cortical recruitment of NuMA, LGN, and Dynein/Dynactin. (**A**) Confocal sections of control shRNA (top) and Afadin shRNA-2 expressing HeLa cells (bottom) in metaphase stained for LGN, NuMA, or p150^{Glued}. Depletion of endogenous Afadin diminishes cortical recruitment of LGN, and abrogates cortical localization of NuMA and Dynactin (p150^{Glued}) above the spindle poles. (**B**) Silencing of Afadin in HeLa cells impairs cortical localization of LGN, NuMA and Dynactin in anaphase. Confocal sections of control shRNA (top) and Afadin shRNA-2 expressing HeLa cells (bottom) in anaphase stained for LGN, NuMA, and p150^{Glued}. In all images, DNA was visualized with DAPI. The scale bar corresponds to 5 μm.

3.3.3 The C-terminal region of Afadin binds directly to LGN^{TPR}

Correct spindle positioning in metaphase relies on the association of LGN with NuMA, which occurs via direct interaction between the TPR domain of LGN and the C-terminal portion of NuMA (Culurgioni et al., 2011; Zhu et al., 2011b).

To gain an understanding of the molecular details of the functional contribution of Afadin to spindle positioning, Manuel Carminati performed *in vitro* reconstitution assays with purified LGN, NuMA and Afadin. He first purified the C-terminal domain of Afadin

encompassing residues 1514-1824 (hereon referred to as Afadin^{Cter}), and tested its direct interaction with LGN^{TPR} and NuMA$^{1861-1824}$. Size exclusion chromatography (SEC) revealed that Afadin^{Cter} enters a stoichiometric 1:1 complex with LGN^{TPR} (Figure 41A), but is unable to bind NuMA$^{1861-1824}$ (Figure 41B). Importantly, when the three proteins where loaded simultaneously on a size exclusion column, LGN^{TPR} co-eluted with NuMA but not with Afadin^{Cter}, indicating that the binding of LGN to Afadin and NuMA is mutually exclusive, and that NuMA is an higher affinity ligand of LGN than Afadin (Figure 41C). To further dissect the requirements for the interaction of Afadin to LGN, he mapped the minimal binding domains required for the binding of the two proteins. He designed complementary constructs of Afadin^{Cter} fused to GST moiety. The ability of the truncated proteins to bind LGN was verified in a pull-down experiment performed with a GST-Afadin fragments immobilized on GSH-beads, and purified LGN^{TPR} in solution. This assays demonstrated that only Afadin$^{1709-1747}$ associated with LGN^{TPR} to the same extent observed for the whole Afadin^{Cter} (Figure 41D) Furthermore, structural and biochemical analysis revealed that the determinants for the specific recognition of the LGN^{TPR} are Phe-1739 and Glu-1735 of Afadin (data not shown).

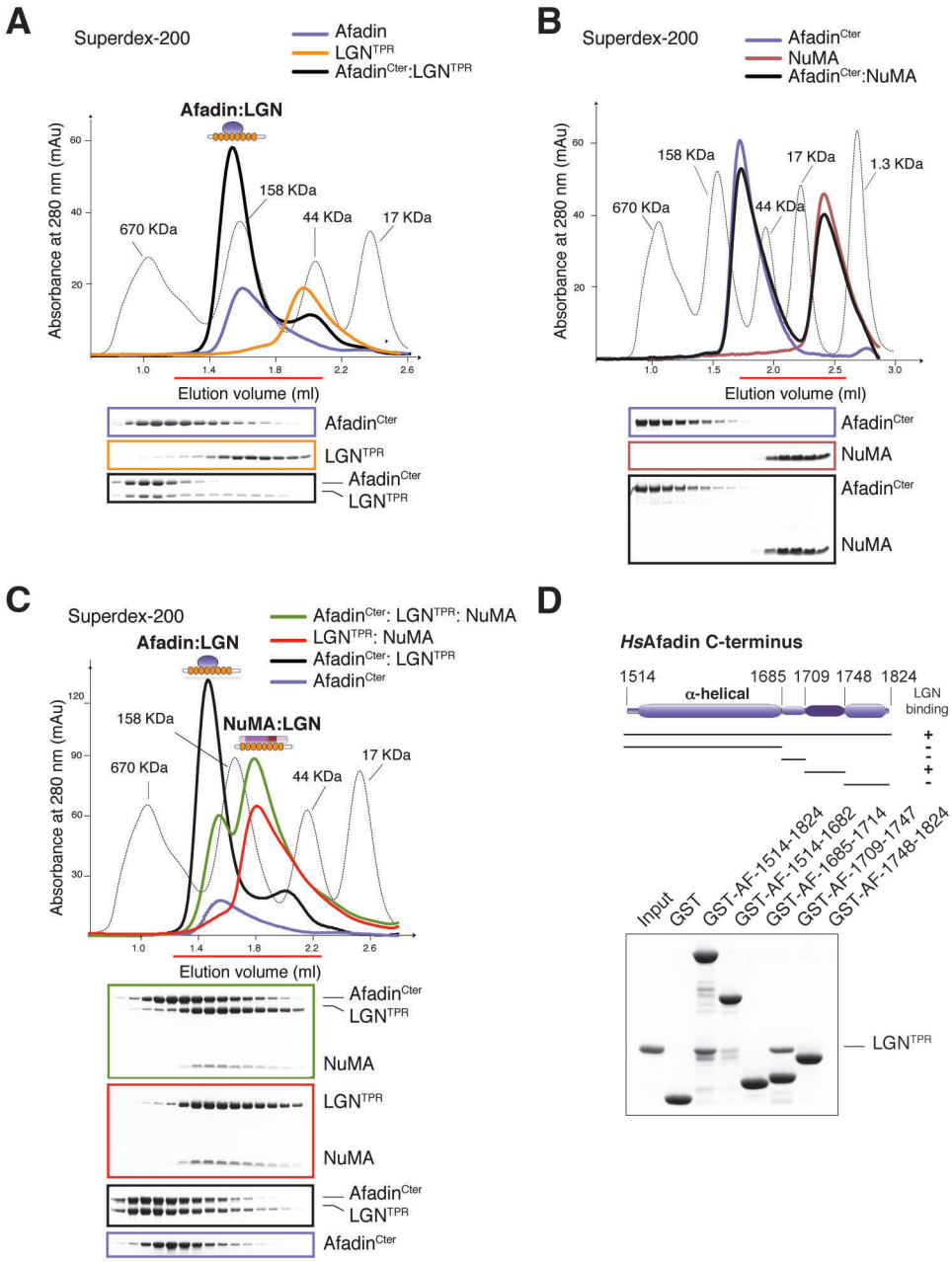

Figure 41 – The C-terminal domain of Afadin binds directly LGN^{TPR}. (**A**) SEC elution profile of the stoichiometric complex formed between Afadin^{Cter} and LGN^{TPR} mixed at 15 µM concentration, and Coomassie-stained SDS-PAGE of the peak fractions corresponding to the horizontal red bar. The elution profile of globular markers is reported as a dashed gray line. Individual runs of Afadin^{Cter} and LGN^{TPR} are shown for comparison. (**B**) An analogous incubation of Afadin^{Cter} with NuMA$^{1861\text{-}1928}$ did not result in a complex formation, as evident by the absence of a peak eluting earlier than the two proteins in isolation. SEC profiles and fraction content are visualized as in (A). (**C**) When loaded simultaneously on a SEC column in equimolar amounts, Afadin^{Cter}, LGN^{TPR} and NuMA$^{1861\text{-}1928}$ eluted in two distinct peaks (green trace). The early eluting peak consists only of Afadin^{Cter}, while the slower migrating peak contains LGN^{TPR} in complex with NuMA$^{1861\text{-}1928}$. This result indicates that Afadin and NuMA are mutually exclusive ligands of LGN, with NuMA displaying a higher affinity. SEC profiles and fraction content are visualized as in (A). (**D**) Mapping of the minimal region of Afadin^{Cter} retaining binding to LGN^{TPR} by GST pull-down.

Complementary fragments of Afadin^{Cter} (1 μM) were adsorbed on GSH-beads, and incubated with 5 μM of purified LGN^{TPR}. After washes, species retained on beads were separated by SDS-PAGE. The binding assay revealed that Afadin$^{1709-1747}$ is the shortest stretch associating to LGN^{TPR} with a binding strength similar to the entire Afadin^{Cter}.

3.3.4 Afadin contributes to spindle orientation by promoting LGN cortical recruitment

Based on the direct binding between Afadin and LGN that we have discovered, we speculated that Afadin could bring LGN to the cortex by interacting with its TPR domain. To test this hypothesis, I attempted to rescue mitotic defects of Afadin-interfered HeLa cells by expressing a mCherry-tagged sh-resistant version of rat Afadin (for the design of the sh-resistant construct see **paragraph 2.2.3** of Material and Methods). For the rescue experiments, I used mCherry-Afadin wild-type (Afadin^{WT}) as a positive control, and an Afadin mutant deleted for the entire LGN binding-interface, referred to as Afadin$^{\Delta LGN}$ hereon. More specifically, the region that we deleted of rat Afadin encompasses residues 1713-1752, which corresponds to the stretch of human Afadin spanning residues 1709-1747, which we had previously shown to be sufficient for the direct interaction of Afadin with LGN^{TPR}. mCherry-Afadin^{WT} and mCherry-Afadin$^{\Delta LGN}$ were cloned in the lentiviral pCDH vector and initially used to generate lentiviruses for stable infection of HeLa cells. Unfortunately, due to the large size of the cloned insert, cells infected with the pCDH vectors expressed Afadin proteins at very low levels, which were not ideal for rescue experiments (data not shown). I next tried to transiently transfect the constructs in HeLa cells. Immunoblotting experiments showed that the expression levels of Afadin^{WT} and Afadin$^{\Delta LGN}$ transiently transfected in Afadin-depleted cells were about ten-fold higher than wild-type cells (Figure 42), which we consider suitable for rescue experiments.

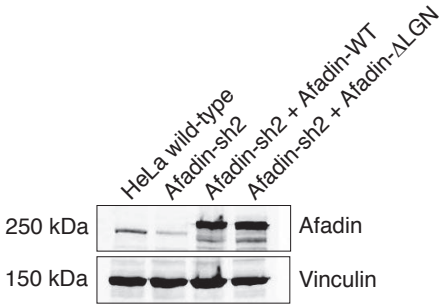

Figure 42 - Expression levels of mCherry-tagged rat Afadin in Afadin-silenced cells. Immunoblotting of HeLa cells transiently transfected with shRNA-Afadin-resistant mCherry-Afadin-WT and -ΔLGN. The immunoblot shows the relative expression levels of the transfected proteins compared to endogenous Afadin. Vinculin was used as loading control.

Analysis of Afadin sh-RNA HeLa cells transfected with the rescue constructs, mCherry-Afadin^{WT} localized uniformly to the cell cortex, and was able to restore normal levels of cortical of LGN, as quantified by intensity line-scan methods (Figure 43A). On the other hand, the analogous overexpression of Afadin$^{\Delta LGN}$ did not rescue the cortical distribution of LGN despite of its proper localization at the cell cortex (Figure 43A-B).

To assess whether impairment of LGN recruitment at the membrane was the main cause of the spindle misorientation phenotype observed in Afadin-depleted cells, I quantified the spindle angle distribution of Afadin knock-down cells expressing the rescue constructs. Spindle angle analysis showed that mCherry-Afadin^{WT} rescued almost completely the spindle alignment defects of Afadin-depleted cells, whereas Afadin$^{\Delta LGN}$ did not (Figure 43C). Together, these results demonstrate that Afadin acts as a scaffolding protein coordinating the correct assembly of force generators at the cortex, this way promoting correct spindle orientation.

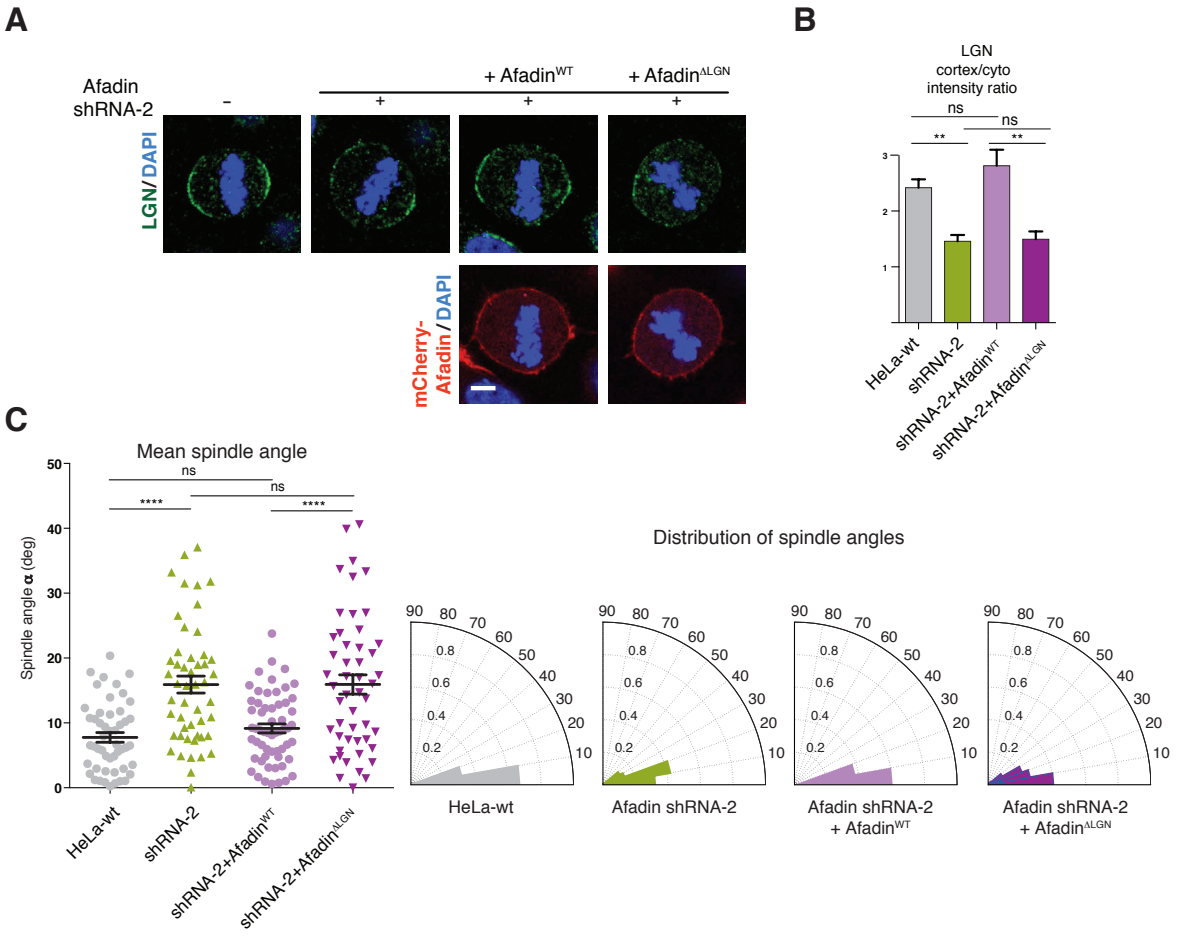

Figure 43 - Afadin contributes to spindle orientation by promoting LGN cortical recruitment. (**A**) Rescue experiments of cortical LGN in HeLa cell lines stably depleted of endogenous Afadin, and transiently transfected with shRNA-resistant rat mCherry-Afadin^{WT} or -Afadin$^{\Delta LGN}$. Whereas Afadin wild-type rescued the cortical localization of LGN above spindle poles in metaphase, expression of the mutant protein Afadin$^{\Delta LGN}$ resulted in poor recruitment of LGN at the cortex. Bottom panels show the uniform cortical localization of the transfected mCherry-Afadin constructs. (**B**) Quantification of cortical LGN in rescue experiments of panel (A). (**C**) Scatter plots illustrating the distribution of the angles measured between the spindle axis and the plane of the coverslip in metaphase HeLa cells wild-type or Afadin-depleted in the presence of rat Afadin rescue constructs. Means and SEM are shown for each experiment with n > 50. Consistent with the LGN localization, mCherry-Afadin^{WT} efficiently rescues spindle misorientation defects observed upon Afadin ablation, while Afadin$^{\Delta LGN}$ does not rescue misorientation. **** indicates P < 0.0001, ** indicates P < 0.01, and * indicates P < 0.05. On the right, the radial histograms illustrate the distributions of the spindle axis angles in HeLa cells in metaphase for Afadin shRNA rescue experiments. All scale bars correspond to 5 μm.

3.3.5 Afadin acts as a linker between F-actin and LGN

At mitotic entry, the actin cytoskeleton reorganizes in a mesh of ordered actin filaments and associated proteins known as cortex, which mediates cell rounding. Recent studies revealed a critical role of the actin cortex in counteracting the action of Dynein/Dynactin, which in the presence of astral MTs exert pulling forces on cortical NuMA:LGN:Gαi complexes to orient the mitotic spindle (Zheng et al., 2013). However, no direct molecular link between spindle orientation proteins and cortical F-actin has been identified so far. Because of its ability to bind directly LGN and to associate with F-actin (Mandai et al., 1997), we reasoned that Afadin could act as a physical tether between actin filaments and the spindle orientation machinery.

3.3.5.1 Afadin interacts simultaneously with LGN and F-actin in vitro

We first determined the interaction surface between Afadin and F-actin by *in vitro* F-actin co-sedimentation assays. These experiments showed that the boundaries of the actin-binding region of Afadin are residues 1514-1682, just upstream of the LGN-binding stretch (data not shown). This finding prompted us to explore the possibility that Afadin could act as a molecular bridge between LGN and F-actin. To test this hypothesis, Manuel Carminati performed high-speed co-sedimentation assays of Afadin^{Cter} with F-actin in the presence of purified LGN^{TPR}. LGN^{TPR} in isolation was found in the supernatant, whereas it cosedimented with F-actin when in complex with Afadin^{Cter} (Figure 44). Consistently, mutations disrupting the Afadin^{Cter}:LGN^{TPR} interaction surface (namely Afadin$^{F1730E/E1735R}$ and LGN $^{R235A-R236A}$) prevented co-sedimentation of LGN with F-actin (Figure 44). These data indicated that Afadin^{Cter} interacts directly and simultaneously with LGN and with F-actin.

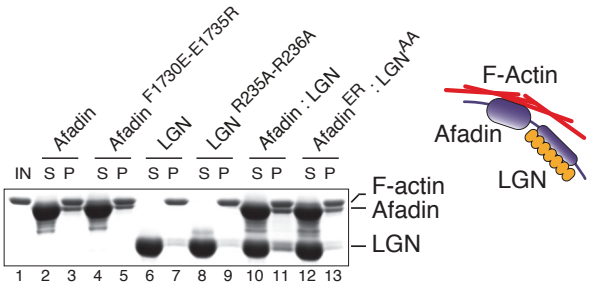

Figure 44 - Afadin interacts simultaneously with LGN and F-actin *in vitro*. To test whether Afadin could physically bridge between LGN and F-actin, cosedimentation assays were performed with 9 μM of Afadin^{Cter} in the presence of equal amounts of LGN^{TPR}. Experiments were carried out with purified wild-type proteins, and with Afadin and LGN mutants unable to interact with one another. Under these conditions, LGN^{TPR} wild-type cosedimented with Afadin^{Cter} and F-actin, whereas the mutant LGN$^{R235A-R236A}$, unable to interact with Afadin$^{F1730E-E1735R}$, was found in the supernatant fraction.

3.3.5.2 Afadin bridges between LGN and F-actin in vivo

To assess whether Afadin connects LGN to F-actin also *in vivo*, I treated HeLa cells with 1 μM of the actin-depolymerizing drug Latrunculin-A, which disassembled the actomyosin cortex almost completely (Figure 45A, left panel) (Spector et al., 1983). Upon Latrunculin-A treatment, LGN was lost from the cortex and localized aberrantly at the spindle poles, as previously reported (Zheng et al., 2013)(Figure 45A). Moreover, also the cortical localization of NuMA was abrogated (Figure 45A). This is consistent with the notion that the integrity of cortical F-actin is critical for association and maintenance of spindle motors at the plasma membrane. To make sure that the spindle orientation defects observed in Afadin-depleted cells were not caused by impairment of cortical F-actin functions, I checked whether cortical F-actin integrity was perturbed by the depletion of Afadin. Phalloidin staining showed that in the absence of Afadin the actomyosin cortex is indistinguishable from the one of wild-type cells, thus indicating that Afadin is not required for mitotic actin organization at the cortex (Figure 45B). Next, I studied the effect of actin-depolymerisation on the distribution of Afadin. In untreated cells, Afadin localized all around the cell cortex but upon Latrunculin-A treatment, Afadin disappeared form the plasma membrane, and redistributed uniformly in the cytoplasm suggesting that the

cortical F-actin is required for the proper localization of Afadin at the plasma membrane (Figure 45A). Together with previous findings showing that Afadin-depletion delocalizes LGN, NuMA and p150^{Glued} from the cortex, these data support the idea that Afadin acts as a direct molecular link between the spindle orientation machinery and cortical F-actin.

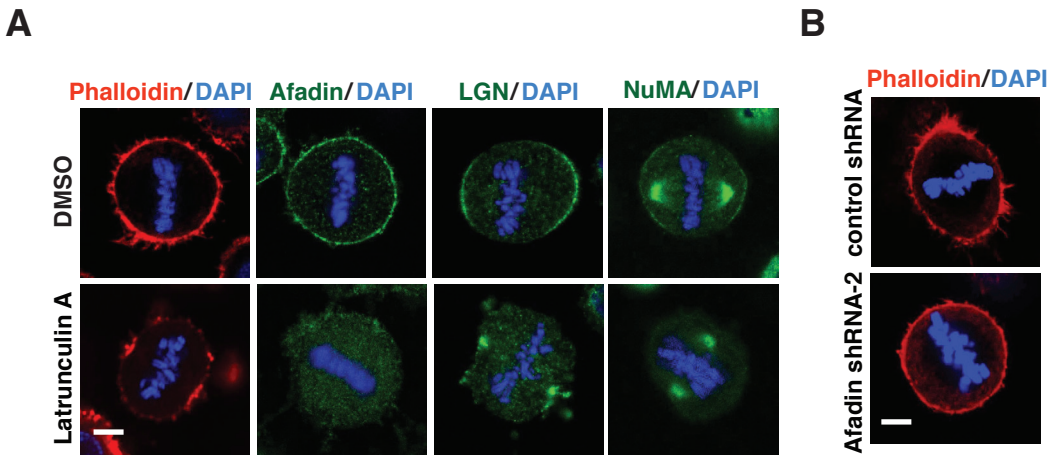

Figure 45 - Afadin bridges between LGN and F-actin *in vivo*. (**A**) HeLa cells in metaphase treated with DMSO (top row) or 1 μM Latrunculin A (bottom row) were fixed and stained for actin (TRITC-conjugated Phalloidin), Afadin, NuMA or LGN. Cells treated with the actin-depolymerizing drug Latrunculin A exhibit a strong reduction of cortical actin, and a concomitant loss of Afadin, NuMA and LGN from the plasma membrane. In the absence of cortical actin, LGN was found at the spindle poles. Scale bars correspond to 5 μm. (B) Confocal sections of control shRNA (top) and Afadin shRNA-2 expressing HeLa cells (bottom) in metaphase stained for actin (Phalloidin). Images showed that loss of Afadin does not alter the integrity of the actomyosin cortex.

4. DISCUSSION

4.1 Aurora-A and NuMA

Aurora-A kinase is a master regulator of mitosis involved in spindle assembly and positioning (Nikonova et al., 2013). My studies showed that the direct phosphorylations of NuMA by Aurora-A on Ser-1969 and on Ser-2047 regulate its distribution at the cortex and at the spindle poles in metaphase, and in this way the correct orientation of the mitotic spindle of adherent cells in culture (Figure 46). Furthermore, we identify a new MT-binding domain on the C-terminal portion of NuMA, which is dispensable for the localization of the protein at the spindle poles and it is compatible with its association to LGN, suggesting a role in spindle positioning.

Aurora-A has been implicated in orienting symmetric and asymmetric divisions from invertebrate to vertebrate (Asteriti et al., 2014; Gillies and Cabernard, 2011; Morin and Bellaiche, 2011; Regan et al., 2013). In asymmetric divisions of *Drosophila* NBs, Aurora-A controls the establishment of apico-basal polarity by phosphorylating D-Lgl (Bell et al., 2014; Carvalho et al., 2014; Wirtz-Peitz et al., 2008), this way affecting indirectly also spindle positioning. Beside that, the molecular events underlying the spindle orientation functions of Aurora-A are still unknown. Our studies reveal that the kinase activity of Aurora-A influences spindle alignment of unpolarized cells by affecting the distribution of NuMA in metaphase. Depletion or chemical inhibition of Aurora-A in metaphase determines an accumulation of NuMA at spindle poles, thus preventing its cortical recruitment with LGN (Figure 46B). The aberrant accumulation of NuMA at the spindle poles in Aurora-A-inhibited condition is also accompanied by reduced mobility, implying that in normal conditions the affinity of NuMA for spindle pole components is diminished by Aurora-A phosphorylation to favor its cortical targeting (Figure 46A).

To demonstrate that the main contribution of Aurora-A to spindle orientation is to allow the recruitment of NuMA at the cortex in metaphase, I ectopically targeted NuMA at the

cortex by chimeric fusion of the GoLoco domain of LGN at the C-terminus of the protein. The expression of NuMA-GoLoco fusion protein restores almost completely the alignment defects observed in MLN8237-treated HeLa cells, supporting the initial hypothesis. Interestingly, the NuMA-GoLoco construct not only rescues misalignment but also shortens the mitotic delay induced by MLN8237 treatment, suggesting a connection between spindle orientation and cell cycle progression. Such link is well documented in yeast (Pereira and Schiebel, 2005) and has been reported in *Drosophila* male germline stem cells (Cheng et al., 2008), but is still largely unexplored in vertebrate cells.

Studies in *Drosophila* NBs suggested that Aurora-A promotes spindle alignment by phosphorylating Pins on a conserved serine residue in the linker region between the TPR domain and the GoLoco motifs, which is important for the interaction between LGN and cortical Dlg (Johnston et al., 2009). Phosphorylation of this serine residue seems to play a role for spindle orientation also in MDCK cysts (Hao et al., 2010) and in neuroepithelial cells (Saadaoui et al., 2014), although it is not clear whether in vertebrate LGN is a direct substrate of Aurora-A. Under the conditions of partial Aurora-A inhibition that I used for my studies, I did not observe a significant reduction in the levels of cortical LGN in metaphase. Therefore, I can conclude that in HeLa cells, cortical targeting of LGN is not affected by Aurora-A or it is not perturbed by partial inhibiting conditions. These finding suggested that instead the spindle misorientation phenotype induced by partial Aurora-A inhibition depends on NuMA delocalization.

The evidence that in MLN8237-treated cells the monomeric C-terminal construct of NuMA spanning residues 1821-2115, exhibits the same polar enrichment displayed by endogenous NuMA allowed us to use this construct to dissect the mitotic effect of Aurora-A on NuMA at a molecular scale, both *in vivo* and *in vitro*. In line with previous proteomic data (Kettenbach et al., 2011), we showed that *in vitro* Aurora-A phosphorylates NuMA on Ser-1969, Ser-1991 and Ser-2047, and demonstrate that these three phosphosites are the determinants of the polar accumulation of NuMA observed in the presence of MLN8237.

In particular, I found that replacement of Ser-1969 with Ala on NuMA^{Cter} recapitulates the enrichment at the poles observed upon Aurora-A inhibition, whereas substitution of Ser-2047 with Ala influences only cortical recruitment (Figure 46A). I propose that in metaphase these two phosphosites synergize to guarantee the correct distribution of NuMA between poles and cortex. In previous studies Kettenbach and colleagues have also analyzed the mutation of Aurora-A phosphosite Ser-1969. They showed that in HeLa cells GFP-NuMA full-length with Ser-1969-Ala substitution displays a perturbed localization at the spindle poles: it is restricted at the PCM and does not reach the MTs near the centrosomes. The same distribution was observed in HeLa cells expressing GFP-NuMA wild-type upon treatment with the Aurora-A inhibitor MLN8054. Together these data seemed to suggest a role of Aurora-A in regulating NuMA-MTs interaction, which was not confirmed by our analyses.

Recent studies demonstrate that Aurora-A phosphorylates the Dynactin subunit p150^{Glued} on Ser-19, which resides in the p150^{Glued} MT-association domain (Reboutier et al., 2013; Rome et al., 2010). Interestingly, substitution of Ser-19 with alanine results in the accumulation of p150^{Glued} at the spindle poles. My analysis in HeLa cells treated with MLN8237 reproduced the accumulation of p150^{Glued} at the spindle poles observed with the Ser-19-Ala mutation. In addition, my results also revealed an impairment of the cortical localization of Dynactin, which could reflect the lack of cortical NuMA. In mitosis NuMA associates with cytoplasmic Dynein/Dynactin, playing different functions at the spindle poles and at the cortex (Kotak et al., 2012; Merdes et al., 2000; Merdes et al., 1996; Zheng et al., 2013). The N-terminal part of NuMA encompassing residues 1-705 has been shown to be required for the interaction with Dynein (Kotak et al., 2012). Since NuMA and Dynactin behave similarly upon Aurora-A inhibition, it was important to clarify whether the delocalization of NuMA and Dynein/Dynactin from the cortex is somehow interdependent. The evidence that NuMA^{Cter} constructs, that cannot bind Dynein/Dynactin, recapitulate the accumulation of NuMA at the spindle poles seems to suggest that Aurora-

A regulates the localization on NuMA by direct phosphorylation. Therefore, I can conclude that Aurora-A can coordinate activities of NuMA and Dynactin at the spindle pole independently and synergically. On one side Aurora-A phosphorylates Dynactin on Ser-19, and on the other it phosphorylates NuMA on Ser-1969, regulating their spindle poles localization. Whether and how these molecular events are coordinated with one another to orient the mitotic spindle remains an open issue.

The evidence that the phosphosite playing a prominent role in setting normal amounts of NuMA at the spindle poles, Ser-1969, lies in a fragment that was previously implicated in MT-binding, prompted us to test the idea that Aurora-A could regulate the interaction between NuMA and MTs. MT cosedimentation and forming assays revealed that the kinase activity of Aurora-A does not influence the affinity of NuMA for MTs, nor its MT organizing ability. Most importantly these analyses, complemented with localizations in mitotic cells, led to the identification of new MT-binding domain of NuMA contained in the fragment 2005-2115. Regardless of Aurora-A activity, I also found that the association of $NuMA^{Cter}$ with MTs is not essential for targeting of the proteins to the spindle poles, hinting at the possibility that the association of NuMA to MTs is important in processes other than spindle pole assembly and aster anchoring to the centrosomes (Silk et al., 2009). The finding that the newly discovered MT-binding domain is compatible with the concomitant binding of NuMA to LGN and MTs suggests that it can sustain spindle orientation. We propose that this MT-binding domain of NuMA works at the cortex, to stabilize the interaction between LGN-engaged NuMA molecules and MT +TIPs, this way assisting the Dynein-mediated sliding of cortical LGN:NuMA complexes along the depolymerizing MTs. This hypothesis is consistent with the propensity of the MT-binding activity of NuMA to promote minus-end directed movements (Forth et al., 2014).

The description of the cross-talk between Aurora-A and NuMA reported in this study introduces an additional element to the regulatory mechanisms controlling NuMA activities throughout mitosis. Analyses in HeLa cells revealed that up to metaphase Plk1

controls the interaction of NuMA with Dynein/Dynactin to center the spindle (Kiyomitsu and Cheeseman, 2012). The phosphorylation of NuMA on Thr-2055 by CDK1 has been shown to timely regulate the cortical enrichment of NuMA observed at the metaphase to anaphase transition, when more cortical Dynein is required to elongate the spindle (Kiyomitsu and Cheeseman, 2013; Kotak et al., 2013; Seldin et al., 2013). Our studies show that the activity of Aurora-A controls cortical targeting of NuMA at metaphase, which determines and maintains the correct orientation of the mitotic spindle in human cells in culture.

Intriguingly, in developing tissues the coordination of the spindle axis with respect to cortical polarity is a prerequisite for asymmetric cell divisions because it defines the unequal segregation of fate determinants and niche contacts (Gonczy, 2002; Knoblich, 2010). In the majority of the asymmetrically dividing systems analyzed so far, in metaphase NuMA polarizes at the apical site above one of the spindle poles (Bowman et al., 2006; Izumi et al., 2006; Lechler and Fuchs, 2005; Seldin et al., 2013; Siller et al., 2006) and promotes spindle alignment along the apico-basal axis (or anterior-posterior axis in *c. elegans* zygotes) (Lorson et al., 2000). Therefore, our findings bear major implications in the context of vertebrate stem cell divisions. We believe that the relevance of the Aurora-A/NuMA pathway in the self-renewal of embryonic and adult stem cells will be an exciting direction for future experiments.

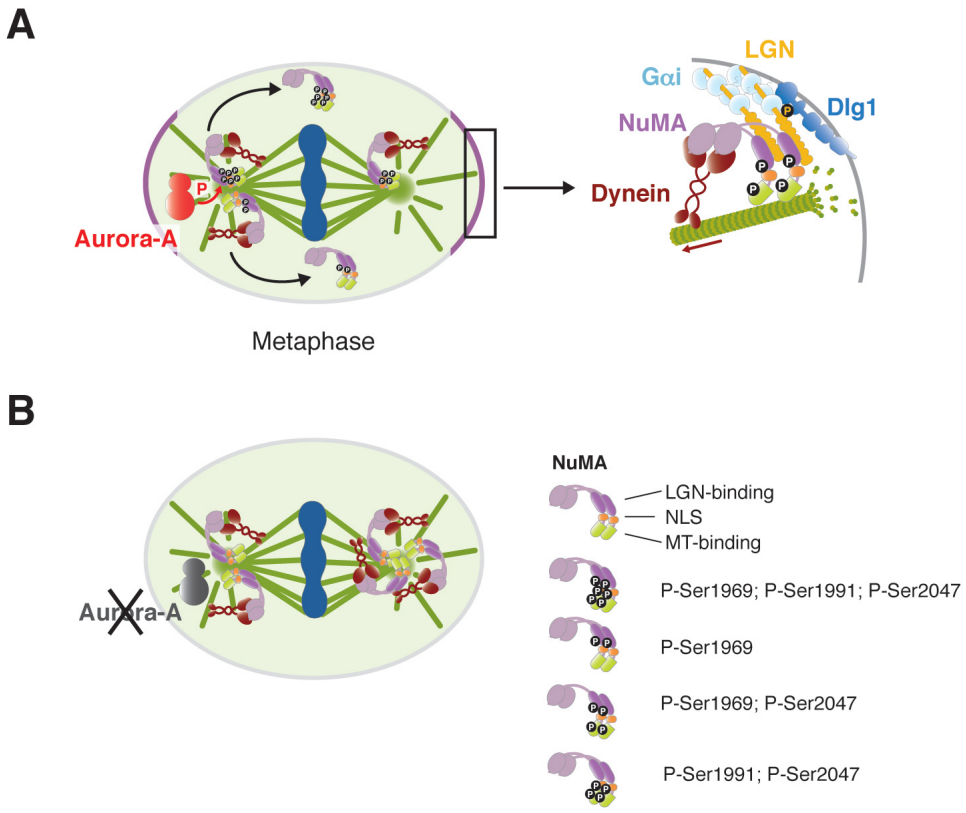

Figure 46 - Schematic representation of the role of Aurora-A in regulating the distribution of NuMA in metaphase according to my study. (**A**) In unperturbed conditions, Aurora-A localized at the spindle poles phosphorylates NuMA on Ser-1969, Ser-1991 and Ser-2047 enhancing its mobility, and allowing a pool of NuMA to reach the polar regions of the cortex above the spindle poles (left panel). In particular, the phosphorylation on Ser-1969 is required to release NuMA from the spindle poles and to its cortical recruitment, whereas the phosphorylation of Ser-2047 influences only its localization at the cell cortex. The receptor for NuMA at the cortex is LGN, which in turn is recruited to the plasma membrane by interaction with four Gαi moieties anchored to the lipid bilayer via myristoyl groups. Phosphorylated LGN is further secured to the membrane by interaction with Dlg1. The N-terminus of NuMA associates with Dynein/Dynactin, while the C-terminal portion binds concomitantly to LGN and to MTs, this way stabilizing the contacts between the Dynein/Dynactin motors and the depolymerizing MT lattice (right panel). (**B**) Aurora-A inhibition results in aberrant accumulation of unphosphorylated NuMA at the spindle poles, and simultaneous loss of NuMA from the cortex.

4.2 Lgl2

In epithelia cells, Lgl2 is required to establish and maintain the apico-basal polarity (Chalmers et al., 2005; Musch et al., 2002; Plant et al., 2003; Yamanaka et al., 2006; Yamanaka et al., 2003). In this context, Lgl2 acts together with Scribble and Dlg to define baso-lateral membrane. Indeed, recent biochemical data demonstrated that Lgl2 is recruited baso-laterally, by direct interaction with Dlg4 (a mammalian homolog of *Drosophila* Dlg), upon aPKC phosphorylation in the central linker region (Zhu et al., 2014). During mitosis, Lgl2 and the *Drosophila* ortholog D-Lgl seem to be involved in the pathway controlling spindle orientation. Yasumi and colleagues have reported an interaction between $Lgl2^{Cter}$ and LGN^{TPR} in mitotic HEK293t cells (Yasumi et al., 2005). On the other hand, recent studies in *Drosophila* imaginal discs and in follicular epithelia showed that during mitosis D-Lgl is direct phosphorylated by Aurora-A, which in turn regulate negatively the cortical D-Lgl:Dlg binding in favour of the Dlg:Pins interaction at the baso-lateral cortex (Bell et al., 2014; Carvalho et al., 2014). Whether this mechanism is conserved in vertebrate is currently unknown.

In this scenario, experiments in HeLa cells showed that Lgl2 distributes uniformly at the cortex throughout mitosis, co-localizing with NuMA and LGN at polar regions above the spindle poles. Spindle orientation analysis in HeLa cells plated on fibronectin showed that the spindle is misaligned compared to the substratum in Lgl2 depleted cells as well as in LGN ablated cells, thus confirming the role of Lgl2 in the spindle orientation pathway. However, my biochemical studies revealed that the Lgl2 and LGN interaction is not reproducible *in vitro* and *ex vivo*. Nevertheless, I scored an interesting interaction between Lgl2 and NuMA in Co-IP experiment, suggesting an alternative explanation for the spindle orientation function of Lgl2. These data, together with the physical interaction between Lgl2 and Dlg4 recently demonstrated, suggest a model whereby cortical Dlg:Lgl2:NuMA complexes capture astral MTs via Dynein/Dynactin and orient the mitotic spindle. To validate this model, I will test whether the phosphorylation of Lgl2 by Aurora-A in the

linker region prevents its cortical localization and its interaction with Dlg in mammalian system, as it was suggested in flies. More in general, I believe it will be worth studying the functional role of the Lgl2:NuMA interaction, and investigating its relevance in polarized system such as Caco-2 cysts. As a start, it will be useful to assess if the Lgl2 and NuMA interact directly, and what are their minimal binding domains.

4.3 Afadin

A second part of my project addressed the functional characterization of the interaction between Afadin and LGN, and provided a molecular explanation for the novel role of Afadin in spindle alignment. I started from the observation that in adherent HeLa cells, Afadin distributes uniformly at the cortex throughout mitosis, and from metaphase to anaphase it co-localizes with LGN and NuMA at polar regions of the cortex above the spindle poles. For this reason, the spindle misorientation observed upon Afadin ablation suggested a direct role of Afadin in cortical targeting of LGN and NuMA. Indeed, our studies demonstrated that Afadin contributes to recruitment of force generators to the cells cortex (Figure 47). Loss of Afadin not only perturbs polar enrichment of LGN in mitosis, but also abolishes cortical accumulation of NuMA. This can be observed both in metaphase, when NuMA is known to be directed to the cortex by LGN-mediated mechanisms (Seldin et al., 2013; Zheng et al., 2014), and in anaphase, when the levels of cortical NuMA increases thanks to its direct interactions with the plasma membrane (Kotak et al., 2013; Kotak and Gonczy, 2014; Zheng et al., 2014). *In vitro* experiments showed that the C-terminal portion of Afadin spanning residues 1709-1747 interacts directly with LGN^{TPR}. LGN^{TPR} is also necessary for the interaction of other spindle orientation actors such as NuMA, Insc, and FRMPD1 (Pan et al., 2013; Zhu et al., 2011b). Therefore, it is not surprising that the association of LGN with Afadin and NuMA is mutually exclusive.

These results suggest that Afadin might influence the distribution of NuMA independently of LGN. Interestingly, induced cell polarity assays in S2 cells showed that the Ras-like domains of Canoe associate with Ran^{GTP}, and are essential for cortical targeting of Mud with Pins (Wee et al., 2011). These findings are consistent with the results of Speichers and coworkers that Canoe acts downstream of Pins and upstream of Mud in regulating spindle orientation of asymmetrically dividing NBs (Speicher et al., 2008). These observations might somehow be correlated with the Ran-dependent cortical regulation of

LGN reported by Cheeseman and co-workers in HeLa cells, although in this system active Ran seems to be required to exclude force generators from the cortical regions above chromosomes rather than for active cortical recruitment. Our findings suggest a model in which, Afadin targets LGN to the cortex by direct interactions with its TPR domain, but at the same time we show that it is involved in the cortical assembly of NuMA:Dynein complexes in more sophisticated ways, whose elucidation required further experiments (Figure 47). At this regard, we consider of particular interest the recent implication of Canoe in the Dishevelled-mediated cortical accumulation of Mud (Johnston et al., 2013), that seems to suggest that Afadin belongs to cortical localized landmarks transducing external signals to orient the divisions (Segalen et al., 2010). From a bread perspective, I believe that Afadin could act in conjunction with Gαi and other cortical anchoring mechanisms, including Dlg (Saadaoui et al., 2014), to ensure timely targeting of LGN and MT-motors at the membrane (Figure 47).

An emerging theme in the field of oriented division is the role of the actin cytoskeleton in spindle positioning. Increasing evidence points at a prominent function of the actomyosin cortex underlying mitotic rounding and in guiding spindle alignment in a variety of cellular contexts, including isolated vertebrate cells in culture (Lancaster and Baum, 2014). The need of an intact actin cortex for orientation is reflected in the requirement of actin regulators controlling actin stability and dynamics in different ways, including ERM family members (Machicoane et al., 2014), Cdc42 (Jaffe et al., 2008), focal adhesion molecules as β1-integrin (Lechler and Fuchs, 2005). However how signals sensed by the actomyosin cortex are communicated to spindle orienting motors is to date largely unclear. Disruption of F-actin results in aberrant displacement of LGN and Gαi from the cortex to the spindle poles (Zheng et al., 2013), suggesting that actomyosin serves as a rigid scaffold counteracting Dynein/Dynactin pulling forces. Our *in vitro* experiments have shown that Afadin interacts directy with F-actin and that this interaction is not mutually exclusive with

LGN binding. Moreover, in HeLa cells Afadin depletion does not perturb the integrity of the actomyosin cortex. Conversely, chemical depolymerization of F-actin by Latrunculin-A impairs Afadin cortical localization suggesting that F-actin is required upstream. I can conclude that Afadin simultaneously binds LGN and cortical F-actin acting as a molecular bridge between the spindle apparatus and the actomyosin cortex (Figure 47).

In epithelial cells, Afadin is found at the lateral membrane (Ooshio et al., 2004), implying that it can act as a lateral cue restricting LGN at the lateral cortex, contributing to orient planarly the spindle axis. In line with this hypothesis, Caco-2 cells lacking Afadin are unable to form three-dimensional cysts with a single inner lumen. The knowledge that Afadin acts as a major organizer of epithelial cell-to-cell junctions, and a hub for small G-protein signaling, makes it an ideal candidate to transfer information from external stimuli and mechano-properties of the cortex to the spindle in order to instruct its position. In this respect, it would be very interesting to investigate the role of the Afadin in cellular system able to switching from planar to vertical divisions such as skin progenitors (Williams et al., 2014), neuroepithelia (Saadaoui et al., 2014), and mammary epithelia (Elias et al., 2014).

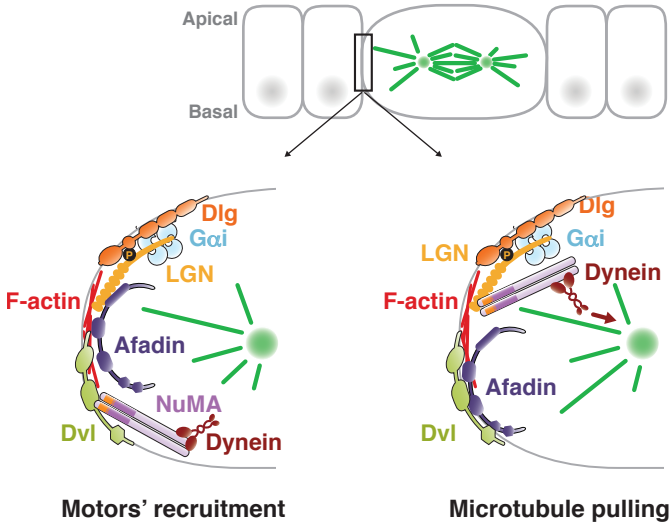

Figure 47 - Schematic representation of the mitotic function of Afadin supported by my study. Afadin localizes at AJs of polarized epithelia, and instructs the localization of MT motors by concomitant binding to cortical F-actin and LGN, and by indirect recruitment of NuMA/Dynein possibly via Dishevelled. Phosphorylated LGN is further secured to the lateral membrane by interaction with Dlg1. Binding of NuMA to LGN ensues MT pulling forces.

5. REFERENCES

Asteriti, I.A., E. Di Cesare, F. De Mattia, V. Hilsenstein, B. Neumann, E. Cundari, P. Lavia, and G. Guarguaglini. 2014. The Aurora-A inhibitor MLN8237 affects multiple mitotic processes and induces dose-dependent mitotic abnormalities and aneuploidy. *Oncotarget*. 5:6229-6242.

Bell, G.P., G.C. Fletcher, R. Brain, and B.J. Thompson. 2014. Aurora Kinases Phosphorylate Lgl to Induce Mitotic Spindle Orientation in Drosophila Epithelia. *Current biology : CB*.

Bellaiche, Y., and M. Gotta. 2005. Heterotrimeric G proteins and regulation of size asymmetry during cell division. *Curr Opin Cell Biol*. 17:658-663.

Bellaiche, Y., A. Radovic, D.F. Woods, C.D. Hough, M.L. Parmentier, C.J. O'Kane, P.J. Bryant, and F. Schweisguth. 2001. The Partner of Inscuteable/Discs-large complex is required to establish planar polarity during asymmetric cell division in Drosophila. *Cell*. 106:355-366.

Bergstralh, D.T., T. Haack, and D. St Johnston. 2013a. Epithelial polarity and spindle orientation: intersecting pathways. *Philos Trans R Soc Lond B Biol Sci*. 368:20130291.

Bergstralh, D.T., H.E. Lovegrove, and D. St Johnston. 2013b. Discs large links spindle orientation to apical-basal polarity in Drosophila epithelia. *Current biology : CB*. 23:1707-1712.

Betschinger, J., F. Eisenhaber, and J.A. Knoblich. 2005. Phosphorylation-induced autoinhibition regulates the cytoskeletal protein Lethal (2) giant larvae. *Curr Biol*. 15:276-282.

Betschinger, J., and J.A. Knoblich. 2004. Dare to be different: asymmetric cell division in Drosophila, C. elegans and vertebrates. *Curr Biol*. 14:R674-685.

Betschinger, J., K. Mechtler, and J.A. Knoblich. 2003. The Par complex directs asymmetric cell division by phosphorylating the cytoskeletal protein Lgl. *Nature*. 422:326-330.

Bilder, D., M. Li, and N. Perrimon. 2000. Cooperative regulation of cell polarity and growth by Drosophila tumor suppressors. *Science*. 289:113-116.

Bowman, S.K., R.A. Neumuller, M. Novatchkova, Q. Du, and J.A. Knoblich. 2006. The Drosophila NuMA Homolog Mud regulates spindle orientation in asymmetric cell division. *Dev Cell*. 10:731-742.

Cabernard, C., and C.Q. Doe. 2009. Apical/basal spindle orientation is required for neuroblast homeostasis and neuronal differentiation in Drosophila. *Dev Cell*. 17:134-141.

Cai, Y., F. Yu, S. Lin, W. Chia, and X. Yang. 2003. Apical complex genes control mitotic spindle geometry and relative size of daughter cells in Drosophila neuroblast and pI asymmetric divisions. *Cell*. 112:51-62.

Cao, F., Y. Miao, K. Xu, and P. Liu. 2015. Lethal (2) giant larvae: an indispensable regulator of cell polarity and cancer development. *Int J Biol Sci*. 11:380-389.

Carmena, A., A. Makarova, and S. Speicher. 2011. The Rap1-Rgl-Ral signaling network regulates neuroblast cortical polarity and spindle orientation. *The Journal of cell biology*. 195:553-562.

Carvalho, C.A., S. Moreira, G. Ventura, C.E. Sunkel, and E. Morais-de-Sa. 2014. Aurora A Triggers Lgl Cortical Release during Symmetric Division to Control Planar Spindle Orientation. *Current biology : CB*.

Caussinus, E., and C. Gonzalez. 2005. Induction of tumor growth by altered stem-cell asymmetric division in Drosophila melanogaster. *Nat Genet*. 37:1125-1129.

Chalmers, A.D., M. Pambos, J. Mason, S. Lang, C. Wylie, and N. Papalopulu. 2005. aPKC, Crumbs3 and Lgl2 control apicobasal polarity in early vertebrate development. *Development*. 132:977-986.

Cheeseman, I.M., S. Anderson, M. Jwa, E.M. Green, J. Kang, J.R. Yates, 3rd, C.S. Chan, D.G. Drubin, and G. Barnes. 2002. Phospho-regulation of kinetochore-microtubule attachments by the Aurora kinase Ipl1p. *Cell*. 111:163-172.

Cheng, J., N. Turkel, N. Hemati, M.T. Fuller, A.J. Hunt, and Y.M. Yamashita. 2008. Centrosome misorientation reduces stem cell division during ageing. *Nature*. 456:599-604.

Ciferri, C., S. Pasqualato, E. Screpanti, G. Varetti, S. Santaguida, G. Dos Reis, A. Maiolica, J. Polka, J.G. De Luca, P. De Wulf, M. Salek, J. Rappsilber, C.A. Moores, E.D. Salmon, and A. Musacchio. 2008. Implications for kinetochore-microtubule attachment from the structure of an engineered Ndc80 complex. *Cell*. 133:427-439.

Clarke, P.R., and C. Zhang. 2008. Spatial and temporal coordination of mitosis by Ran GTPase. *Nat Rev Mol Cell Biol*. 9:464-477.

Couwenbergs, C., J.C. Labbe, M. Goulding, T. Marty, B. Bowerman, and M. Gotta. 2007. Heterotrimeric G protein signaling functions with dynein to promote spindle positioning in C. elegans. *J Cell Biol*. 179:15-22.

Crane, R., A. Kloepfer, and J.V. Ruderman. 2004. Requirements for the destruction of human Aurora-A. *J Cell Sci*. 117:5975-5983.

Culurgioni, S., A. Alfieri, V. Pendolino, F. Laddomada, and M. Mapelli. 2011. Inscuteable and NuMA proteins bind competitively to Leu-Gly-Asn repeat-enriched protein (LGN) during asymmetric cell divisions. *Proc Natl Acad Sci U S A*. 108:20998-21003.

De Luca, M., L. Brunetto, I.A. Asteriti, M. Giubettini, P. Lavia, and G. Guarguaglini. 2008. Aurora-A and ch-TOG act in a common pathway in control of spindle pole integrity. *Oncogene*. 27:6539-6549.

den Elzen, N., C.V. Buttery, M.P. Maddugoda, G. Ren, and A.S. Yap. 2009. Cadherin adhesion receptors orient the mitotic spindle during symmetric cell division in mammalian epithelia. *Mol Biol Cell*. 20:3740-3750.

Desai, A., and T.J. Mitchison. 1997. Microtubule polymerization dynamics. *Annu Rev Cell Dev Biol*. 13:83-117.

Du, Q., and I.G. Macara. 2004. Mammalian Pins is a conformational switch that links NuMA to heterotrimeric G proteins. *Cell*. 119:503-516.

Du, Q., P.T. Stukenberg, and I.G. Macara. 2001. A mammalian Partner of inscuteable binds NuMA and regulates mitotic spindle organization. *Nat Cell Biol*. 3:1069-1075.

Du, Q., L. Taylor, D.A. Compton, and I.G. Macara. 2002. LGN blocks the ability of NuMA to bind and stabilize microtubules. A mechanism for mitotic spindle assembly regulation. *Curr Biol*. 12:1928-1933.

Elias, S., M.S. Thion, H. Yu, C.M. Sousa, C. Lasgi, X. Morin, and S. Humbert. 2014. Huntingtin regulates mammary stem cell division and differentiation. *Stem cell reports*. 2:491-506.

Elting, M.W., C.L. Hueschen, D.B. Udy, and S. Dumont. 2014. Force on spindle microtubule minus ends moves chromosomes. *J Cell Biol*. 206:245-256.

Fant, X., A. Merdes, and L. Haren. 2004. Cell and molecular biology of spindle poles and NuMA. *Int Rev Cytol*. 238:1-57.

Ferrari, S., O. Marin, M.A. Pagano, F. Meggio, D. Hess, M. El-Shemerly, A. Krystyniak, and L.A. Pinna. 2005. Aurora-A site specificity: a study with synthetic peptide substrates. *Biochem J*. 390:293-302.

Fink, J., N. Carpi, T. Betz, A. Betard, M. Chebah, A. Azioune, M. Bornens, C. Sykes, L. Fetler, D. Cuvelier, and M. Piel. 2011. External forces control mitotic spindle positioning. *Nat Cell Biol*. 13:771-778.

Forth, S., K.C. Hsia, Y. Shimamoto, and T.M. Kapoor. 2014. Asymmetric friction of nonmotor MAPs can lead to their directional motion in active microtubule networks. *Cell*. 157:420-432.

Fuchs, E., and T. Chen. 2013. A matter of life and death: self-renewal in stem cells. *EMBO Rep*. 14:39-48.

Gadde, S., and R. Heald. 2004. Mechanisms and molecules of the mitotic spindle. *Curr Biol*. 14:R797-805.

Giet, R., D. McLean, S. Descamps, M.J. Lee, J.W. Raff, C. Prigent, and D.M. Glover. 2002. Drosophila Aurora A kinase is required to localize D-TACC to centrosomes and to regulate astral microtubules. *J Cell Biol*. 156:437-451.

Giet, R., R. Uzbekov, F. Cubizolles, K. Le Guellec, and C. Prigent. 1999. The Xenopus laevis aurora-related protein kinase pEg2 associates with and phosphorylates the kinesin-related protein XlEg5. *J Biol Chem*. 274:15005-15013.

Gillies, T.E., and C. Cabernard. 2011. Cell division orientation in animals. *Current biology : CB*. 21:R599-609.

Glotzer, M. 2009. The 3Ms of central spindle assembly: microtubules, motors and MAPs. *Nat Rev Mol Cell Biol*. 10:9-20.

Gonczy, P. 2002. Mechanisms of spindle positioning: focus on flies and worms. *Trends Cell Biol*. 12:332-339.

Gonczy, P., and L.S. Rose. 2005. Asymmetric cell division and axis formation in the embryo. *WormBook*:1-20.

Gorlich, D., and U. Kutay. 1999. Transport between the cell nucleus and the cytoplasm. *Annu Rev Cell Dev Biol*. 15:607-660.

Gotta, M., Y. Dong, Y.K. Peterson, S.M. Lanier, and J. Ahringer. 2003. Asymmetrically distributed C. elegans homologs of AGS3/PINS control spindle position in the early embryo. *Curr Biol*. 13:1029-1037.

Grill, S.W., P. Gonczy, E.H. Stelzer, and A.A. Hyman. 2001. Polarity controls forces governing asymmetric spindle positioning in the Caenorhabditis elegans embryo. *Nature*. 409:630-633.

Gruss, O.J., and I. Vernos. 2004. The mechanism of spindle assembly: functions of Ran and its target TPX2. *J Cell Biol*. 166:949-955.

Gueth-Hallonet, C., K. Weber, and M. Osborn. 1996. NuMA: a bipartite nuclear location signal and other functional properties of the tail domain. *Exp Cell Res*. 225:207-218.

Hao, Y., Q. Du, X. Chen, Z. Zheng, J.L. Balsbaugh, S. Maitra, J. Shabanowitz, D.F. Hunt, and I.G. Macara. 2010. Par3 controls epithelial spindle orientation by aPKC-mediated phosphorylation of apical Pins. *Curr Biol*. 20:1809-1818.

Harborth, J., J. Wang, C. Gueth-Hallonet, K. Weber, and M. Osborn. 1999. Self assembly of NuMA: multiarm oligomers as structural units of a nuclear lattice. *EMBO J*. 18:1689-1700.

Harborth, J., K. Weber, and M. Osborn. 1995. Epitope mapping and direct visualization of the parallel, in-register arrangement of the double-stranded coiled-coil in the NuMA protein. *EMBO J*. 14:2447-2460.

Haren, L., N. Gnadt, M. Wright, and A. Merdes. 2009. NuMA is required for proper spindle assembly and chromosome alignment in prometaphase. *BMC Res Notes*. 2:64.

Haren, L., and A. Merdes. 2002. Direct binding of NuMA to tubulin is mediated by a novel sequence motif in the tail domain that bundles and stabilizes microtubules. *J Cell Sci*. 115:1815-1824.

Heald, R., R. Tournebize, T. Blank, R. Sandaltzopoulos, P. Becker, A. Hyman, and E. Karsenti. 1996. Self-organization of microtubules into bipolar spindles around artificial chromosomes in Xenopus egg extracts. *Nature*. 382:420-425.

Hertwig, W.A.O., Hertwig, and R. Hertwig. 1884. Untersuchungen zur Morphologie und Physiologie der Zelle. Jena.

Humbert, P.O., N.A. Grzeschik, A.M. Brumby, R. Galea, I. Elsum, and H.E. Richardson. 2008. Control of tumourigenesis by the Scribble/Dlg/Lgl polarity module. *Oncogene*. 27:6888-6907.

Hutterer, A., J. Betschinger, M. Petronczki, and J.A. Knoblich. 2004. Sequential roles of Cdc42, Par-6, aPKC, and Lgl in the establishment of epithelial polarity during Drosophila embryogenesis. *Dev Cell*. 6:845-854.

Ikeda, W., H. Nakanishi, J. Miyoshi, K. Mandai, H. Ishizaki, M. Tanaka, A. Togawa, K. Takahashi, H. Nishioka, H. Yoshida, A. Mizoguchi, S. Nishikawa, and Y. Takai. 1999. Afadin: A key molecule essential for structural organization of cell-cell junctions of polarized epithelia during embryogenesis. *J Cell Biol*. 146:1117-1132.

Izumi, Y., N. Ohta, K. Hisata, T. Raabe, and F. Matsuzaki. 2006. Drosophila Pins-binding protein Mud regulates spindle-polarity coupling and centrosome organization. *Nat Cell Biol*. 8:586-593.

Jaffe, A.B., N. Kaji, J. Durgan, and A. Hall. 2008. Cdc42 controls spindle orientation to position the apical surface during epithelial morphogenesis. *J Cell Biol*. 183:625-633.

Johnston, C.A., K. Hirono, K.E. Prehoda, and C.Q. Doe. 2009. Identification of an Aurora-A/PinsLINKER/Dlg spindle orientation pathway using induced cell polarity in S2 cells. *Cell*. 138:1150-1163.

Johnston, C.A., L. Manning, M.S. Lu, O. Golub, C.Q. Doe, and K.E. Prehoda. 2013. Formin-mediated actin polymerization cooperates with Mushroom body defect (Mud)-Dynein during Frizzled-Dishevelled spindle orientation. *Journal of cell science*. 126:4436-4444.

Kalab, P., and R. Heald. 2008. The RanGTP gradient - a GPS for the mitotic spindle. *J Cell Sci*. 121:1577-1586.

Kardon, J.R., and R.D. Vale. 2009. Regulators of the cytoplasmic dynein motor. *Nat Rev Mol Cell Biol*. 10:854-865.

Kettenbach, A.N., D.K. Schweppe, B.K. Faherty, D. Pechenick, A.A. Pletnev, and S.A. Gerber. 2011. Quantitative phosphoproteomics identifies substrates and functional modules of Aurora and Polo-like kinase activities in mitotic cells. *Science signaling*. 4:rs5.

Khodjakov, A., L. Copenagle, M.B. Gordon, D.A. Compton, and T.M. Kapoor. 2003. Minus-end capture of preformed kinetochore fibers contributes to spindle morphogenesis. *J Cell Biol*. 160:671-683.

Kisurina-Evgenieva, O., G. Mack, Q. Du, I. Macara, A. Khodjakov, and D.A. Compton. 2004. Multiple mechanisms regulate NuMA dynamics at spindle poles. *Journal of cell science*. 117:6391-6400.

Kiyomitsu, T. 2015. Mechanisms of daughter cell-size control during cell division. *Trends Cell Biol*. 25:286-295.

Kiyomitsu, T., and I.M. Cheeseman. 2012. Chromosome- and spindle-pole-derived signals generate an intrinsic code for spindle position and orientation. *Nat Cell Biol*.

Kiyomitsu, T., and I.M. Cheeseman. 2013. Cortical dynein and asymmetric membrane elongation coordinately position the spindle in anaphase. *Cell*. 154:391-402.

Knoblich, J.A. 2010. Asymmetric cell division: recent developments and their implications for tumour biology. *Nat Rev Mol Cell Biol*. 11:849-860.

Knoblich, J.A., L.Y. Jan, and Y.N. Jan. 1995. Asymmetric segregation of Numb and Prospero during cell division. *Nature*. 377:624-627.

Kobayashi, R., S. Kurita, M. Miyata, T. Maruo, K. Mandai, Y. Rikitake, and Y. Takai. 2014. s-Afadin binds more preferentially to the cell adhesion molecules nectins than l-afadin. *Genes to cells : devoted to molecular & cellular mechanisms*. 19:853-863.

Konno, D., G. Shioi, A. Shitamukai, A. Mori, H. Kiyonari, T. Miyata, and F. Matsuzaki. 2008. Neuroepithelial progenitors undergo LGN-dependent planar divisions to maintain self-renewability during mammalian neurogenesis. *Nat Cell Biol*. 10:93-101.

Kotak, S., C. Busso, and P. Gonczy. 2012. Cortical dynein is critical for proper spindle positioning in human cells. *The Journal of cell biology*. 199:97-110.

Kotak, S., C. Busso, and P. Gonczy. 2013. NuMA phosphorylation by CDK1 couples mitotic progression with cortical dynein function. *The EMBO journal*. 32:2517-2529.

Kotak, S., and P. Gonczy. 2013. Mechanisms of spindle positioning: cortical force generators in the limelight. *Current opinion in cell biology*. 25:741-748.

Kotak, S., and P. Gonczy. 2014. NuMA phosphorylation dictates dynein-dependent spindle positioning. *Cell cycle*. 13:177-178.

Kufer, T.A., H.H. Sillje, R. Korner, O.J. Gruss, P. Meraldi, and E.A. Nigg. 2002. Human TPX2 is required for targeting Aurora-A kinase to the spindle. *J Cell Biol*. 158:617-623.

Kulukian, A., and E. Fuchs. 2013. Spindle orientation and epidermal morphogenesis. *Philos Trans R Soc Lond B Biol Sci*. 368:20130016.

Kunda, P., and B. Baum. 2009. The actin cytoskeleton in spindle assembly and positioning. *Trends Cell Biol*. 19:174-179.

Lancaster, O.M., and B. Baum. 2014. Shaping up to divide: Coordinating actin and microtubule cytoskeletal remodelling during mitosis. *Seminars in cell & developmental biology*.

Lechler, T., and E. Fuchs. 2005. Asymmetric cell divisions promote stratification and differentiation of mammalian skin. *Nature*. 437:275-280.

Lee, C.Y., R.O. Andersen, C. Cabernard, L. Manning, K.D. Tran, M.J. Lanskey, A. Bashirullah, and C.Q. Doe. 2006a. Drosophila Aurora-A kinase inhibits neuroblast self-renewal by regulating aPKC/Numb cortical polarity and spindle orientation. *Genes Dev*. 20:3464-3474.

Lee, C.Y., B.D. Wilkinson, S.E. Siegrist, R.P. Wharton, and C.Q. Doe. 2006b. Brat is a Miranda cargo protein that promotes neuronal differentiation and inhibits neuroblast self-renewal. *Dev Cell*. 10:441-449.

Letessier, A., S. Garrido-Urbani, C. Ginestier, G. Fournier, B. Esterni, F. Monville, J. Adelaide, J. Geneix, L. Xerri, P. Dubreuil, P. Viens, E. Charafe-Jauffret, J. Jacquemier, D. Birnbaum, M. Lopez, and M. Chaffanet. 2007. Correlated break at PARK2/FRA6E and loss of AF-6/Afadin protein expression are associated with poor outcome in breast cancer. *Oncogene*. 26:298-307.

Lioutas, A., and I. Vernos. 2013. Aurora A kinase and its substrate TACC3 are required for central spindle assembly. *EMBO Rep*. 14:829-836.

Littlepage, L.E., and J.V. Ruderman. 2002. Identification of a new APC/C recognition domain, the A box, which is required for the Cdh1-dependent destruction of the kinase Aurora-A during mitotic exit. *Genes Dev*. 16:2274-2285.

Littlepage, L.E., H. Wu, T. Andresson, J.K. Deanehan, L.T. Amundadottir, and J.V. Ruderman. 2002. Identification of phosphorylated residues that affect the activity of the mitotic kinase Aurora-A. *Proc Natl Acad Sci U S A*. 99:15440-15445.

Livak, K.J., and T.D. Schmittgen. 2001. Analysis of relative gene expression data using real-time quantitative PCR and the 2(-Delta Delta C(T)) Method. *Methods*. 25:402-408.

Lorger, M., and K. Moelling. 2006. Regulation of epithelial wound closure and intercellular adhesion by interaction of AF6 with actin cytoskeleton. *J Cell Sci*. 119:3385-3398.

Lorson, M.A., H.R. Horvitz, and S. van den Heuvel. 2000. LIN-5 is a novel component of the spindle apparatus required for chromosome segregation and cleavage plane specification in Caenorhabditis elegans. *The Journal of cell biology*. 148:73-86.

Lu, M.S., and C.A. Johnston. 2013. Molecular pathways regulating mitotic spindle orientation in animal cells. *Development*. 140:1843-1856.

Luderus, M.E., J.L. den Blaauwen, O.J. de Smit, D.A. Compton, and R. van Driel. 1994. Binding of matrix attachment regions to lamin polymers involves single-stranded regions and the minor groove. *Mol Cell Biol*. 14:6297-6305.

Machicoane, M., C.A. de Frutos, J. Fink, M. Rocancourt, Y. Lombardi, S. Garel, M. Piel, and A. Echard. 2014. SLK-dependent activation of ERMs controls LGN-NuMA localization and spindle orientation. *The Journal of cell biology*. 205:791-799.

Manahan, C.L., M. Patnana, K.J. Blumer, and M.E. Linder. 2000. Dual lipid modification motifs in G(alpha) and G(gamma) subunits are required for full activity of the pheromone response pathway in Saccharomyces cerevisiae. *Mol Biol Cell*. 11:957-968.

Mandai, K., H. Nakanishi, A. Satoh, H. Obaishi, M. Wada, H. Nishioka, M. Itoh, A. Mizoguchi, T. Aoki, T. Fujimoto, Y. Matsuda, S. Tsukita, and Y. Takai. 1997. Afadin: A novel actin filament-binding protein with one PDZ domain localized at cadherin-based cell-to-cell adherens junction. *The Journal of cell biology*. 139:517-528.

Manfredi, M.G., J.A. Ecsedy, A. Chakravarty, L. Silverman, M. Zhang, K.M. Hoar, S.G. Stroud, W. Chen, V. Shinde, J.J. Huck, D.R. Wysong, D.A. Janowick, M.L. Hyer, P.J. Leroy, R.E. Gershman, M.D. Silva, M.S. Germanos, J.B. Bolen, C.F. Claiborne, and T.B. Sells. 2011. Characterization of Alisertib (MLN8237), an investigational small-molecule inhibitor of aurora A kinase using novel in vivo pharmacodynamic assays. *Clin Cancer Res*. 17:7614-7624.

Marumoto, T., S. Honda, T. Hara, M. Nitta, T. Hirota, E. Kohmura, and H. Saya. 2003. Aurora-A kinase maintains the fidelity of early and late mitotic events in HeLa cells. *The Journal of biological chemistry*. 278:51786-51795.

Matsumura, S., M. Hamasaki, T. Yamamoto, M. Ebisuya, M. Sato, E. Nishida, and F. Toyoshima. 2011. ABL1 regulates spindle orientation in adherent cells and mammalian skin. *Nat Commun*. 3:626.

Mattaj, I.W., and L. Englmeier. 1998. Nucleocytoplasmic transport: the soluble phase. *Annu Rev Biochem*. 67:265-306.

Mayer, T.U., T.M. Kapoor, S.J. Haggarty, R.W. King, S.L. Schreiber, and T.J. Mitchison. 1999. Small molecule inhibitor of mitotic spindle bipolarity identified in a phenotype-based screen. *Science*. 286:971-974.

McCloy, R.A., B.L. Parker, S. Rogers, R. Chaudhuri, V. Gayevskiy, N.J. Hoffman, N. Ali, D.N. Watkins, R.J. Daly, D.E. James, T. Lorca, A. Castro, and A. Burgess. 2015. Global Phosphoproteomic Mapping of Early Mitotic Exit in Human Cells Identifies Novel Substrate Dephosphorylation Motifs. *Mol Cell Proteomics*. 14:2194-2212.

Mechler, B.M., W. McGinnis, and W.J. Gehring. 1985. Molecular cloning of lethal(2)giant larvae, a recessive oncogene of Drosophila melanogaster. *EMBO J*. 4:1551-1557.

Meraldi, P., and E.A. Nigg. 2002. The centrosome cycle. *FEBS Lett*. 521:9-13.

Merdes, A., and D.W. Cleveland. 1998. The role of NuMA in the interphase nucleus. *Journal of cell science*. 111 (Pt 1):71-79.

Merdes, A., R. Heald, K. Samejima, W.C. Earnshaw, and D.W. Cleveland. 2000. Formation of spindle poles by dynein/dynactin-dependent transport of NuMA. *J Cell Biol*. 149:851-862.

Merdes, A., K. Ramyar, J.D. Vechio, and D.W. Cleveland. 1996. A complex of NuMA and cytoplasmic dynein is essential for mitotic spindle assembly. *Cell*. 87:447-458.

Mora-Bermudez, F., F. Matsuzaki, and W.B. Huttner. 2014. Specific polar subpopulations of astral microtubules control spindle orientation and symmetric neural stem cell division. *eLife*. 3.

Morgan, D.O. 2006. The cell cycle : principles of control. New Science Press, London.

Morin, X., and Y. Bellaiche. 2011. Mitotic Spindle Orientation in Asymmetric and Symmetric Cell Divisions during Animal Development. *Dev Cell*. 21:102-119.

Morin, X., F. Jaouen, and P. Durbec. 2007. Control of planar divisions by the G-protein regulator LGN maintains progenitors in the chick neuroepithelium. *Nat Neurosci*. 10:1440-1448.

Musch, A., D. Cohen, C. Yeaman, W.J. Nelson, E. Rodriguez-Boulan, and P.J. Brennwald. 2002. Mammalian homolog of Drosophila tumor suppressor lethal (2) giant larvae interacts with basolateral exocytic machinery in Madin-Darby canine kidney cells. *Mol Biol Cell*. 13:158-168.

Nachury, M.V., T.J. Maresca, W.C. Salmon, C.M. Waterman-Storer, R. Heald, and K. Weis. 2001. Importin beta is a mitotic target of the small GTPase Ran in spindle assembly. *Cell*. 104:95-106.

Nakajima, Y., E.J. Meyer, A. Kroesen, S.A. McKinney, and M.C. Gibson. 2013. Epithelial junctions maintain tissue architecture by directing planar spindle orientation. *Nature*. 500:359-362.

Neer, E.J. 1995. Heterotrimeric G proteins: organizers of transmembrane signals. *Cell*. 80:249-257.

Nguyen-Ngoc, T., K. Afshar, and P. Gonczy. 2007. Coupling of cortical dynein and G alpha proteins mediates spindle positioning in Caenorhabditis elegans. *Nat Cell Biol*. 9:1294-1302.

Niessen, C.M., and C.J. Gottardi. 2008. Molecular components of the adherens junction. *Biochimica et biophysica acta*. 1778:562-571.

Nikonova, A.S., I. Astsaturov, I.G. Serebriiskii, R.L. Dunbrack, Jr., and E.A. Golemis. 2013. Aurora A kinase (AURKA) in normal and pathological cell division. *Cellular and molecular life sciences : CMLS*. 70:661-687.

Ogo, N., S. Oishi, K. Matsuno, J. Sawada, N. Fujii, and A. Asai. 2007. Synthesis and biological evaluation of L-cysteine derivatives as mitotic kinesin Eg5 inhibitors. *Bioorg Med Chem Lett*. 17:3921-3924.

Ohshiro, T., T. Yagami, C. Zhang, and F. Matsuzaki. 2000. Role of cortical tumour-suppressor proteins in asymmetric division of Drosophila neuroblast. *Nature*. 408:593-596.

Ooshio, T., N. Fujita, A. Yamada, T. Sato, Y. Kitagawa, R. Okamoto, S. Nakata, A. Miki, K. Irie, and Y. Takai. 2007. Cooperative roles of Par-3 and afadin in the formation of adherens and tight junctions. *Journal of cell science*. 120:2352-2365.

Ooshio, T., K. Irie, K. Morimoto, A. Fukuhara, T. Imai, and Y. Takai. 2004. Involvement of LMO7 in the association of two cell-cell adhesion molecules, nectin and E-cadherin, through afadin and alpha-actinin in epithelial cells. *The Journal of biological chemistry*. 279:31365-31373.

Pan, Z., J. Zhu, Y. Shang, Z. Wei, M. Jia, C. Xia, W. Wen, W. Wang, and M. Zhang. 2013. An autoinhibited conformation of LGN reveals a distinct interaction mode between GoLoco motifs and TPR motifs. *Structure*. 21:1007-1017.

Park, D.H., and L.S. Rose. 2008. Dynamic localization of LIN-5 and GPR-1/2 to cortical force generation domains during spindle positioning. *Dev Biol*. 315:42-54.

Peng, C.Y., L. Manning, R. Albertson, and C.Q. Doe. 2000. The tumour-suppressor genes lgl and dlg regulate basal protein targeting in Drosophila neuroblasts. *Nature*. 408:596-600.

Pereira, G., and E. Schiebel. 2005. Kin4 kinase delays mitotic exit in response to spindle alignment defects. *Molecular cell*. 19:209-221.

Peset, I., J. Seiler, T. Sardon, L.A. Bejarano, S. Rybina, and I. Vernos. 2005. Function and regulation of Maskin, a TACC family protein, in microtubule growth during mitosis. *J Cell Biol*. 170:1057-1066.

Peset, I., and I. Vernos. 2008. The TACC proteins: TACC-ling microtubule dynamics and centrosome function. *Trends Cell Biol*. 18:379-388.

Petronczki, M., and J.A. Knoblich. 2001. DmPAR-6 directs epithelial polarity and asymmetric cell division of neuroblasts in Drosophila. *Nat Cell Biol*. 3:43-49.

Peyre, E., F. Jaouen, M. Saadaoui, L. Haren, A. Merdes, P. Durbec, and X. Morin. 2011. A lateral belt of cortical LGN and NuMA guides mitotic spindle movements and planar division in neuroepithelial cells. *J Cell Biol*. 193:141-154.

Peyre, E., and X. Morin. 2012. An oblique view on the role of spindle orientation in vertebrate neurogenesis. *Development, growth & differentiation*. 54:287-305.

Pinyol, R., J. Scrofani, and I. Vernos. 2013. The role of NEDD1 phosphorylation by Aurora A in chromosomal microtubule nucleation and spindle function. *Curr Biol*. 23:143-149.

Plant, P.J., J.P. Fawcett, D.C. Lin, A.D. Holdorf, K. Binns, S. Kulkarni, and T. Pawson. 2003. A polarity complex of mPar-6 and atypical PKC binds, phosphorylates and regulates mammalian Lgl. *Nat Cell Biol*. 5:301-308.

Ragkousi, K., and M.C. Gibson. 2014. Cell division and the maintenance of epithelial order. *J Cell Biol*. 207:181-188.

Reboutier, D., M.B. Troadec, J.Y. Cremet, L. Chauvin, V. Guen, P. Salaun, and C. Prigent. 2013. Aurora A is involved in central spindle assembly through phosphorylation of Ser 19 in P150Glued. *The Journal of cell biology*. 201:65-79.

Regan, J.L., T. Sourisseau, K. Soady, H. Kendrick, A. McCarthy, C. Tang, K. Brennan, S. Linardopoulos, D.E. White, and M.J. Smalley. 2013. Aurora A kinase regulates mammary epithelial cell fate by determining mitotic spindle orientation in a Notch-dependent manner. *Cell reports*. 4:110-123.

Rome, P., E. Montembault, N. Franck, A. Pascal, D.M. Glover, and R. Giet. 2010. Aurora A contributes to p150(glued) phosphorylation and function during mitosis. *J Cell Biol*. 189:651-659.

Saadaoui, M., M. Machicoane, F. di Pietro, F. Etoc, A. Echard, and X. Morin. 2014. Dlg1 controls planar spindle orientation in the neuroepithelium through direct interaction with LGN. *The Journal of cell biology*. 206:707-717.

Saito, S., M. Matsushima, S. Shirahama, T. Minaguchi, Y. Kanamori, M. Minami, and Y. Nakamura. 1998. Complete genomic structure DNA polymorphisms, and alternative splicing of the human AF-6 gene. *DNA Res*. 5:115-120.

Sandquist, J.C., A.M. Kita, and W.M. Bement. 2011. And the dead shall rise: actin and myosin return to the spindle. *Dev Cell*. 21:410-419.

Sans, N., P.Y. Wang, Q. Du, R.S. Petralia, Y.X. Wang, S. Nakka, J.B. Blumer, I.G. Macara, and R.J. Wenthold. 2005. mPins modulates PSD-95 and SAP102 trafficking and influences NMDA receptor surface expression. *Nat Cell Biol*. 7:1179-1190.

Sardon, T., R.A. Pache, A. Stein, H. Molina, I. Vernos, and P. Aloy. 2010. Uncovering new substrates for Aurora A kinase. *EMBO Rep*. 11:977-984.

Sardon, T., I. Peset, B. Petrova, and I. Vernos. 2008. Dissecting the role of Aurora A during spindle assembly. *EMBO J*. 27:2567-2579.

Sawin, K.E., K. LeGuellec, M. Philippe, and T.J. Mitchison. 1992. Mitotic spindle organization by a plus-end-directed microtubule motor. *Nature*. 359:540-543.

Sawyer, J.K., W. Choi, K.C. Jung, L. He, N.J. Harris, and M. Peifer. 2011. A contractile actomyosin network linked to adherens junctions by Canoe/afadin helps drive convergent extension. *Mol Biol Cell*. 22:2491-2508.

Sawyer, J.K., N.J. Harris, K.C. Slep, U. Gaul, and M. Peifer. 2009. The Drosophila afadin homologue Canoe regulates linkage of the actin cytoskeleton to adherens junctions during apical constriction. *J Cell Biol*. 186:57-73.

Schindelin, J., I. Arganda-Carreras, E. Frise, V. Kaynig, M. Longair, T. Pietzsch, S. Preibisch, C. Rueden, S. Saalfeld, B. Schmid, J.Y. Tinevez, D.J. White, V. Hartenstein, K. Eliceiri, P. Tomancak, and A. Cardona. 2012. Fiji: an open-source platform for biological-image analysis. *Nat Methods*. 9:676-682.

Schober, M., M. Schaefer, and J.A. Knoblich. 1999. Bazooka recruits Inscuteable to orient asymmetric cell divisions in Drosophila neuroblasts. *Nature*. 402:548-551.

Scita, G., P. Tenca, L.B. Areces, A. Tocchetti, E. Frittoli, G. Giardina, I. Ponzanelli, P. Sini, M. Innocenti, and P.P. Di Fiore. 2001. An effector region in Eps8 is responsible for the activation of the Rac-specific GEF activity of Sos-1 and for the proper localization of the Rac-based actin-polymerizing machine. *The Journal of cell biology*. 154:1031-1044.

Segalen, M., C.A. Johnston, C.A. Martin, J.G. Dumortier, K.E. Prehoda, N.B. David, C.Q. Doe, and Y. Bellaiche. 2010. The Fz-Dsh planar cell polarity pathway induces oriented cell division via Mud/NuMA in Drosophila and zebrafish. *Dev Cell*. 19:740-752.

Seldin, L., N.D. Poulson, H.P. Foote, and T. Lechler. 2013. NuMA localization, stability, and function in spindle orientation involve 4.1 and Cdk1 interactions. *Molecular biology of the cell*. 24:3651-3662.

Silk, A.D., A.J. Holland, and D.W. Cleveland. 2009. Requirements for NuMA in maintenance and establishment of mammalian spindle poles. *The Journal of cell biology*. 184:677-690.

Siller, K.H., C. Cabernard, and C.Q. Doe. 2006. The NuMA-related Mud protein binds Pins and regulates spindle orientation in Drosophila neuroblasts. *Nat Cell Biol*. 8:594-600.

Siller, K.H., and C.Q. Doe. 2009. Spindle orientation during asymmetric cell division. *Nat Cell Biol*. 11:365-374.

Spector, I., N.R. Shochet, Y. Kashman, and A. Groweiss. 1983. Latrunculins: novel marine toxins that disrupt microfilament organization in cultured cells. *Science*. 219:493-495.

Speicher, S., A. Fischer, J. Knoblich, and A. Carmena. 2008. The PDZ protein Canoe regulates the asymmetric division of Drosophila neuroblasts and muscle progenitors. *Curr Biol*. 18:831-837.

Srinivasan, D.G., R.M. Fisk, H. Xu, and S. van den Heuvel. 2003. A complex of LIN-5 and GPR proteins regulates G protein signaling and spindle function in C elegans. *Genes Dev*. 17:1225-1239.

Sun, T.T., Y. Wang, H. Cheng, X.H. Zhang, J.J. Xiang, J.T. Zhang, S.B. Yu, T.A. Martin, L. Ye, L.L. Tsang, W.G. Jiang, X. Jiang, and H.C. Chan. 2013. Disrupted interaction between CFTR and AF-6/afadin aggravates malignant phenotypes of colon cancer. *Biochimica et biophysica acta*. 1843:618-628.

Takai, Y., W. Ikeda, H. Ogita, and Y. Rikitake. 2008. The immunoglobulin-like cell adhesion molecule nectin and its associated protein afadin. *Annu Rev Cell Dev Biol*. 24:309-342.

Tanaka-Okamoto, M., Y. Itoh, J. Miyoshi, A. Mizoguchi, K. Mizutani, Y. Takai, and M. Inoue. 2014. Genetic ablation of afadin causes mislocalization and deformation of Paneth cells in the mouse small intestinal epithelium. *PLoS One*. 9:e110549.

Tanentzapf, G., and U. Tepass. 2003. Interactions between the crumbs, lethal giant larvae and bazooka pathways in epithelial polarization. *Nat Cell Biol*. 5:46-52.

Tawa, H., Y. Rikitake, M. Takahashi, H. Amano, M. Miyata, S. Satomi-Kobayashi, M. Kinugasa, Y. Nagamatsu, T. Majima, H. Ogita, J. Miyoshi, K. Hirata, and Y. Takai. 2010. Role of afadin in vascular endothelial growth factor- and sphingosine 1-phosphate-induced angiogenesis. *Circulation research*. 106:1731-1742.

Thery, M., V. Racine, A. Pepin, M. Piel, Y. Chen, J.B. Sibarita, and M. Bornens. 2005. The extracellular matrix guides the orientation of the cell division axis. *Nat Cell Biol*. 7:947-953.

Toughiri, R., X. Li, Q. Du, and C.J. Bieberich. 2012. Phosphorylation of NuMA by Aurora-A kinase in PC-3 prostate cancer cells affects proliferation, survival and interphase NuMA localization. *J Cell Biochem*.

Toyoshima, F., and E. Nishida. 2007. Integrin-mediated adhesion orients the spindle parallel to the substratum in an EB1- and myosin X-dependent manner. *The EMBO journal*. 26:1487-1498.

Vassilev, L.T., C. Tovar, S. Chen, D. Knezevic, X. Zhao, H. Sun, D.C. Heimbrook, and L. Chen. 2006. Selective small-molecule inhibitor reveals critical mitotic functions of human CDK1. *Proc Natl Acad Sci U S A*. 103:10660-10665.

Vidi, P.A., G. Chandramouly, M. Gray, L. Wang, E. Liu, J.J. Kim, V. Roukos, M.J. Bissell, P.V. Moghe, and S.A. Lelievre. 2012. Interconnected contribution of tissue morphogenesis and the nuclear protein NuMA to the DNA damage response. *J Cell Sci*. 125:350-361.

Vidi, P.A., J. Liu, D. Salles, S. Jayaraman, G. Dorfman, M. Gray, P. Abad, P.V. Moghe, J.M. Irudayaraj, L. Wiesmuller, and S.A. Lelievre. 2014. NuMA promotes homologous recombination repair by regulating the accumulation of the ISWI ATPase SNF2h at DNA breaks. *Nucleic Acids Res*. 42:6365-6379.

Walter, A.O., W. Seghezzi, W. Korver, J. Sheung, and E. Lees. 2000. The mitotic serine/threonine kinase Aurora2/AIK is regulated by phosphorylation and degradation. *Oncogene*. 19:4906-4916.

Wang, G., Q. Jiang, and C. Zhang. 2014. The role of mitotic kinases in coupling the centrosome cycle with the assembly of the mitotic spindle. *J Cell Sci*. 127:4111-4122.

Wang, H., G.W. Somers, A. Bashirullah, U. Heberlein, F. Yu, and W. Chia. 2006. Aurora-A acts as a tumor suppressor and regulates self-renewal of Drosophila neuroblasts. *Genes Dev*. 20:3453-3463.

Wee, B., C.A. Johnston, K.E. Prehoda, and C.Q. Doe. 2011. Canoe binds RanGTP to promote Pins(TPR)/Mud-mediated spindle orientation. *The Journal of cell biology*. 195:369-376.

Wei, C., V.K. Bhattaram, J.C. Igwe, E. Fleming, and J.S. Tirnauer. 2012. The LKB1 tumor suppressor controls spindle orientation and localization of activated AMPK in mitotic epithelial cells. *PLoS One*. 7:e41118.

Williams, S.E., S. Beronja, H.A. Pasolli, and E. Fuchs. 2011. Asymmetric cell divisions promote Notch-dependent epidermal differentiation. *Nature*. 470:353-358.

Williams, S.E., L.A. Ratliff, M.P. Postiglione, J.A. Knoblich, and E. Fuchs. 2014. Par3-mInsc and Galphai3 cooperate to promote oriented epidermal cell divisions through LGN. *Nature cell biology*. 16:758-769.

Wirtz-Peitz, F., T. Nishimura, and J.A. Knoblich. 2008. Linking cell cycle to asymmetric division: Aurora-A phosphorylates the Par complex to regulate Numb localization. *Cell*. 135:161-173.

Wodarz, A., A. Ramrath, A. Grimm, and E. Knust. 2000. Drosophila atypical protein kinase C associates with Bazooka and controls polarity of epithelia and neuroblasts. *J Cell Biol*. 150:1361-1374.

Wodarz, A., A. Ramrath, U. Kuchinke, and E. Knust. 1999. Bazooka provides an apical cue for Inscuteable localization in Drosophila neuroblasts. *Nature*. 402:544-547.

Woodard, G.E., N.N. Huang, H. Cho, T. Miki, G.G. Tall, and J.H. Kehrl. 2011. Ric-8A and Gi alpha recruit LGN, NuMA, and dynein to the cell cortex to help orient the mitotic spindle. *Mol Cell Biol*. 30:3519-3530.

Xu, Y., R. Chang, Z. Peng, Y. Wang, W. Ji, J. Guo, L. Song, C. Dai, W. Wei, Y. Wu, X. Wan, C. Shao, and L. Zhan. 2015. Loss of polarity protein AF6 promotes pancreatic cancer metastasis by inducing Snail expression. *Nat Commun*. 6:7184.

Yamamoto, H., T. Maruo, T. Majima, H. Ishizaki, M. Tanaka-Okamoto, J. Miyoshi, K. Mandai, and Y. Takai. 2013. Genetic deletion of afadin causes hydrocephalus by destruction of adherens junctions in radial glial and ependymal cells in the midbrain. *PLoS One*. 8:e80356.

Yamanaka, T., Y. Horikoshi, N. Izumi, A. Suzuki, K. Mizuno, and S. Ohno. 2006. Lgl mediates apical domain disassembly by suppressing the PAR-3-aPKC-PAR-6 complex to orient apical membrane polarity. *J Cell Sci*. 119:2107-2118.

Yamanaka, T., Y. Horikoshi, Y. Sugiyama, C. Ishiyama, A. Suzuki, T. Hirose, A. Iwamatsu, A. Shinohara, and S. Ohno. 2003. Mammalian Lgl forms a protein complex with PAR-6 and aPKC independently of PAR-3 to regulate epithelial cell polarity. *Curr Biol*. 13:734-743.

Yang, C.H., E.J. Lambie, and M. Snyder. 1992. NuMA: an unusually long coiled-coil related protein in the mammalian nucleus. *J Cell Biol*. 116:1303-1317.

Yang, Y., M. Liu, D. Li, J. Ran, J. Gao, S. Suo, S.C. Sun, and J. Zhou. 2014. CYLD regulates spindle orientation by stabilizing astral microtubules and promoting dishevelled-NuMA-dynein/dynactin complex formation. *Proc Natl Acad Sci U S A*. 111:2158-2163.

Yang, Z., S. Zimmerman, P.R. Brakeman, G.M. Beaudoin, 3rd, L.F. Reichardt, and D.K. Marciano. 2013. De novo lumen formation and elongation in the developing nephron: a central role for afadin in apical polarity. *Development*. 140:1774-1784.

Yasumi, M., T. Sakisaka, T. Hoshino, T. Kimura, Y. Sakamoto, T. Yamanaka, S. Ohno, and Y. Takai. 2005. Direct binding of Lgl2 to LGN during mitosis and its requirement for normal cell division. *J Biol Chem*. 280:6761-6765.

Zhadanov, A.B., D.W. Provance, Jr., C.A. Speer, J.D. Coffin, D. Goss, J.A. Blixt, C.M. Reichert, and J.A. Mercer. 1999. Absence of the tight junctional protein AF-6 disrupts epithelial cell-cell junctions and cell polarity during mouse development. *Current biology : CB*. 9:880-888.

Zheng, Z., Q. Wan, J. Liu, H. Zhu, X. Chu, and Q. Du. 2013. Evidence for dynein and astral microtubule-mediated cortical release and transport of Galphai/LGN/NuMA complex in mitotic cells. *Molecular biology of the cell*. 24:901-913.

Zheng, Z., Q. Wan, G. Meixiong, and Q. Du. 2014. Cell cycle-regulated membrane binding of NuMA contributes to efficient anaphase chromosome separation. *Molecular biology of the cell*. 25:606-619.

Zheng, Z., H. Zhu, Q. Wan, J. Liu, Z. Xiao, D.P. Siderovski, and Q. Du. 2010. LGN regulates mitotic spindle orientation during epithelial morphogenesis. *J Cell Biol*. 189:275-288.

Zhu, J., Y. Shang, Q. Wan, Y. Xia, J. Chen, Q. Du, and M. Zhang. 2014. Phosphorylation-dependent interaction between tumor suppressors Dlg and Lgl. *Cell Res*. 24:451-463.

Zhu, J., Y. Shang, C. Xia, W. Wang, W. Wen, and M. Zhang. 2011a. Guanylate kinase domains of the MAGUK family scaffold proteins as specific phospho-protein-binding modules. *The EMBO journal*. 30:4986-4997.

Zhu, J., W. Wen, Z. Zheng, Y. Shang, Z. Wei, Z. Xiao, Z. Pan, Q. Du, W. Wang, and M. Zhang. 2011b. LGN/mInsc and LGN/NuMA complex structures suggest distinct functions in asymmetric cell division for the Par3/mInsc/LGN and Galphai/LGN/NuMA pathways. *Molecular cell*. 43:418-431.

Zorba, A., V. Buosi, S. Kutter, N. Kern, F. Pontiggia, Y.J. Cho, and D. Kern. 2014. Molecular mechanism of Aurora A kinase autophosphorylation and its allosteric activation by TPX2. *Elife*. 3:e02667.

ACKNOWLEDGMENTS

First, I want to thank all of my colleagues of the Lab: Manuel, Laura, Sara and Valentina for their scientific and personal support. They are both colleagues and friends that have definitely helped me throughout these difficult four years.

A special mention goes also to my friend Federico Boem, who never stopped to encourage me.

Of course, I am grateful to Marina Mapelli for the opportunity that she gave me to work in her group, especially on these challenging projects. Moreover, she helped me a lot with the entire revision of my thesis.

I also would like to thank Emanuele Martini and Amanda Oldani for their technical support on confocal microscope and FRAP analysis. Another thanks go to Giulia Guarguaglini's Lab that contributes to Aurora-A/NuMA project.

Last but not least, a special thanks to my family, I am grateful to my mother Annalisa, and my father Loris for all of the sacrifices that they have made on my behalf. I would not be here without their encouragement and their love.